The fabrication of nanogap electrodes using nanoskiving

Pourhossein Aghbolagh, Parisa

The Fabrication of Nanogap Electrodes Using Nanoskiving

Parisa Pourhossein Aghbolagh

The Fabrication of Nanogap Electrodes Using Nanoskiving

Parisa Pourhossein Aghbolagh

PhD Thesis

University of Groningen
The Netherlands

ISBN:978-90-367-7071-2 (Printed version)
ISBN:978-90-367-7072-9 (Electronic version)

This project was carried out in the research group of Chemistry of (Bio)Molecular Materials and Devices part of the Stratingh Institute for Chemistry, University of Groningen, The Netherlands. This work is part of the Joint Solar Program (JSP) of Hyet Solar and the Stichting voor Fundamentaal Onderzoek der Materie FOM, which is part of the Netherlands Organisation for Scientific Research (NWO).

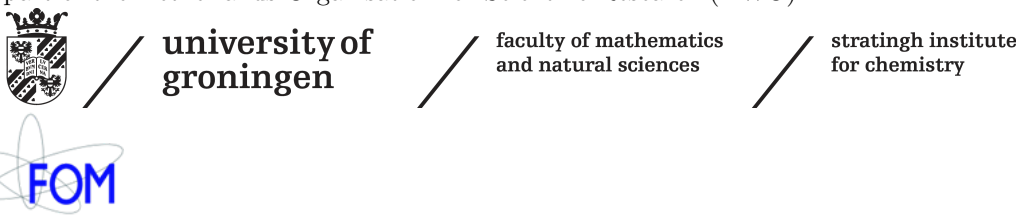

university of groningen

The Fabrication of Nanogap Electrodes Using Nanoskiving

PhD thesis

to obtain the degree of PhD at the
University of Groningen
on the authority of the
Rector Magnificus Prof. E. Sterken
and in accordance with
the decision by the College of Deans.

This thesis will be defended in public on

Friday 20 June 2014 at 16.15 hours

by

Parisa Pourhossein Aghbolagh

born on 24 April 1981
in Tehran, Iran

Supervisor
Prof. J.C. Hummelen

Co-supervisor
Dr. R.C. Chiechi

Assessment committee
Prof. E.M.J. Verpoorte
Prof. S.C.J. Meskers
Prof. D.J. Lipomi

To my dear parents

Contents

Chapter 1

Introduction

1.1 What is nanotechnology?

The origin of the word nano is in the Greek word "nanos" which means dwarf. In the International System of Units, the prefix nano means one-billionth, which is a factor of 10^{-9} and is used mostly in association with time interval and length scale (*i.e.*, one nanometer is one billionth of a meter). It is quite difficult to imagine how small one nanometer is. A sheet of paper is about $100,000$ nanometers thick. A strand of human DNA is 2.5 nanometers in diameter. The width of a human hair is $\sim 80,000 - 100,000$ nanometers. Figure 1.1 elucidates the length scale of things. This illustration shows how small things are at the nanoscale.

The terms nanotechnology and nanoscience refer to the study and application of extremely small things—often at the molecular scale—and they comprise an interdisciplinary field that includes aspects of chemistry, biology, physics, materials science, and engineering. In 1959, Richard Feynman gave an inspiring talk, "There's Plenty of Room at the Bottom" at an American Physical Society meeting at California Institute of Technolgy (CalTech); He introduced the

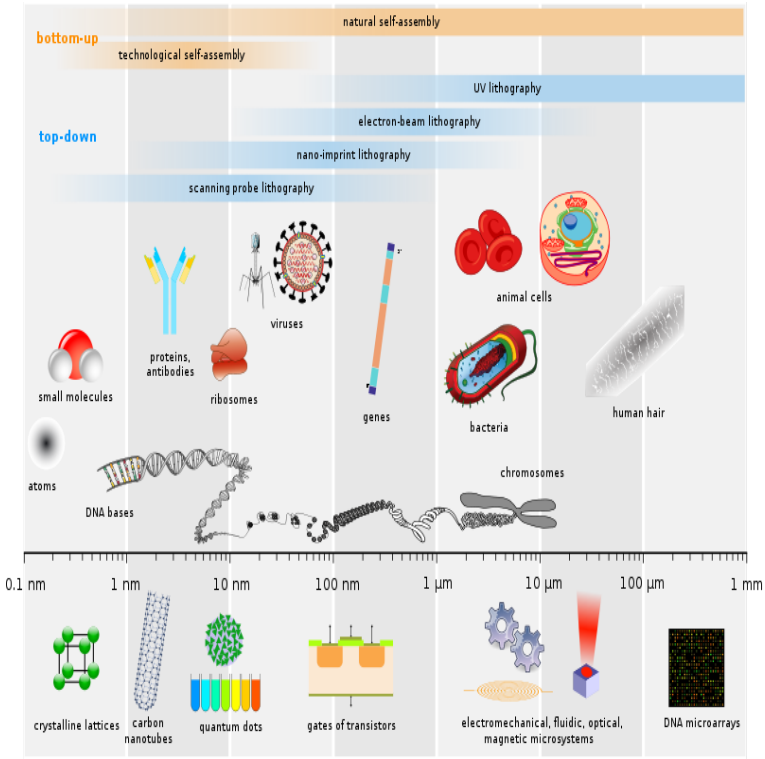

Figure 1.1: A comparison of the scales of various biological and technological objects. Adapted from the Wikimedia Commons file:"Biological and technological scales compared-en.svg".

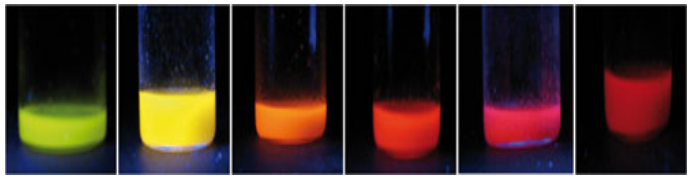

Figure 1.2: Size makes the difference: silicon nanoparticles luminesce–depending on diameter–in different colours. Reproduced with permission from Ref. [1].

idea of nanotechnology long before the term nanotechnology was used. Modern nanotechnology arguably began with the development of scanning tunneling microscope in 1981.

The nanoscale is the scale at which the properties of materials change from those in bulk materials (larger scales). At this scale quantum mechanical effects become dominant and the properties of materials such as melting point, fluorescence, electrical conductivity, etc. are size-dependent. As a result, by changing the size of particles one can tune a property of interest. For example, the effect of size (or quantum) confinement on the fluorescence of Si nanoparticles is shown in Figure 1.2 which shows the dependence of light emission color on size of the nanoparticles.[1,2] Tunneling is another phenomenon that arises at the nanoscale. Charge transport through individual molecules typically occurs via non-resonant tunneling, which is length dependent. Extensive studies have been done on charge transport through molecules.[3–14] Scanning tunneling microscopy is based on this property.

Nanotechnology can potentially revolutionize electronics and information technology, sustainable energy and medical and health applications to name few. In the electronics industry, nanotechnology can be used to provide faster, smaller, and more portable systems that can manage and store larger and larger amounts of information. Nanotechnology can be a solution to provide clean, affordable, and renewable energy sources. One approach is to make solar cells of cheaper materials (*e.g.*, inorganic or organic nanoscale materials). Increasing the efficiency of solar cells by using new nanostructures to collect wavelengths of solar energy

that are currently wasted can be another option. Green energy can be provided by utilizing new, cheaper, nanoscale catalysts to convert biofuels (which are renewable sources) to diesel. The current semiconductor industry uses complex and sophisticated processes to manufacture electronic devices. Photolithography equipment is expensive and incompatibility with organic and some other class of materials is an issue. Thus, the demand is to develop methods of patterning and manufacturing nanostructures, devices and systems that are simple, reliable, cost-effective and accessible.

1.2 Nanofabrication

Fabrication at the nanoscale–in which at least one lateral dimension is between 1 nm and 100 nm–is known as nanofabrication and can be thought of an extension of microfabrcation.[15] There are two main approaches of nanofabrication, top-down or bottom-up. In top-down fabrication large pieces of materials are broken all the way down to the nanoscale. The bottom-up approach to nanofabrication generates products by building them up from atomic- and molecular-scale components.

1.3 Nanogap electrodes

Nanogap electrodes comprise a pair of electrodes that are separated from each other by a nanoscale gap.[16–21] Most metal/molecule/metal devices are nanogaps because most molecules of interest are < 5 nm. There are two options for the insertion of such molecules. The molecular components can be inserted after the fabrication of electrodes or, taking advantage of the formation of self-assembled monolayers (SAMs), molecules can be arranged in the gap during the fabrication procedure.[22] In SAMs, molecules self-organize without the involvement of humans.[23] Highly ordered monolayers on substrates can spontaneously form from solution.[24] Molecules that form SAMs have three main components; a

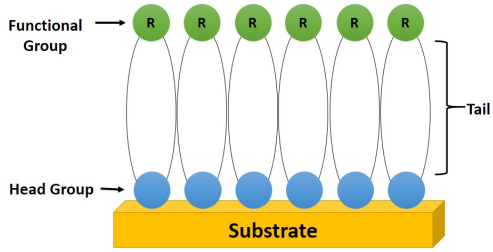

Figure 1.3: A schematic (not to scale) representation of SAMs. Each molecule is composed of three parts: a head group, a spacer and a functional end group.

head (or anchoring) group, a spacer (or tail) and a functional end group.[25] A schematic representation of a SAM is shown in Figure 5.1. The head groups of the molecules form a covalent bond with the substare. The most studied SAMs are SAMs of alkanethiols on gold substrates.[26–31] The sulphur atom of thiols is chemisorbed on a gold surface and alkyl chains are closely packed by van der waals forces.

1.4 Fabrication of nanogap electrodes

As I mentioned earlier, target molecules with dimensions below 5 nm are of interest for metal/molecule/metal devices. Thus, the precise control of the gap size is an important issue to avoid any anomalies that will result in unexpected performancs. Over nearly 20 years of research on nanogap electrodes, several methods of fabrication with controlled spacing have been reported in literature: mechanical break junctions,[32] electron-beam lithography,[33] electrochemical plating,[34] electromigration,[35] focused ion beam lithography,[21] shadow mask evaporation,[36] scanning probe and atomic force lithography,[37] on-wire lithography,[38] molecular rulers[39] etc.; The method that we have de-

veloped is based on nanoskiving.[40] In the following, I will introduce some of these techniques.

1.4.1 Mechanical Controllable Break Junctions

Reed et al. adopted the mechanical controllable break junction (MCBJ) method that had been introduced by Moreland to fabricate nanogap electrodes.[32,41,42] Figure 1.4 presents the MCBJ technique. As it is shown in the schematic drawing (Figure 1.4A), small metallic wires (mostly gold wires) are glued to a flexible substrate. A fracture is made in the wire by bending the substrate. The size of the formed gap can be controlled using a piezoelectric element. To aquire two atomically clean surfaces, the breaking process mostly takes place at low temperature and high vacuum conditions.[17,43,44] MCBJs are used in single molecule devices (even single atom devices)[43–51] and metal-molecule-metal junctions.[13,17,32,42,52–54] The drawback of this method is that fabricating devices with three or even more electrodes is complicated and it is not easy to fabricate highly integrated molecular devices. There is no control on the actual geometry of the electrodes and the stability and reproducibility of the junction is often unsatisfactory. The metal/molecule/metal "devices" are also transient.

1.4.2 Electrochemical and Chemical Deposition

A reproducible way to fabricate nanogap electrodes is using electrochemical and chemical deposition methods, which are combined with lithography techniques.[55] First, electrodes with a relatively large gap are fabricated using lithography techniques and then gap is scaled down to a smaller gap by depositing specific atoms onto the electrodes. The reverse process to widen the gaps is also possible. With these methods gaps within the range of few angstroms to 10 nm can be formed. These facile methods can be promising to fabricate large scale and highly integrated devices; however, addressability of the electrodes is still a challenge. Figure 1.5 and Figure 1.6 shows nanogaps fabricated using

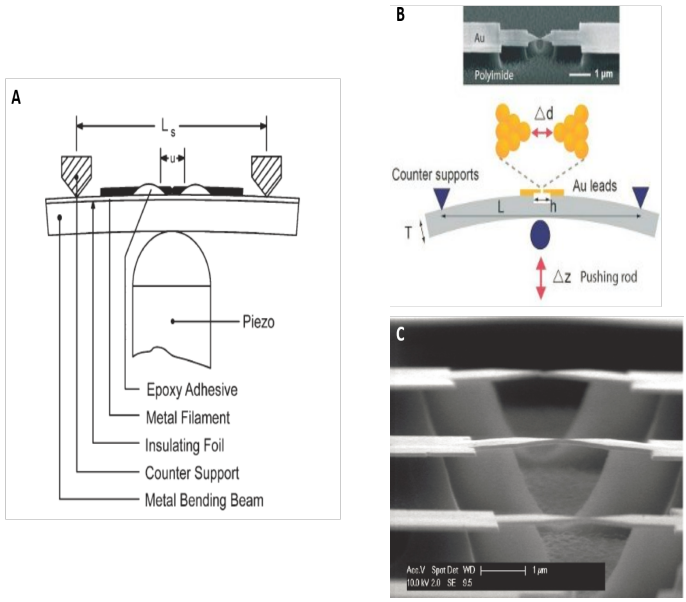

Figure 1.4: The sample mounting of a three point bending conguration. The bending beam consists of flexible phosphorus bronze covered with an insulating layer of Capton. The junction is formed by breaking the electrode material, which is achieved by bending the beam. The elongation of the unglued section, u, is concentrated on the notch and will result in a fracture of the material. A voltage on the piezo element is used for fine adjustment of the coupling between the two electrodes. Reproduced with permission from Ref. [42,44].

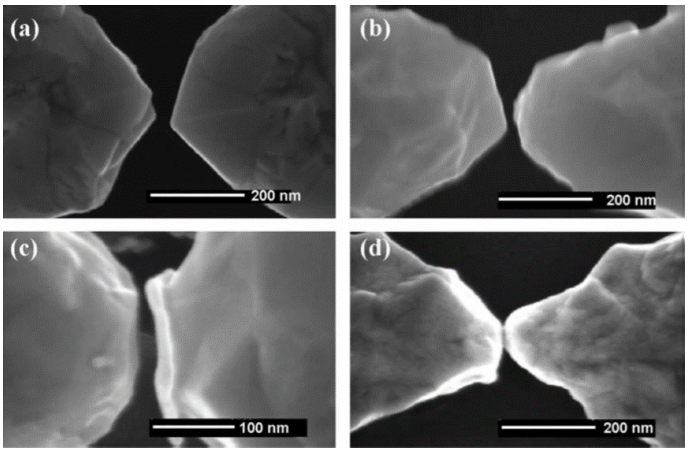

Figure 1.5: SEM images of gaps prepared at 3 kHz with different Δt values: a) $\Delta t = 9$ s, d=26 nm; b)$\Delta t = 25$ s, d=16 nm; c) $\Delta t = 42$ s, d=7 nm; d) $\Delta t = 62$ s, d ~ 1 nm. Reproduced with permission from Ref. [20].

electrochemical and chemical deposition respectively.[20,56]

1.4.3 Electromigration

In electromigration, the passage of a high density of current or application of direct current (DC) through a thin metal wire (that has been predefined by electron-beam lithography) results in breakage of the nanowire.[57–59] In essence, the electromigration of metal atoms causes this breakage. This method is useful for fabricating three-electrode nanodevices because a gate electrode can easily be fabricated on the substrate before electrical fracture takes place. Figure 1.7 is a scanning electron micrograph of a nanogap fabricated using this technique.[19] A 1 nm gap between two gold nanowires is formed in this case. Observations of Coulomb blockade and Kondo effect in single-atom and single-molecule transistors and temperature dependence have been reported in junctions fabricated using electromigration.[60,61] Two important issues that have to be taken into account are as follow: electromigration is a thermally-assisted process, but excessive heating must be avoided since it will cause melting of the metal, so the

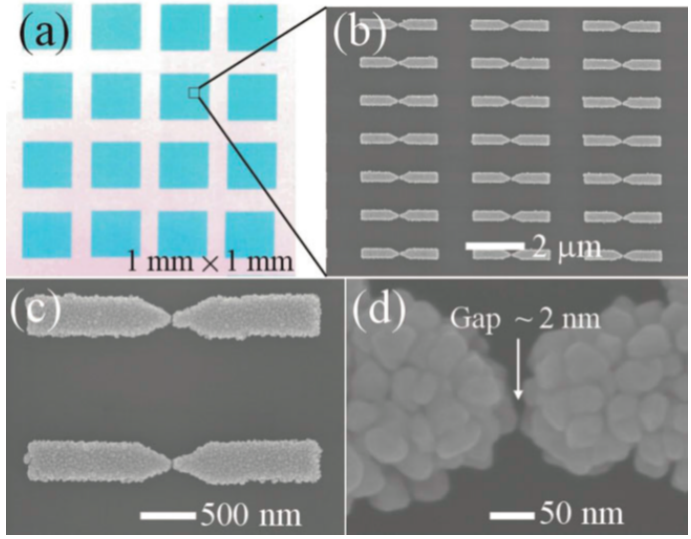

Figure 1.6: a) Optical and b) field emission scanning electron microscopy (FESEM) images of an array of nanogaps with sub-5nm separations after surface-catalyzed chemical deposition. FESEM images of two-fingered nanogap electrodes with magnifications of c) $\times 40000$ and d)$\times 320000$. Reproduced with permission from Ref. [56].

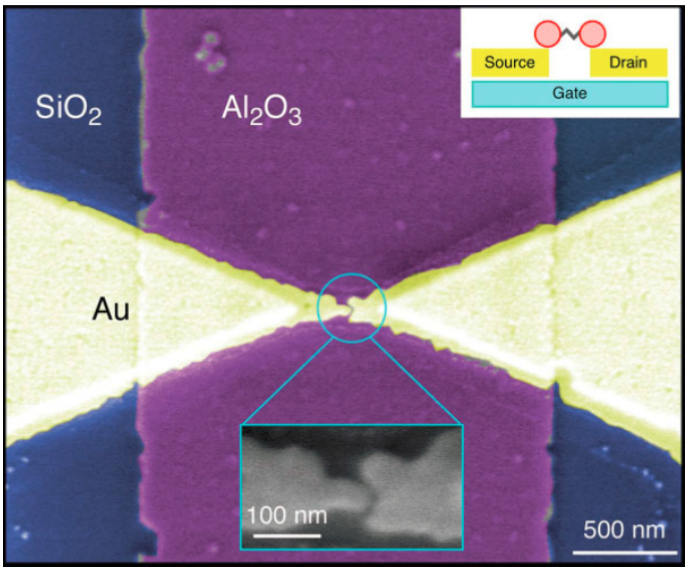

Figure 1.7: SEM image (false color) of the metallic electrodes fabricated by electron beam lithography and the electromigration-induced break junction technique. The image shows two gold electrodes separated by 1 nm above an aluminium pad, which is covered with a 3 nm thick layer of aluminium oxide. The whole structure was defined on a silicon wafer. The bright yellow regions corresponds to a gold bridge with a thickness of 15 nm and a minimum lateral size of 100 nm. The paler yellow regions represent portions of the gold electrodes with a thickness of 100 nm. Inset: schematic diagram of single-molecule transistors that contain individual divanadium molecules. Reproduced with permission from Ref. [19].

temperature should be kept low during the process. Another issue is related to the metal debris in the nanogap after fabrication which will affect the insertion of molecules in the gap.

1.4.4 Molecular Ruler

The gap size can be defined using molecules as gap template. Hatzor and Weiss constructed nanostructures using mercaptoalkanoic acids as molecular templates.[39] By combining metal deposition via electron-beam lithography and etching out mercaptoalkanoic acid–that serves as resist in this case–nanogaps can

be fabricated.[62,63] The size of this spacing is dictated by the thickeness of mercaptoalkanoic acid layer. The so-called "molecular lithography" is a promissing method to construct arrays of moleuclar circuits (Figure 1.8).[22]

1.4.5 On-wire Lithography

Mirkin et al. developed a method of fabricating nanogaps with spacing from a few to several hundred nanometers.[38,64] On-wire Lithography (OWL) combines template-directed synthesis of nanowires with electrochemical deposition and wet-chemical etching to remove the sacrificial segment. Figure 1.9 shows the SEM images of multisegment metallic Au-Ag nanowires. A gap of 5 nm is depicted in Figure 1.9F. Organic field effect transistors (OFETs) of conjugated polymer based on nanogap electrodes using OWL have been fabricated. However, addressing these nanogaps requires serial e-beam lithography.

1.4.6 Nanoskiving

Nanoskiving is a method that is derived from edge-lithography techniques;[65] We have adopted this method for the purpose of fabrication to construct nanogap electrodes.[40] This technique combines metal deposition and sectioning; SAMs or sacrificial layers are utilized to tune the gap size. Sectioning is done using an ultramicrotome. Microtomes have been used to slice thin sections since 1770.[66] However, the application of this instrument was mostly limited to biology; with the advent of electorn microscopes (*e.g.*, the transmission electron microscope in 1930s), sections below 100 nm were required for imaging.[67] Thus, the microtome became known as the ultramicrotome and using ultramicrotomy sections of inorganic and polymeric materials could be cut.[68] Whitesides and co-workers developed nanoskiving to fabricate nanostructures that are difficult or impossible to make using other techniques.[69]

We used nanoskiving to overcome some of the disadvantages of the aforementioned methods. Nanoskiving provides us a truly simple platform to fabricate

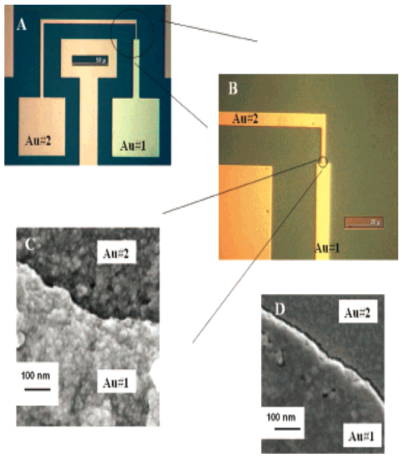

Figure 1.8: Optical and scanning electron micrographs showing an electrode structure fabricated on a silicon substrate via photolithography. (A) Optical micrograph showing an individual electrode structure. The initial electrode is labeled Au$\neq 1$, and the electrode that was deposited second is labeled as Au$\neq 2$. The scale bar is $50\ \mu\mathrm{m}$. (B) High resolution optical micrograph showing the interface between the two metallic electrodes, labeled Au$\neq 1$ and Au$\neq 2$. The scale bar is $20\ \mu\mathrm{m}$. (C) Scanning electron micrograph of the interface between the two metallic layers, labeled Au$\neq 1$ and Au$\neq 2$. The scale bar is 100 nm. The separation between the electrodes is observable but is difficult to resolve. (D) A similar scanning electron micrograph taken of an electrode pair on a second substrate fabricated using a multilayered resist to achieve a larger separation distance between two electrodes. The scale bar is 100 nm. Reproduced with permission from Ref. [22]

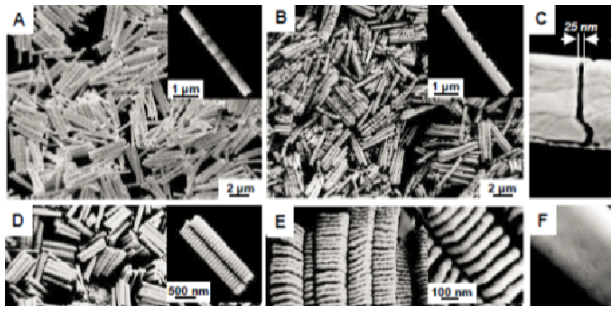

Figure 1.9: FESEM images of multisegment metallic Au-Ag nanowires (A) before and (B) after coating with a bilayer consisting of 10 nm of Ti and 40 nm of Au and subsequent wet-chemical etching of the Ag segments. Insets show magnified images. (C) Side view of a nanogap wire with gap sizes of 25, 50, and 100 nm. Multisegment metallic Au-Ni nanowires (D) before and (E) after coating one side with 50 nm of silica and subsequent wet-chemical etching of the Ni segments. Each Au and Ni segment length is 40 nm. Insets are magnified images. (F) An Au nanowire with a 5-nm gap. Every nanowire in the batch has a well-defined gap. Reproduced with permission from Ref. [38].

hundreds of thousands of directly addressable nanogaps on demand in a short time (with the rate of one nanogap per second). This inexpensive and high throughput method enables us to fabricate high aspect ratio nanostructures which is not achievable with any other method.

1.5 Potential Applications of Nanogap Electrodes

1.5.1 Solar cells

In bulk heterojunction organic photovoltaic (OPV) devices, upon exposure to solar light, a photoinduced electron transfer between donor- and acceptor-type semiconducting polymers or molecules takes place. In order to achieve charge separation, excitons created in either material should be able to diffuse to the interface. Due to their short lifetime and low mobility, the diffusion length of excitons in organic semiconductors is limited to few nanometers. Photogenerated

charges must be able to migrate to the collecting electrodes through the donor-acceptor blend.

Electrodes are an indispensable component of OPV devices, yet most OPVs utilize the same basic combinations of high- and low-work-function electrodes in planar architectures. This design has remained popular because it is simple to fabricate using techniques that were handed down from the crystalline solar cell work that began in the middle of the 20th century. The notion that it is the best architecture for organic system belies the principle advantage of using organic materials—processability. The conformal nature of organic materials is such that the introduction of a simple method for generating non-planar electrode architectures that are tailored to the quirks of excitonic solar cells (a category to which all existing OPVs belong) carries the potential to improve the efficiencies of all OPVs by retaining the gains that have been made through the optimization of organic materials over the last decade. The principle mechanism for loss in excitonic solar cells is the recombination of charges that can occur after they are created by the scission of excitons, but before they are able to drift to the collection electrodes. The simplest way to prevent this loss is to put the collection electrodes within the exciton diffusion length of the active materials of the device. In planar architectures this can only be accomplished by making thinner films, however this decreases the amount of light that can be captured. The current trend in research is to create stacked, planar devices, but this increases the complexity of fabrication (and reproducibility) and offsets one of the primary advantages of using organic materials to begin with. The introduction of a new, simple, scalable, and commercially viable means to produce non-planar electrodes on the length scale of the exciton diffusion length of common organic materials would obviate all of these trade-offs and potentially make OPVs viable and competitive for local power generation in consumer electronic products. Thus we need to produce non-planar architectures for organic, nanocrystal-based, and hybrid photovoltaic devices in which the configuration of the electrodes and the active materials is controlled on the length scale of

the exciton diffusion radii (10-20 nm) inherent to the active materials of the device.[70–72] In other words, we are thinking of a generalizable platform in which the absorption of a photon in an arbitrary material occurs within the exciton diffusion radius of a charge-separation interface and both collection electrodes, thus maximizing the scission of excitons in to charge pairs and the injection of those charges in to electrodes. The fabrication of nanogap electrodes would be the first step towards this goal.

1.5.2 Molecular Electronics

The level of miniaturization in the semiconductor industry is reaching its limits; To follow the well–known Moore's law, the dream of using molecules as circuit elements may come true.[73] In 1974, Aviram and Ratner proposed a simple molecular electronic device, which was a rectifier and was similar to a p–n junction.[74] Molecular–based devices for electronic applications offer unique advantages such as lower cost, higher efficiency, lower energy dissipation etc.[75] However, the challenge of integrating molecules to electronic circuits still remains. One way to wire up molecules in devices is to utilize nanogap electrodes.

1.6 Outline of the thesis

The two applications of nanogap electrodes that I have mentioned in the previous section and the fact that none of the aforementioned methods of fabricating nanogaps combines simplicity, high throughput and direct addressability, motivated us to come up with a new method of nanofabrication. In this thesis, I introduce nanoskiving–a form of edge lithography technique–as a simple method to fabricate addressable nanogap electrodes. In Chapter 2 a detailed description of the method of nanoskiving along with the embedding resin that we have developed is presented. In Chapter 3 the fabrication of electrically addressable sub-3 nm nanogap electrodes using SAMs as gap templates is described. I have fabricated SAM-templated addressable nanogap electrodes (STANs) using

three different alkanedithiols. Electron microscopy and electrical characterizations have been performed and length dependent electrical measurements show that the molecules are indeed determining the gap size. We observed an excellent agreement between the obtained value of tunneling deacy constant (β) and the values which have been reported in literature. In Chapter 4 I describe the fabrication of nanogap electrodes using sacrificial layers of Al and Ag to obtain gaps > 5 nm. Also, I present the results of the fabrication of the nanogap electrodes using two different work function metals as electrodes. In Chapter 5 we investigated the fabrication of nanogap electrodes from arbitrary symmetric dithiols. I used dynamic exchange of SAMs to exchange alkanedithiols in prefabricated STANs with oligo(phenylene ethynylenes) (OPEs). Electrical measurements were performed which indicates the increase in current density uopn exchange of alkanedithiols with OPEs. In Chapter 6 I have fabricated STANs using SAMs of hemicyanine molecules. Charge transport in these devices was investigated in dark and uopn irradiation with different wavelengths.

Bibliography

[1] A. Gupta, M. T. Swihart, and H. Wiggers. Luminescent colloidal dispersion of silicon quantum dots from microwave plasma synthesis: Exploring the photoluminescence behavior across the visible spectrum. *Adv. Funct. Mater.*, 19(5):696–703, 2009.

[2] C. Meier, A. Gondorf, S. Lüttjohann, A. Lorke, and H. Wiggers. Silicon nanoparticles: Absorption, emission, and the nature of the electronic bandgap. *J. Appl. Phys.*, 101(10):103112, 2007.

[3] C. A. Martin, D. Ding, H. S. van der Zant, and J. M. van Ruitenbeek. Lithographic mechanical break junctions for single-molecule measurements in vacuum: possibilities and limitations. *New J. Phys.*, 10(6):065008, 2008.

[4] E. H. Huisman, M. L. Trouwborst, F. L. Bakker, B. de Boer, B. J. van Wees, and S. J. van der Molen. Stabilizing single atom contacts by molecular bridge formation. *Nano Lett.*, 8(10):3381–3385, 2008. PMID: 18771330.

[5] C. M. Guèdon, J. Zonneveld, H. Valkenier, J. C. Hummelen, and S. J. van der Molen. Controlling the interparticle distance in a 2d molecule-nanoparticle network. *Nanotechnology*, 22(12):125205, 2011.

[6] D. Fracasso, H. Valkenier, J. C. Hummelen, G. C. Solomon, and R. C. Chiechi. Evidence for Quantum Interference in SAMs of Arylethynylene Thiolates in Tunneling Junctions with Eutectic Ga-In (EGaIn) Top-Contacts. *J. Am. Chem. Soc.*, 133(24):9556–9563, May 2011.

[7] B. de Boer, M. M. Frank, Y. J. Chabal, W. Jiang, E. Garfunkel, and Z. Bao. Metallic contact formation for molecular electronics: Interactions between vapor-deposited metals and self-assembled monolayers of conjugated mono- and dithiols. *Langmuir*, 20(5):1539–1542, 2004. PMID: 15801409.

[8] H. B. Akkerman, P. W. M. Blom, D. M. de Leeuw, and B. de Boer. Towards molecular electronics with large-area molecular junctions. *Nature*, 441(7089):69–72, May 2006.

[9] V. B. Engelkes, J. M. Beebe, and C. D. Frisbie. Length-dependent transport in molecular junctions based on sams of alkanethiols and alkanedithiols: Effect of metal work function and applied bias on tunneling efficiency and contact resistance. *J. Am. Chem. Soc.*, 126(43):14287–14296, 2004. PMID: 15506797.

[10] J. M. Beebe, V. B. Engelkes, L. L. Miller, and C. D. Frisbie. Contact resistance in metal-molecul-metal junctions based on aliphatic sams: Effects of surface linker and metal work function. *J. Am. Chem. Soc.*, 124(38):11268–11269, 2002. PMID: 12236731.

[11] C. Chu, J.-S. Na, and G. N. Parsons. Conductivity in alkylamine/gold and alkanethiol/gold molecular junctions measured in molecule/nanoparticle/molecule bridges and conducting probe structures. *J. Am. Chem. Soc.*, 129(8):2287–2296, 2007.

[12] E. A. Weiss, R. C. Chiechi, G. K. Kaufman, J. K. Kriebel, Z. Li, M. Duati, M. A. Rampi, and G. M. Whitesides. Influence of defects on the electrical characteristics of mercury-drop junctions: Self-assembled monolayers of n-alkanethiolates on rough and smooth silver. *J. Am. Chem. Soc.*, 129(14):4336–4349, 2007. PMID: 17358061.

[13] J. Reichert, R. Ochs, D. Beckmann, H. B. Weber, M. Mayor, and H. v. Löhneysen. Driving current through single organic molecules. *Phys. Rev. Lett.*, 88:176804, Apr 2002.

[14] B. Xu and N. J. Tao. Measurement of single-molecule resistance by repeated formation of molecular junctions. *Science*, 301(5637):1221–1223, 2003.

[15] B. D. Gates, Q. Xu, M. Stewart, D. Ryan, C. G. Willson, and G. M. Whitesides. New approaches to nanofabrication: Molding, printing, and other techniques. *Chem. Rev.*, 105(4):1171–1196, 2005. PMID: 15826012.

[16] T. Li, W. Hu, and D. Zhu. Nanogap electrodes. *Adv. Mater.*, 22(2):286–300, 2010.

[17] C. Kergueris, J.-P. Bourgoin, S. Palacin, D. Esteve, C. Urbina, M. Magoga, and C. Joachim. Electron transport through a metal-molecule-metal junction. *Phys. Rev. B*, 59:12505–12513, May 1999.

[18] M. S. M. Saifullah, T. Ondarçuhu, D. K. Koltsov, C. Joachim, and M. E. Welland. A reliable scheme for fabricating sub-5 nm co-planar junctions for single-molecule electronics. *Nanotechnology*, 13(5):659, 2002.

[19] W. Liang, M. P. Shores, M. Bockrath, J.. R. Long, and H. Park. Kondo resonance in a single-molecule transistor. *Nature*, 417:725–729, 2002.

[20] Q. Qing, F. Chen, P. Li, W. Tang, Z. Wu, and Z. Liu. Finely tuning metallic nanogap size with electrodeposition by utilizing high-frequency impedance in feedback. *Angew. Chem. Int. Ed.*, 44(47):7771–7775, 2005.

[21] T. Nagase, T. Kubota, and S. Mashiko. Fabrication of nano-gap electrodes for measuring electrical properties of organic molecules using a focused ion beam. *Thin Solid Films*, 438-439(0):374 – 377, 2003. ¡ce:title¿The 5th International Conference on Nano-Molecular Electronics¡/ce:title¿.

[22] G. S. McCarty. Molecular lithography for wafer-scale fabrication of molecular junctions. *Nano Lett.*, 4(8):1391–1394, 2004.

[23] J. Sagiv. Organized monolayers by adsorption. 1. formation and structure of oleophobic mixed monolayers on solid surfaces. *J. Am. Chem. Soc.*, 102(1):92–98, 1980.

[24] R. G. Nuzzo and D. L. Allara. Adsorption of bifunctional organic disulfides on gold surfaces. *J. Am. Chem. Soc.*, 105(13):4481–4483, 1983.

[25] J. C. Love, L. A. Estroff, J. K. Kriebel, R. G. Nuzzo, and G. M. Whitesides. Self-assembled monolayers of thiolates on metals as a form of nanotechnology. *Chem. Rev.*, 105(4):1103–1170, 2005.

[26] C. D. Bain and G. M. Whitesides. Formation of monolayers by the coadsorption of thiols on gold: variation in the length of the alkyl chain. *J. Am. Chem. Soc.*, 111(18):7164–7175, 1989.

[27] M. M. Walczak, C. Chung, S. M. Stole, C. A. Widrig, and M. D. Porter. Structure and interfacial properties of spontaneously adsorbed n-alkanethiolate monolayers on evaporated silver surfaces. *J. Am. Chem. Soc.*, 113(7):2370–2378, 1991.

[28] K. Shimazu, I. Yagi, Y. Sato, and K. Uosaki. In situ and dynamic monitoring of the self-assembling and redox processes of a ferrocenylundecanethiol monolayer by electrochemical quartz crystal microbalance. *Langmuir*, 8(5):1385–1387, 1992.

[29] G. K. Rowe and S. E. Creager. Redox and ion-pairing thermodynamics in self-assembled monolayers. *Langmuir*, 7(10):2307–2312, 1991.

[30] T. W. Schneider and D. A. Buttry. Electrochemical quartz crystal microbalance studies of adsorption and desorption of self-assembled monolayers of alkyl thiols on gold. *J. Am. Chem. Soc.*, 115(26):12391–12397, 1993.

[31] F. Nüesch, F. Rotzinger, L. Si-Ahmed, and L. Zuppiroli. Chemical potential shifts at organic device electrodes induced by grafted monolayers. *Chem. Phys. Lett*, 288(5 - 6):861 – 867, 1998.

[32] M. A. Reed, C. Zhou, C. J. Muller, T. P. Burgin, and J. M. Tour. Conductance of a molecular junction. *Science*, 278(5336):252–254, 1997.

[33] W. Chen, H. Ahmed, and K. Nakazoto. Coulomb blockade at 77 k in nanoscale metallic islands in a lateral nanostructure. *Appl. Phys. Lett.*, 66(24):3383–3384, 1995.

[34] A.F. Morpurgo, C.M. Marcus, and D.B. Robinson. Controlled fabrication of metallic electrodes with atomic separation. *Applied Physics Letters*, 74(14):2084–2086, 1999.

[35] J. Park, A. N. Pasupathy, J. I. Goldsmith, C. Chang, Y. Yaish, J. R. Petta, M. Rinkoski, J. P. Sethna, H. D. Abruna, P.L. McEuen, and D. C. Ralph. Coulomb blockade and the kondo effect in single-atom transistors. *Nature*, 417:722–725, 2002.

[36] S. Kubatkin, A. Danilov, M. Hjort, J. Cornil, J. Brédas, N. Stuhr-Hansen, P. Hedegård, and T. Bjørnholm. Single-electron transistor of a single organic molecule with access to several redox states. *Nature*, 425:698–701, 2003.

[37] A. Notargiacomo, V. Foglietti, E. Cianci, G. Capellini, M. Adami, P. Faraci, F. Evangelisti, and C. Nicolini. Atomic force microscopy lithography as a nanodevice development technique. *Nanotechnology*, 10(4):458, 1999.

[38] L. Qin, S. Park, L. Huang, and C. A. Mirkin. On-wire lithography. *Science*, 309(5731):113–115, 2005.

[39] A. Hatzor and P. S. Weiss. Molecular rulers for scaling down nanostructures. *Science*, 291:1019–1020, 2001.

[40] P. Pourhossein and R. C. Chiechi. Directly addressable sub-3 nm gold nanogaps fabricated by nanoskiving using self-assembled monolayers as templates. *ACS Nano*, 6(6):5566–5573, 2012.

[41] J. Moreland and J. W. Ekin. Electron tunneling experiments using nb-sn break junctions. *J. Appl. Phys.*, 58(10):3888–3895, 1985.

[42] C. J. Muller, B. J. Vleeming, M. A. Reed, J. J. S. Lamba, R. Hara, L. II. Jones, and J. M. Tour. Atomic probes: a search for conduction through a single molecule. *Nanotechnology*, 7(4):409, 1996.

[43] J. M. Krans, C. J. Muller, I. K. Yanson, Th. C. M. Govaert, R. Hesper, and J. M. van Ruitenbeek. One-atom point contacts. *Phys. Rev. B*, 48:14721–14724, Nov 1993.

[44] J.M. Van Ruitenbeek, A. Alvarez, I. Pineyro, C. Grahmann, P. Joyez, M.H. Devoret, D. Esteve, and C. Urbina. Adjustable nanofabricated atomic size contacts. *Review of Scientific Instruments*, 67(1):108–111, 1996.

[45] J. M. Krans and J. M. van Ruitenbeek. Subquantum conductance steps in atom-sized contacts of the semimetal sb. *Phys. Rev. B*, 50:17659–17661, Dec 1994.

[46] C. J. Muller, J. M. van Ruitenbeek, and L. J. de Jongh. Conductance and supercurrent discontinuities in atomic-scale metallic constrictions of variable width. *Phys. Rev. Lett.*, 69:140–143, Jul 1992.

[47] I. K. Yanson, V. V. Fisun, R. Hesper, A. V. Khotkevich, J. M. Krans, J. A. Mydosh, and J. M. van Ruitenbeek. Size dependence of kondo scattering in point contacts. *Phys. Rev. Lett.*, 74:302–305, Jan 1995.

[48] N. van der Post, E. T. Peters, I. K. Yanson, and J. M. van Ruitenbeek. Subgap structure as function of the barrier in atom-size superconducting tunnel junctions. *Phys. Rev. Lett.*, 73:2611–2613, Nov 1994.

[49] J. M. Krans, J. M. van Ruitenbeek, V. V. Fisun, I. K. Yanson, and L. J. de Jongh. The signature of conductance quantization in metallic point contacts. *Nature*, 375:767–769, 1995.

[50] A. I. Yanson, G. R. Boolinger, H. E. van den Brom, N. N. Agrait, and J. M. van Ruitenbeek. Formation and manipulation of a metallic wire of single gold atoms. *Nature*, 395:783, 1998.

[51] C. Zhou, C. J. Muller, M. R. Deshpande, J. W. Sleight, and M.A. Reed. Microfabrication of a mechanically controllable break junction in silicon. *Applied Physics Letters*, 67(8):1160–1162, 1995.

[52] H.B Weber, J. Reichert, F. Weigend, R. Ochs, D. Beckmann, M. Mayor, R. Ahlrichs, and H. v. Löhneysen. Electronic transport through single conjugated molecules. *Chem. Phys*, 281(2 - 3):113 – 125, 2002.

[53] J. Reichert, H. B. Weber, M. Mayor, and H. v. Löhneysen. Low-temperature conductance measurements on single molecules. *Appl. Phys. Lett.*, 82(23):4137–4139, 2003.

[54] D. Djukic and J. M. van Ruitenbeek. Shot noise measurements on a single molecule. *Nano Letters*, 6(4):789–793, 2006.

[55] J. Xiang, B. Liu, S.-T. Wu, B. Ren, F.-Z. Yang, B.-W. Mao, Y. L. Chow, and Z.-Q. Tian. A controllable electrochemical fabrication of metallic electrodes with a nanometer/angstrom-sized gap using an electric double layer as feedback. *Angew. Chem. Int. Ed.*, 44(8):1265–1268, 2005.

[56] C. S. Ah, Y. J. Yun, J. S. Lee, H. J. Park, D. H. Ha, and W. S. Yun. Fabrication of integrated nanogap electrodes by surface-catalyzed chemical deposition. *Appl. Phys. Lett.*, 88(13):133116, 2006.

[57] H. Park, A. K. L. Lim, A. P. Alivisatos, J. Park, and P. L. McEuen. Fabrication of metallic electrodes with nanometer separation by electromigration. *Appl. Phys. Lett.*, 75(2):301–303, 1999.

[58] D. R. Strachan, D. E. Smith, D. E. Johnston, T.-H. Park, Michael J. Therien, D. A. Bonnell, and A. T. Johnson. Controlled fabrication of nanogaps in ambient environment for molecular electronics. *Appl. Phys. Lett.*, 86(4):043109, 2005.

[59] A. K. Mahapatro, J. Ying, T. Ren, and D. B. Janes. Electronic transport through ruthenium-based redox-active molecules in metal-molecule-metal nanogap junctions. *Nano Lett.*, 8(8):2131–2136, 2008. PMID: 18582119.

[60] H. B. Heersche, Z. de Groot, J. A. Folk, L. P. Kouwenhoven, H. S. J. van der Zant, A. A. Houck, J. Labaziewicz, and I. L. Chuang. Kondo effect in the presence of magnetic impurities. *Phys. Rev. Lett.*, 96:017205, 2006.

[61] M. Poot, E. Osorio, K. O'Neill, J. M. Thijssen, D. Vanmaekelbergh, C. A. van Walree, L. W. Jenneskens, and H. S. J. van der Zant. Temperature dependence of three-terminal molecular junctions with sulfur end-functionalized tercyclohexylidenes. *Nano Lett.*, 6(5):1031–1035, 2006.

[62] M. E. Anderson, L. P. Tan, H. Tanaka, M. Mihok, H. Lee, M. W. Horn, and P. S. Weiss. Advances in nanolithography using molecular rulers. *J. Vac. Sci. Technol. B*, 21(6):3116–3119, 2003.

[63] R. Negishi, T. Hasegawa, K. Terabe, M. Aono, T. Ebihara, H. Tanaka, and T. Ogawa. Fabrication of nanoscale gaps using a combination of self-assembled molecular and electron beam lithographic techniques. *Appl. Phys. Lett.*, 88(22):223111, 2006.

[64] L. Qin, J. Jang, L. Huang, and C. A. Mirkin. Sub-5-nm gaps prepared by on-wire lithography: Correlating gap size with electrical transport. *Small*, 3(1):86–90, 2007.

[65] D. J. Lipomi, R. V. Martinez, and G. M. Whitesides. Use of thin sectioning (nanoskiving) to fabricate nanostructures for electronic and optical applications. *Angew. Chem. Int. Ed.*, 50(37):8566–8583, 2011.

[66] J. Hill. *The Construction of Timber*. Imperial Academy, London, 1770.

[67] D..C. Pease and K. R. Porter. Electron microscopy and ultramicrotomy. *J. Cell Biol*, 91:287s, 1981.

[68] T.F. Malis and D. Steele. Ultramicrotomy for materials science. *Mater. Res. Soc. Symp. Proc.*, 199:3, 1990.

[69] Q. Xu, R. M. Rioux, M. D. Dickey, and G. M. Whitesides. Nanoskiving: A new method to produce arrays of nanostructures. *Acc. Chem. Res.*, 41(12):1566–1577, 2008.

[70] P. Peumans, A. Yakimov, and S. R. Forrest. Small molecular weight organic thin-film photodetectors and solar cells. *J. Appl. Phys.*, 93(7):3693–3723, 2003.

[71] W. A. Luhman and R. J. Holmes. Investigation of energy transfer in organic photovoltaic cells and impact on exciton diffusion length measurements. *Adv. Funct. Mater.*, 21(4):764–771, 2011.

[72] O. V. Mikhnenko, F. Cordella, A. B. Sieval, J. C. Hummelen, P. W. M. Blom, and M. A. Loi. Temperature dependence of exciton diffusion in conjugated polymers. *J. Phys. Chem. B*, 112(37):11601–11604, 2008.

[73] G. E. Moore. Cramming more components onto integrated circuit. *Electronics*, 38:114, 1965.

[74] A. Aviram and M. A. Ratner. Molecular rectifiers. *Chem. Phys. Lett.*, 29(2):277 – 283, 1974.

[75] J. R. Heath and M. A. Ratner. Molecular electronics. *Phys. Today*, 56:43, 2003.

Chapter 2

Nanoskiving: Method and Materials

2.1 Introduction

Nanoskiving is a simple and convenient edge lithography technique for fabricating nanostructures by sectioning embedded films (typically metals or polymers) using an ultramicrotome.[1] Figure 2.1 outlines the procedure for fabricating nanostructures by nanoskiving.[2] Preparing the sample (or 'block') for sectioning by microtome is a key aspect of nanoskiving. Typically, the fabrication process begins with a substrate consisting of a cured embedding resin that can either be flat or have topography (defined by soft lithography,[3–5] for example). Thin films can be deposited onto this substrate with precise thickness by a number of methods (e.g., spin coating, physical vapor deposition or sputtering). The entire substrate is then embedded in additional resin. Prior to sectioning, the face of the block is trimmed manually into a trapezoidal shape ($\sim 1 - 1.5$ mm^2) using a razor blade. Sectioning the resulting block with an ultramicro-

∗ Parts of this chapter have been published in: Robin L. Mays, Parias Pourhossein, Dhanalekshmi Savithri, Jan Genzer, Ryan C. Chiechi and Michael D. Dickey, J. Mater. Chem. C, 2013, 1, 121-130. I would like to thank Robin L. Mays, Dhanalekshmi Savithri, Jan Genzer and Michael D. Dickey for the fruitful collaboration.

tome equipped with a diamond knife attached to a boat filled with water yields thin polymer slabs that float on the surface of the water and that can be transferred to a substrate directly (e.g., by dipping a substrate in the boat) or via a drop of water. Structures formed by nanoskiving are often composed of gold because it is easy to deposit, does not oxidize in air, and is soft relative to most metals, which facilitates sectioning and results in stable, electrically continuous nanostructures. Exposure to oxygen (or air) plasma selectively removes the embedding resin and generates freestanding nanostructures. The topography of the original substrate, the thickness of the deposited film, and the thickness of the sections cut by the ultramicrotome (as thin as 10 nm) determine the dimensions of these nanostructures. The ability to control the dimensions of the nanostructures without the use of sophisticated lithographic tools and without the use of a clean room makes this technique very attractive for rapid prototyping and nanostructures can be fabricated from materials that are not compatible with conventional photolithography/etching. Nanoskiving produces hundreds of thousands of identical sections from a single block and the thin polymeric sections can be positioned onto various substrates. [6]

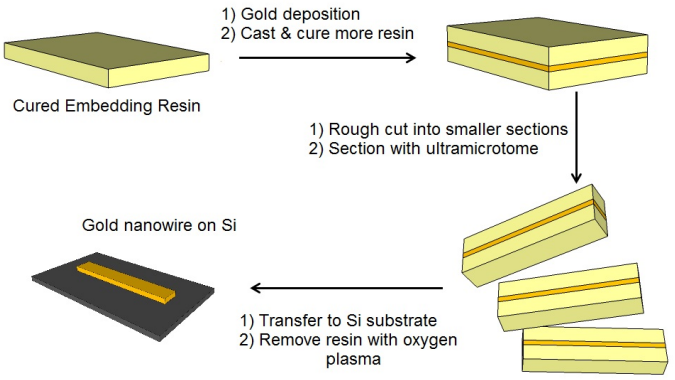

Figure 2.1: A schematic of the fabrication of a gold nanowire by nanoskiving. Reproduced with permission from Ref.[2].

Biologists and material scientists use ultramicrotomy conventionally to pro-

duce thin ($\sim$ 100 nm thick) sections of cells, tissues, and materials for analysis by electron microscopy.[7,8] Embedding is done by the infiltration of the sample with a liquid embedding medium that polymerizes to produce a solid block that can be handled and sectioned using a microtome. An embedding medium for conventional biological samples should have the following properties: commercial availability, uniformity from one batch to another, solubility in dehydrating agents, low viscosity as a monomer for ease of handling, uniform polymerization, minimal volume change upon polymerization to avoid distortion of the sample, and ease of sectioning and stability in an electron beam.[7] Embedding resins for nanoskiving do not require solubility in dehydrating agents or stability in an electron beam, but should be able to be etched by oxygen plasma.

None of the embedding media developed so far possesses all the desired qualities for microtomy, although several commercial epoxies (*e.g.*, Araldite and Epofix) work very well for most microtome applications.[1,9] Epoxies are generally cross-linked and possess relatively large elastic moduli (Youngs modulus, E $>$ 1500 MPa), which is well suited for sectioning at room temperature.[10] Hardening of epoxies occurs via an addition reaction that results in very little change of volume. Epoxy resins also adhere well to many materials with polar surfaces (*i.e.*, surface oxides) by hydrogen bonding.[11]

2.2 The ultramicrotome and process of sectioning

As it is shown in Figure 2.2, an ultramicrotome is eqquiped with different parts including a stereomicroscope, sample (or block) arm that holds the block, and a movable stage that the knife is mounted on. The controlled mechanical approach of the sample arm to the edge of the knife is the basis of ultramicrotomy. Each time that the sample arm touches the edge of the knife, the resulting section or ribbon of sections floats onto the surface of the water in the boat. Two general mechanisms are proposed in the literature for the process of sectioning: true sectioning and crack initiation and propagation.[9] True sectioning involves shear

lamellae. This mechanism dominates in metals and alloys.[12] In brittle materials *e.g.*, minerals and ceramics, crack initiation and propagation dominates.[12] In sections of high-strength steel both mechanisms can exist.[12]

2.3 Fabrication of nanostructures from different materials

Nanowires are the simplest nanostructures that can be fabricated using nanoskiving. Nanowires with rectangular cross sections can be obtained from sectioning a metallic, ceramic, semiconducting, polymeric thin films. Nanowires of gold, aluminum, silver, copper, lead, bismuth, palladium, platinum, nickel, germanium, silicon oxide, all conducting and semiconducting polymers and lead sulfide nanocrystals can be fabricated.[9] Figure 2.3 summarizes the materials that can be sectioned using nanoskiving and makes predictions for the class of materials that have not been sectioned yet. In this figure term 'intact' means that the material can be sectioned without fragmantation to yield unbroken nanowires. 'Fragmentation' applies when nanowires are broken into segments of < 10 μm. 'Borderline' is used when the rate of fragmentation of the material depends on the method of deposition, the size and geometry of the structure and the orientation of the thin film with respect to sectioning. Designations 'predicted to be fragmented' and 'predicted to be intact' are used based on the probable mechanical properties of a thin film of the material assuming that the film can be formed and sectioned in an inert atmosphere.

Photolithography and soft lithography can be used to pattern the films prior to sectioning.[1] Sectioning the patterned films result in more complex nanostructures than nanowires and that are challenging to fabricate using conventional techniques (*e.g.*, photo- or e-beam lithography and focused ion beam).[3,4,13] Figure 2.4 shows gold nanostructures with different geometries that have been fabricated using nanoskiving. These nanostructers can have electronic or optical applications.[6,14–20] For instance, nanostructures in 2.4A have optical properties whereas nanostructures in 2.4B are electrically addressable.

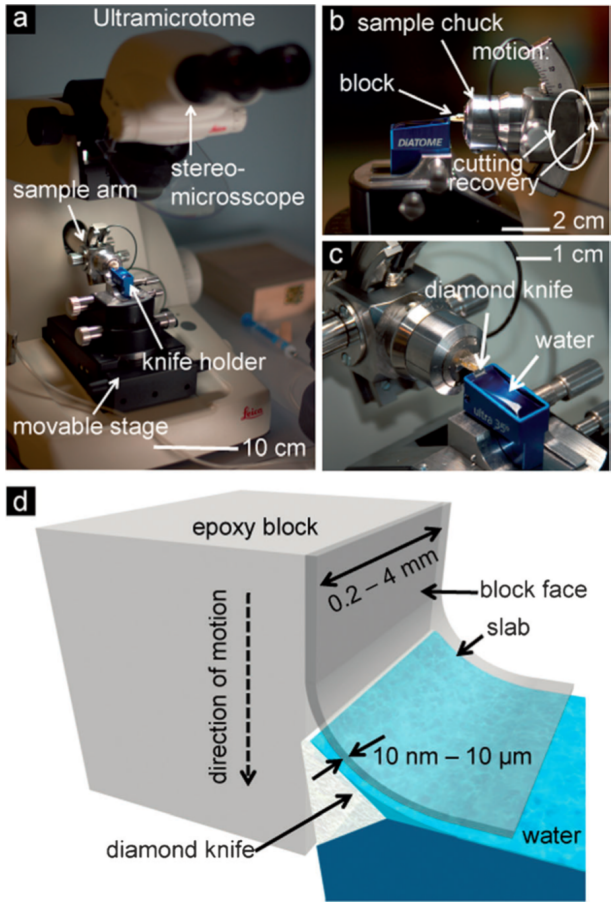

Figure 2.2: A diagram of an ultramicrotome and how it is used in nanoskving. The epoxy block containing the thin-film structures is mounted on the articulating arm, which holds the block above the diamond knife. The knife is wetted on one side by a boat of water, onto which the sections float as the block is pushed against the edge of the knife. Reproduced with permission from Ref. [23].

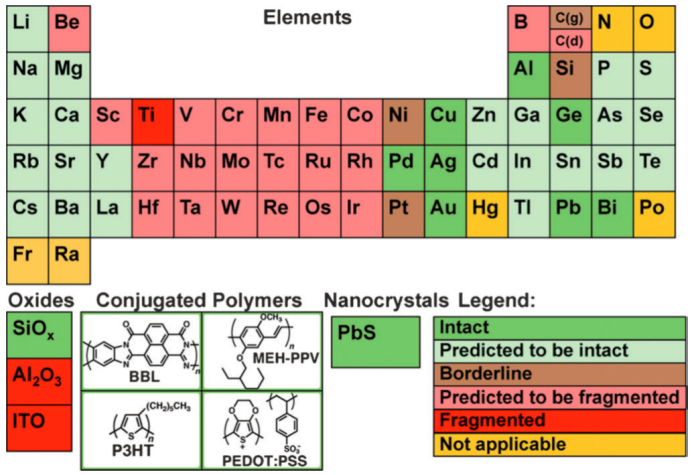

Figure 2.3: Summary of findings and predictions regarding the abilities of elements, oxides, polymers, and nanocrystals to form nanowires by sectioning thin films. Reproduced with permission from Ref. [9].

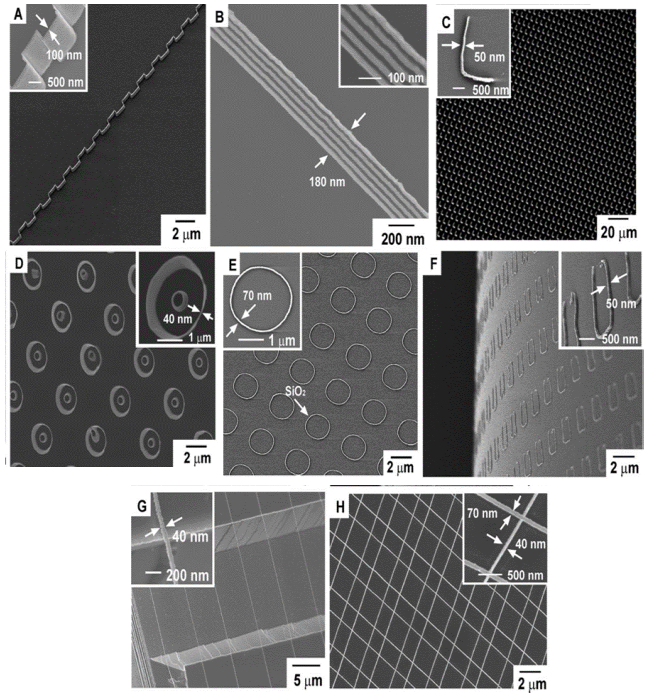

Figure 2.4: (A) SEM image of 100-nm wide, $1\ \mu\mathrm{m}$ high 'step-shaped' nanostructures fabricated by nanoskiving a metal-coated epoxy substrate prepatterned with $1\ \mu\mathrm{m}$ wide lines with $1\ \mu\mathrm{m}$ spacing.[21] (B) SEM image of parallel gold nanowires with 20-nm spacing by nanoskiving, a flat epoxy substrate coated with a multilayer, composite Au/SiO_2 film, followed by complete etching of the SiO_2 spacing layers using reactive ionetching.[21] (C) Dark-field optical microscopy image of 'L-shaped' nanostructures patterned over a ~ 3- mm^2 area by nanoskiving in a direction parallel to the patterned substrate.[5] (D) SEM image of double 'loop-shaped' gold nanostructures.[22] (E) SEM image of loop-shaped SiO_2 nanostructures on a $SiO_2/Si(100)$ substrate by using gold loop-shaped nanostructures as a physical mask during reactive ion etching with CF_4. (F) SEM image of an array of 'U-shaped' gold nanostructures positioned on the curved surface of a glass rod.[21] (G) SEM image of parallel gold nanowires draped over $20\ \mu\mathrm{m}$ wide 'truncated-V'-shaped trenches, etched in a Si(100) surface.[21] (H) Crossbar nanostructures fabricated by the orthogonal stacking of two epoxy slabs containing arrays of gold nanowires on top of each other. The insets are high-magnification SEM images of the nanostructures. Reproduced with permission from Ref.[1]

.

2.4 Embedding resins

One of the essential steps in nanoskiving is embedding the films in resins to support the resulting structures. We have developed and evaluated new thiol-containing embedding resins specifically for nanoskiving gold structures and compared these polymeric materials to conventional, epoxy-based embedding resins. The conventional polymers used for embedding films are typically liquid pre-polymers that cure with minimal shrinkage to produce a hard bulk polymer that facilitates handling and that is necessary for sectioning. Adhesion between the sample (*i.e.*, typically a metal film in the case of nanoskiving) and the polymer resin is important in order to assure that the final composite does not disintegrate during sectioning. Epoxies are popular embedding resins for microtomy because they are hard, shrink minimally during curing, and adhere conformally to most materials. Epoxies, however, do not adhere well to gold (or other smooth, metallic structures), which is often used for nanoskiving because gold is easy to deposit and section, is not brittle, and does not oxidize readily. The two most commonly used, commercially available epoxides are Araldite and Epofix. Araldite is advantageous because it is easy to trim (a necessary first step in nanoskiving) and forms mechanically stable sections even at very thin (< 100 nm) thicknesses that are common in nanoskiving. However, Araldite is a three-part epoxy with a lengthy curing time (~ 48 hours for optimal mechanical properties) and it is optimized for soft materials (*e.g.*, biological specimens). Epofix is a two-part, thermally-curable epoxy that is designed specifically for sectioning hard materials, but it is considerably harder than Araldite, which leads to unstable sections and an increased susceptibility to chattering, where the diamond knife skips across the surface of the epoxy block leading to non-uniform thicknesses in the resulting sections. Neither Araldite nor Epofix adhere particularly well to smooth metal surfaces, in particular to gold.

We hypothesized that incorporating monomers with thiol functionality into the embedding polymer would improve the adhesion between gold and the poly-

mer during sectioning by introducing chemisorption via the spontaneous formation of gold-thiolate bonds. We evaluated photocurable thiol-ene polymers because they possess properties that are well suited for microtomy, *i.e.*, : (1) their mechanical properties can be tailored by the choice of monomers, (2) they have low viscosity before curing, which facilitates embedding, (3) they photocure quickly on demand to deep thicknesses, which allows for rapid prototyping, and (4) they cure by step-growth polymerization, which leads to low shrinkage compared to most free-radical polymerizations. We also studied a thiol-epoxy formulation, which has many of the same desirable attributes of the epoxy networks, but which includes thiol functionality. We fabricated gold nanowires of various dimensions and examined the resulting sections by optical microscopy, measured the conductance of the nanowires, and compared the etching rates by plasma oxidation to demonstrate that the thiol-containing embedding resins are superior to conventional epoxy resins for nanoskiving. Most nanoskiving work to date relied on Araldite and Epofix epoxy resins, which offer convenience at the expense of performance.[8,23] Unfortunately, epoxy-based embedding resins exhibit poor adhesion to gold, which can lead to catastrophic delamination of the nanostructures from the embedding resin during sectioning or during preparation of the sample blocks (Figure 2.6). Sectioning is a mechanical cutting process and relies on the smooth and continuous advance of the block passing the edge of the knife. Delamination significantly diminishes the quality of the sectioning process and should be mitigated when possible. For applications in which the epoxy matrix is used to electrically isolate the top face of gold nanostructures, delamination is catastrophic.[24] Delamination between the epoxy and gold has been minimized–but not eliminated–previously by careful handling and ensuring that the epoxy completely encapsulates the gold film on all sides.[1]

We sought to evaluate polymeric embedding materials that possess the important material characteristics required for microtoming, while enhancing the binding to gold and increasing the rate of curing with minimal shrinkage. We chose polymers that contained thiols because they form strong bonds with many

metals including gold, silver, palladium, copper, and many others.[13] Although in some circumstances it may be possible to improve adhesion between metal and the embedding resin by modifying the gold films with self-assembled monolayers (SAMs), we have had limited success with epoxide and carboxylate-terminated SAMs with both Epofix and Araldite. Thus, we sought to develop a simpler and more universally useful resin that contained thiols so that no additional steps would be required to improve adhesion to gold. We evaluated the critical properties of several thiol-containing resins within the context of microtomy and demonstrate the utility of these materials in nanoskiving.

2.4.1 Experimental Design

Table 2.1 summarizes the materials studied as embedding resins. Epofix and Araldite serve as commercial benchmarks against which we compare the thiol-containing resins.

Table 2.1: Materials studied as embedding resins for nanoskiving

Material	**Polymer Type**
Epofix	Epoxy
Araldite 502	Epoxy
NOA 63	Thiol-Ester
NOA 81	Thiol-Ester
PETMP/TATATO (1:1)	Thiol-ene
PETMP/TATATO (3:4)	Thiol-ene
PETMP/Epofix	Thiol-Epoxy

Thiol-esters: We evaluated two commercially available, photocurable, mercapto-ester systems: NOA 63 and NOA 81. Norland Products sells many photocurable adhesives, but we selected these polymers because they possess elastic moduli similar to that of conventional epoxy resins. The manufacturer does not provide chemical information other than to call these products mercapto-esters and we

use thiol-ester to be consistent with our other notations. These resins are also sold in smaller quantities than Araldite and Epofix, as they are optical adhesives that are optimized for transparency, not embedding.

Thiol-enes: The photopolymerization of mixtures of thiols and alkenes is an efficient method for the rapid production of crosslinked polymer networks.[25] Thiol-ene photopolymerization proceeds rapidly by a step-growth free-radical chain transfer reaction.[25] We formulated thiol-ene resins using commercially available monomers, pentaerythritol tetra(3-mercaptopropionate) and triallyl-1,3,5-triazine-2,4,6-trione (referred to as PETMP and TATATO, respectively). Figure 2.5 depicts the chemical structures of the monomers. PETMP/TATATO has been studied as potential dental restorative material, which also has the requirements of minimal shrinkage and hardness.[26] The properties of this formulation can be tuned by varying the composition and stoichiometry of the reacting monomers. We evaluated 3:4 and 1:1 molar compositions of PETMP/TATATO. The 3:4 molar mixtures have stoichiometric amounts of functional groups, whereas 1:1 mixture has an excess of thiol functional groups but comprises stoichiometric amounts of monomer molecules.

Thiol-epoxies: We also evaluated a thiol-epoxy catalyzed by an amine, which involves a multistep reaction resulting in the opening of the epoxide ring followed by the addition of a thiol anion.[27] The motivation for using these materials is driven by the low shrinkage and mechanical properties enabled by epoxies and by the ease with which a commercial thiol (PETMP) can be added to a commercial epoxy embedding resin (Epofix).[28] These materials are cured thermally at room temperature using the chemistry developed for conventional resins (*i.e.*, using an amine [triethylenetetramine] initiator).

Benchmark embedding resins: We selected two conventional epoxy-based resins, Araldite 502 and Epofix, as benchmarks to compare the thiol containing resins. Both embedding resins have been used previously for nanoskiving.[5,24] Araldite cures at 60 °C over a 24-48 h period, whereas Epofix cures at room temperature over 8-10 h. The main difference between these two epoxies is

the nature of the curing agent that adds across the epoxy groups of the resin molecules to provide cross linking. In Araldite, the curing agent is an anhydride, whereas in Epofix, it is an aliphatic amine.

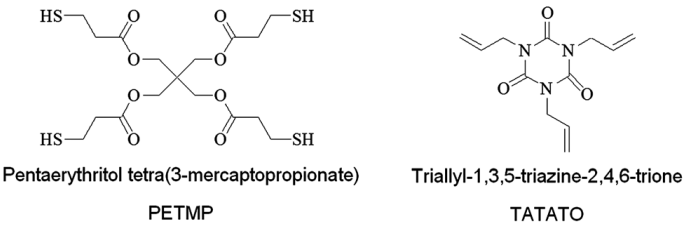

Figure 2.5: Chemical structures of the thiol and ene monomers.

2.4.2 Characterization

We sought to measure the properties and compare the performance of the new resins to the benchmark resins. Previous studies have shown that stress-strain tensile measurements provide the best metric for predicting a priori whether a material will be a satisfactory embedding resin.[10] Ideal materials are hard enough to prevent sample deformation (*i.e.*, they possess a large modulus), but are not too brittle so as to prevent cracking. We therefore use stress-strain behavior as a primary metric for predicting ideal embedding resins. Of course, the ultimate metric for evaluating new resins is their performance during nanoskiving.

There are also some additional fundamental properties of polymer networks that help predict whether a resin will perform well; these include glass transition temperature (T_g), shrinkage, and adhesion to gold.[10] Thermomechanical analysis provides insight into the glass transition temperature of the polymer networks. The T_g is a physical property of polymers that can indicate the best temperature settings needed for microtomy. As a general rule, polymers that are hard ($T_g >$ room temperature) can be sectioned at room temperature while soft materials ($T_g <$ room temperature) need to be sectioned at lower tem-

peratures.[10] Shrinkage of the resin during preparation of the block should be minimized to avoid sample distortion and adhesion of the resin to gold during sectioning should be maximized to avoid delamination.

We prepared the specimen samples for ultramicrotome sectioning by first depositing a thin film of gold (thickness 50 or 100 nm) on a silicon wafer by e-beam evaporation. We spin coated (or drop cast for Epofix) the pre-polymer on the gold surface and cured it. The gold-film adhered to the polymer as it was peeled from the Si surface and cut into small strips of (5-7 mm long, 1 mm wide). Embedding the gold strips in more pre-polymer formulation in a mold produced the block. I used a Leica UC-6 Ultramicrotome to prepare sections from the blocks containing gold films with thicknesses of 50, 100, 150, and 200 nm using a 2 mm 35° Diatome diamond knife at 1 mm/s except for the 50 nm sections which were sectioned at 0.8 mm/s. The sample blocks for each polymer system contained an embedded film of gold (50 or 100 nm-thick). Prior to sectioning with the ultramicrotome, I trimmed these specimens to a rough trapezoid shape (∼1 x 1 mm) as shown in Figure 2.6. In some cases, the brittle nature of Epofix, combined with its poor adhesion to gold, caused the polymer to delaminate and break away in chips, requiring the block to be rough-cut and re-trimmed. An example of this type of failure is shown in Figure 2.6A. The blocks formed from 1:1 PETMP/TATATO (Figure 2.6B) represent the other extreme; excellent adhesion, but polymer blocks that were too soft to be sectioned (Figure 2.7).

I successfully sectioned blocks of four polymers; Araldite, Epofix, NOA 81, and 3:4 PETMP/TATATO. The mechanical properties of the blocks formed from the other embedding resins precluded trimming and sectioning, primarily because they were too soft and deformed during the trimming process (Figure 2.7). Optical micrographs of the resulting sections of thicknesses of 50, 100, 150, and 200 nm are shown in Figure 2.8. With the exception of NOA 81, I produced sections down to 40 nm (not shown) before they became too fragile to handle, though the technical limit of the ultramicrotome is 15 nm. Although the resolution of these micrographs (250X magnification) is not sufficient to image

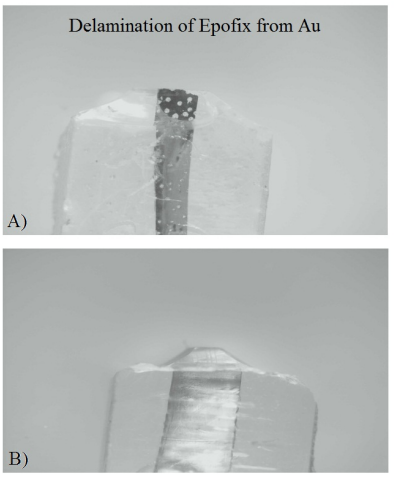

Figure 2.6: Photographs of sample blocks prepared by cutting polymer with a razor blade. A) Epofix, which does not contain thiol, delaminates from gold. B) PETMP/TATATO (1:1), which does contain thiol, has good adhesion to gold. Reproduced with permission from Ref.[2].

the gold structures directly, which are 50-100 nm thick, the mismatch in the indices of refraction between the embedding resins and the gold appears as a dark line, which is indicated with vertical arrows in the left side of each image in Figure 2.8. The numbers in the lower-right corner of each image indicate the thickness at which the ultramicrotome was set during sectioning. This set-thickness can be verified by the color of the sections, which results from thickness-dependent interference; 50 nm appears grey, 100 nm turquoise, 150 nm blue, and 200 nm orange-brown. The NOA 81 sections all appear blue-turquoise, however, indicating that the actual thickness of the sections deviated from the set thickness. This deviation is the result of the mechanical properties of the NOA 81 which is likely too compressible and produces too much friction against the advancing edge of the diamond knife. The result is uneven sections, which is the case in Figure 2.8 (lower-left) where only a band of orange-brown (*i.e.*, 200 nm-thick resin) is apparent in the 200 nm section. The average thickness of these

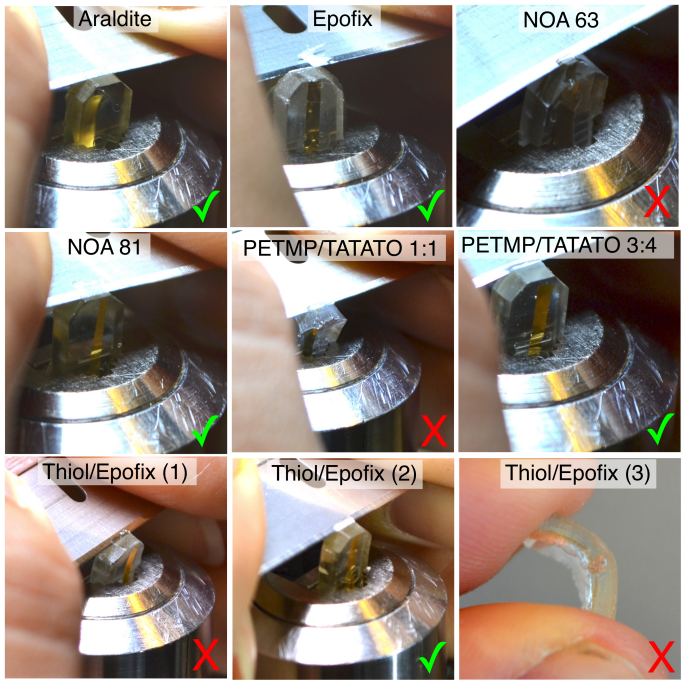

Figure 2.7: Photographs of the blocks of the different embedding resins being trimmed with a razor blade prior to sectioning. The photographs marked with a red X indicate blocks that could not be trimmed because the polymers were too soft, causing the block to deform, and/or the stress induced by the razor blade caused macroscopic adhesive failure–*i.e.*, the block fell apart. The photographs marked with a green $\surd$ indicate blocks that could be trimmed, but not necessarily sectioned. Three different blocks of thiol/Epofix are pictured, highlighting the block-to-block variability; one block (bottom-left) was too soft to be trimmed, one (bottom-center) could be trimmed (but was not sectioned), and one (bottom-right) was too flexible to be mounted for trimming. Reproduced with permission from Ref.[2].

sections also alternates as the block advances by the set-thickness before each stroke, but differing thicknesses of epoxy are skived. The result is that NOA 81 is unsuitable for forming gold nanowires by nanoskiving at any thickness.

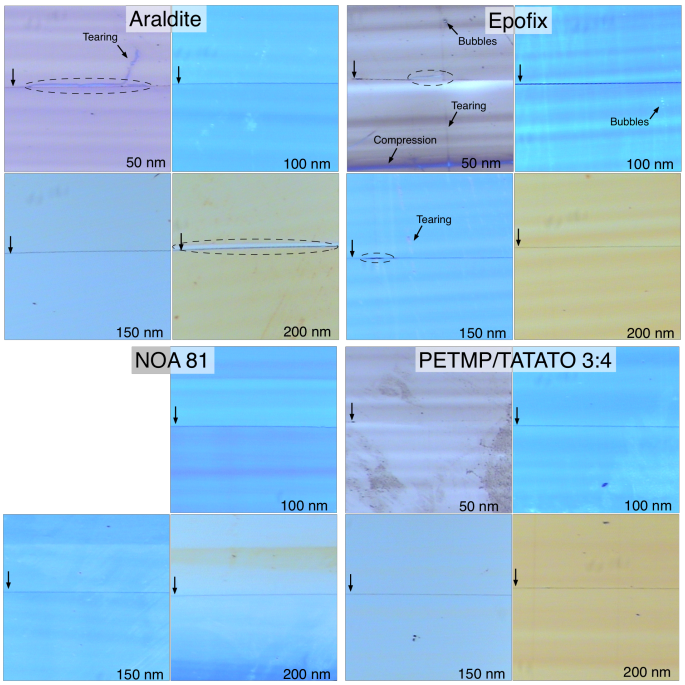

Figure 2.8: Optical micrographs (250X) of sections of the four embedding resins that could be nanoskived. The vertical arrows at the left of each image indicate the position of the gold nanowire and the dashed ovals indicate delamination of the resin from the gold. The thickness of each section is indicated in the lower left corner, which is confirmed by the color of the section resulting from thickness-dependent interference. The horizontal bands present in some images are the result of chattering, the severity of which depends on the mechanical properties of each resin. Sections of NOA 81 < 50 nm disintegrated upon formation and chattering was severe enough to preclude accurate section-thicknesses, which is evident from the predominantly blue color in the 200 nm section. Tearing, bubbles, and compression artifacts were predominant in the Epofix sections, while Araldite exhibited the most severe delamination. Reproduced with permission from Ref.[2].

The most obvious feature of the Araldite (Figure 2.8; top-left) sections is delamination, which is indicated with dashed ovals and appears as almost complete adhesive failure in the 50 and 200 nm sections. While the degree of delamination varies between sections, the images shown in Figure 2.8 are representative (of all of the polymers). Aside from delamination, Araldite produces–unsurprisingly–very high quality sections with minimal chattering, which appears as horizontal bands of color. These bands of color are the result of the knife skipping (chattering) as it passes through the polymer and are the result of the compressibility of the polymer and the amount of friction generated at the trailing edge of the knife. Chattering should not be confused with ambient vibrations, which can be controlled externally (*e.g.*, with a dampening table). From these results we conclude that Araldite, while functional, is not an ideal embedding resin for gold structures.

Epofix, which is designed for ultramicrotomy on hard materials, performs very poorly at thicknesses below 100 nm. The 50 nm-thick section pictured in Figure 2.8 (top-right) is rife with artifacts, the most severe of which is the compression visible in the lower part of the section. Also present are bubbles, which form when the two parts of the pre-polymer are mixed and which cannot be removed completely before the resin cures. There is also significant tearing, which is usually the result of a nick in the diamond knife, but can also be caused by dust particles. In this case, we ascribe the tearing to a minor defect in the knife (which is very common) that is only apparent in the 50 nm-thick sections of Epofix because of the brittle nature of that resin. In addition to being difficult to trim (Figure 2.6a), this brittleness also leads to sections that craze and are predisposed to separating into pieces in the boat (not shown) as a result of tearing and compression artifacts. The most prominent artifact in the Epofix sections, surprisingly, is not delamination–which is visible to some extent in 50 and 150 nm-thick sections–but chattering, which is evident as prominent bands of color in all of the sections. While chattering is not necessarily detrimental to the formation of nanowires of gold, which are cut parallel to the edge of the

knife, more complex metallic structures will not have a uniform height/thickness when sectioned using Epofix.

Though the measurements of the mechanical properties of the thiol/Epofix mixture suggest that it is ideal for nanoskiving, I found the mixture impossible to trim, which is directly contradicted by the tensile test and the elastic modulus, which are ideal. This inconsistency arises because the addition of PETMP to Epofix initiates an exothermic polymerization that precludes efficient mixing on the microscale. Thus, while the relatively large widgets used for mechanical testing show ideal properties, the relatively small blocks (and extremely small slabs formed during nanoskiving) are sensitive to small, localized variation in mechanical properties arising from the inefficient mixing. This variation manifested itself as block-to-block inconsistencies; some of the blocks could, in fact, be trimmed (Figure 2.7) but I did not continue the nanoskiving test because of the irreproducibility of the blocks.

The only embedding resin that produced sections (nearly) free of artifacts and with no delamination at all thicknesses was 3:4 PETMP/TATATO. The only visible artifacts are smudges, which are the most pronounced in the 50 nm-thick sections shown in Figure 2.8 (bottom-right). It is not clear what causes these smudges, but they are not tears, bubbles, compression artifacts or the result of chattering nor do they appear to affect the nanoskiving process negatively. The 3:4 PETMP/TATATO sections were the easiest to trim and section, show almost no chattering, and form very stable sections even at thicknesses below 50 nm. Interestingly, the dark line indicating the position of the gold is barely discernable in the 50 nm-thick sections, which we ascribe to the small dimension of the gold wire (50 x 50 nm) and the excellent adhesion of the polymer to gold. It is clearly visible and free of any signs of delamination in the 100, 150, and 200 nm-thick sections.

To verify that the embedding resins do not interfere with the electrical properties of the gold nanowires, I measured I/V curves for 100 nm-thick sections of Araldite, Epofix, NOA 81, and 3:4 PETMP/TATATO. I measured 50 nm-thick

gold nanowires (∼1 mm x 50 nm x 100 nm) by painting small (∼ 1 mm^2) pads of silver paste at either end of each nanowire and contacting them in a home-built probe station. The resulting data are plotted in Figure 2.9 and show ohmic conduction for all four nanowires, indicating that none of the embedding resins affected the electrical properties of the gold nanowires. The magnitude of the current (∼ 10^{-4} A) is consistent with previous measurements on gold nanowires of similar dimensions fabricated using nanoskiving.[29] The slightly lower conductivities of NOA 81 and Araldite are the result of differences in the lengths of the nanowires. From these measurements and the optical micrographs in Figure 2.8, we can conclude that all four resins are capable of producing electrically continuous gold nanowires; however, 3:4 PETMP/TATATO yields the least delamination and, qualitatively, the highest quality sectioning and general ease of handling the sections. Moreover, 3:4 PETMP/TATATO is photo-curable in a fraction of the time of the thermally-curable Araldite and Epofix epoxies. While delamination is, in this case, not a critical parameter–it leads to some deformation of the wires, but not catastrophic failure–it is of critical importance for delicate and/or complex metallic features and for applications that leverage the insulation that the polymer slab provides. For instance, nanowires fabricated using 3:4 PETMP/TATATO can be contacted using silver paste with no leakage (hence electrical shorts) to the supporting substrate, and the top face of the wire can be selectively functionalized with, for example, a self-assembled monolayer (SAM) or addressed by a fluid for sensing applications.

For applications in which it is desirable to remove the polymer slab, leaving only the metallic nanostructure–in our case nanowires–on the substrate, we compared the time required to ash 100 nm-thick slabs of each of the four resins completely using oxygen plasma. I exposed each to 1 mbar of pure oxygen plasma until there were no traces of polymer remaining by optical microscopy. These results are summarized in Table 2.2 and show that the thiol-containing polymers (3:4 PETMP/TATATO and NOA 81) take considerably longer (30 min) to ash than do the epoxies, and that Araldite ashes in about one third the

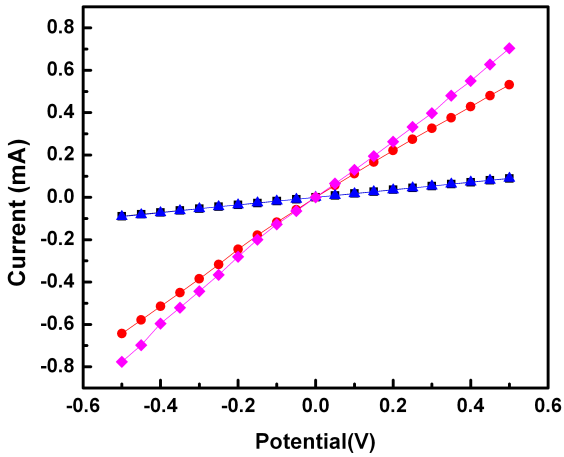

Figure 2.9: Plots of current versus potential for 50 nm-thick gold nanowires fabricated using 100 nm-thick sections of Araldite (black squares), NOA 81 (blue triangles), Epofix (red squares), and 3:4 PETMP/TATATO (pink diamonds). Each trace is an average of four sections. All four wires exhibit ohmic I/V characteristics indicating that the wires are electrically continuous. The slightly lower conductivities of the wires in NOA 81 and Araldite are the result of differences in the lengths of the wires. Reproduced with permission from Ref. [2].

time (5 min) of Epofix (15 min). We expect these times to scale according to the power output of the plasma oxidizer; we used a relatively low power plasma cleaner.

Table 2.2: Time required to ash 100 nm-thick sections completely with oxygen plasma (1 mbar)

Material	**Oxygen Plasma Exposure (min)**
Epofix	15
Araldite 502	5
NOA 81	30
PETMP/TATATO (3:4)	30

2.5 Conclusions

We developed new embedding resins for nanoskiving that have similar properties to conventional epoxy-based embedding resins, but that are photocurable and have improved adhesion to gold because of the inclusion of thiol functional groups. I compared these thiol-containing resins to two conventional, benchmark epoxy-based resins (Araldite and Epofix). Of the thiol-containing materials in my study, the 3:4 PETMP/TATATO appears to have the most promising properties for nanoskiving. It cures quickly, possesses mechanical properties similar to commercial resins, adheres well to gold, and produces high-quality microtome sections. A drawback of the 3:4 PETMP/TATATO system is that it shrinks slightly more than conventional epoxies, which may result in some deformation or stress in delicate samples. We observed no evidence of this being an issue in our samples as determined by measuring the electrical properties of the gold nanowires, but it may be an issue for more sensitive geometries (*e.g.*, fragile gold structures that might deform under stress). For particularly sensitive samples, users may consider exploring techniques from the literature to reduce thiol-ene

shrinkage such as allyl sulfide addition-fragmentation chain transfer.[30,31] The ability to partially cure thiol-enes to produce oligomers prior to embedding provides an additional route to lower the shrinkage. The improved adhesion of the thiol-containing embedding polymers to the metal reduces the occurrence of delamination during sample preparation and microtome sectioning. We anticipate that the enhanced properties offered by thiol-containing systems, such as reduced cure time, excellent adhesion to gold, and sufficient hardness, will be useful to those that use nanoskiving. The use of light to initiate the reaction allows for rapid prototyping, but may also enable better spatial-temporal control of the resin during sample preparation. Nanoskiving of gold nanowires has already proven useful to numerous applications,[23,29] and with this new embedding resin there is increased potential for further use of this unconventional nanofabrication technique in a wider range of areas with more reliable sectioning.

Bibliography

[1] Q. Xu, R. M. Rioux, M. D. Dickey, and G. M. Whitesides. Nanoskiving: A new method to produce arrays of nanostructures. *Acc. Chem. Res.*, 41(12):1566–1577, 2008.

[2] R. L. Mays, P. Pourhossein, D. Savithri, J. Genzer, R. C. Chiechi, and M. D. Dickey. Thiol-containing polymeric embedding materials for nanoskiving. *J. Mater. Chem. C*, 1:121–130, 2013.

[3] B. D. Gates, Q. Xu, J. C. Love, D. B. Wolfe, and G. M. Whitesides. Unconventional nanofabrication. *Annu. Rev. Mater. Res.*, 34(1):339–372, 2004.

[4] B. D. Gates, Q. Xu, M. Stewart, D. Ryan, C. G. Willson, and G. M. Whitesides. New approaches to nanofabrication: Molding, printing, and other techniques. *Chem. Rev.*, 105(4):1171–1196, 2005. PMID: 15826012.

[5] Q. Xu, J. Bao, R. M. Rioux, R. Perez-Castillejos, F. Capasso, and G. M. Whitesides. Fabrication of large-area patterned nanostructures for optical applications by nanoskiving. *Nano Lett.*, 7(9):2800–2805, 2007.

[6] D. J. Lipomi, F. Ilievski, B. J. Wiley, P. B. Deotare, M. Loncčar, and G. M. Whitesides.

Integrated fabrication and magnetic positioning of metallic and polymeric nanowires embedded in thin epoxy slabs. *ACS Nano*, 3(10):3315–3325, 2009.

[7] A. M. Glauert. *Practical Methods in Electron Microscopy.* American Elsevier Publishing Co. Inc, 1974.

[8] H. K Plummer. Reflections on the use of microtomy for materials science specimen preparation. *Microsc. Microanal*, 3:239–260, 1997.

[9] D. J. Lipomi, R. V. Martinez, R. M. Rioux, L. Cademartiri, W. F. Reus, and G. M. Whitesides. Survey of materials for nanoskiving and influence of the cutting process on the nanostructures produced. *ACS Appl. Mater. Interfaces*, 2(9):2503–2514, 2010.

[10] J. D. Acetarin, E. Carlemalm, E. Kellenberger, and W. Villiger. Correlation of some mechanical properties of embedding resins with their behaviour in microtomy. *J. Electron Microsc. Tech.*, 6(1):63–79, 1987.

[11] E. M. Petrie. *Epoxy Adhesive Formulations.* McGraw-Hill, 2005.

[12] T.F. Malis and D. Steele. Ultramicrotomy for materials science. *Mater. Res. Soc. Symp. Proc.*, 199:3, 1990.

[13] J. C. Love, L. A. Estroff, J. K. Kriebel, R. G. Nuzzo, and G. M. Whitesides. Self-assembled monolayers of thiolates on metals as a form of nanotechnology. *Chem. Rev.*, 105(4):1103–1170, 2005.

[14] Q. Xu, B. D. Gates, and G. M. Whitesides. Fabrication of metal structures with nanometer-scale lateral dimensions by sectioning using a microtome. *J. Am. Chem. Soc.*, 126(5):1332–1333, 2004. PMID: 14759178.

[15] M. D. Dickey, D. J. Lipomi, P. J. Bracher, and G. M. Whitesides. Electrically addressable parallel nanowires with 30 nm spacing from micromolding and nanoskiving. *Nano Lett.*, 8(12):4568–4573, 2008.

[16] D. J. Lipomi, R. C. Chiechi, M. D. Dickey, and G. M. Whitesides. Fabrication of conjugated polymer nanowires by edge lithography. *Nano Lett.*, 8(7):2100–2105, 2008. PMID: 18517256.

[17] D. J. Lipomi, R. C. Chiechi, W. F. Reus, and G. M. Whitesides. Laterally ordered bulk heterojunction of conjugated polymers: Nanoskiving a jelly roll. *Adv. Funct. Mater.*, 18(21):3469–3477, 2008.

[18] Q. B. Xu, J. M. Bao, F. Capasso, and G. M. Whitesides. Surface plasmon resonances of free-standing gold nanowires fabricated by nanoskiving. *Angew.Chem*, 118:3713, 2006.

[19] Q. Xu, J. Bao, F. Capasso, and G. M. Whitesides. Surface plasmon resonances of free-standing gold nanowires fabricated by nanoskiving. *Angewandte Chemie International Edition*, 45(22):3631–3635, 2006.

[20] B. J. Wiley, D. J. Lipomi, J. Bao, F. Capasso, and G. M. Whitesides. Fabrication of surface plasmon resonators by nanoskiving single-crystalline gold microplates. *Nano Lett.*, 8(9):3023–3028, 2008. PMID: 18720977.

[21] Q. Xu, R. M. Rioux, and G. M. Whitesides. Fabrication of complex metallic nanostructures by nanoskiving. *ACS Nano*, 1(3):215–227, 2007.

[22] Q. Xu, R. Perez-Castillejos, Z. Li, and G. M. Whitesides. Fabrication of high-aspect-ratio metallic nanostructures using nanoskiving. *Nano Lett.*, 6(9):2163–2165, 2006.

[23] D. J. Lipomi, R. V. Martinez, and G. M. Whitesides. Use of thin sectioning (nanoskiving) to fabricate nanostructures for electronic and optical applications. *Angew. Chem. Int. Ed.*, 50(37):8566–8583, 2011.

[24] P. Pourhossein and R. C. Chiechi. Directly addressable sub-3 nm gold nanogaps fabricated by nanoskiving using self-assembled monolayers as templates. *ACS Nano*, 6(6):5566–5573, 2012.

[25] C. E. Hoyle, T. Y. Lee, and T. Roper. Thiol-enes: Chemistry of the past with promise for the future. *Journal of Polymer Science Part A: Polymer Chemistry*, 42(21):5301–5338, 2004.

[26] H. Lu, J. A. Carioscia, and C. N. Stansbury, J. W.and N. Bowman. Investigations of step-growth thiol-ene polymerizations for novel dental restoratives. *Dental Materials*, 21(12):1129 – 1136, 2005.

[27] C. E. Hoyle, A. B. Lowe, and C. N. Bowman. Thiol-click chemistry: a multifaceted toolbox for small molecule and polymer synthesis. *Chem. Soc. Rev.*, 39:1355–1387, 2010.

[28] J. A. Carioscia, J. W. Stansbury, and C. N. Bowman. Evaluation and control of thiol-ene/thiol-epoxy hybrid networks. *Polymer*, 48(6):1526 – 1532, 2007.

[29] K. Dawson, J. Strutwolf, K. P. Rodgers, G. Herzog, D. W. M. Arrigan, A. J. Quinn, and A. O'Riordan. Single nanoskived nanowires for electrochemical applications. *Anal. Chem.*, 83(14):5535–5540, 2011.

[30] T. F. Scott, A. D. Schneider, W. D. Cook, and C. N. Bowman. Photoinduced plasticity in cross-linked polymers. *Science*, 308(5728):1615–1617, 2005.

[31] C. J. Kloxin, T. F. Scott, and C. N. Bowman. Stress relaxation via addition-fragmentation chain transfer in a thiol-ene photopolymerization. *Macromolecules*, 42(7):2551–2556, 2009.

Chapter 3

Fabrication of Sub-3 nm Nanogap Electrodes by Nanoskiving

3.1 Introduction

A central challenge to interfacing molecules electrically from our macro world is producing nanostructures that possess both features on the molecular scale–single nanometers–and on a scale large enough to connect to external circuitry.[1,2] Several methods of fabricating nanoscale gaps with controlled spacing have been reported, including mechanical break junctions,[3] electron-beam lithography,[4] electrochemical plating,[5,6] electromigration,[7] focused ion beam lithography,[8] shadow evaporation,[9] scanning probe and atomic force microscopy,[10] on-wire lithography,[11] and molecular rulers.[12] Each of these methods have their own applications and limitations, but despite all the progress in this field, there remain challenges to producing electrodes with single-nanometer spacings that can be fabricated and positioned in a precise and controllable manner and that are

∗This chapter has been published in: Parisa Pourhossein and Ryan C. Chiechi, ACS Nano, 2012, 6, 5566-5573.

readily electrically-addressable. The most common approach is to fabricate the "nano" part of the device, containing a nascent gap (*e.g.*, the sacrificial metal in on-wire lithography or the constriction point in break junctions) and then using a lithographic process to connect it to wires and contact pads before unmasking the nanogap. This approach is effective, but laborious, and because gap-sizes of single nanometers also demand sub-nanometer resolutions, they push modern nanofabrication methods to their technical limits. The resulting complexity necessitates specialized infrastructure (clean rooms, e-beam/photolithography equipment, etc.) and the commensurate overhead–cost, training, and time. A more desirable approach is to start from a simple technique that is far from its technical limits, leaving plenty of room for improvement and adaptation to specific experiments/applications.[13]

3.2 Fabrication

We are particularly interested in the application of nanogap structures to construct metal-molecule-metal tunneling junctions, where molecules are placed between electrodes through which they can be addressed from the macro world. There are three general approaches to addressing molecules electrically; i) forming gaps in electrode materials that are on the same length scale as the molecules of interest and then allowing (typically only a few of) these molecules to self-assemble into the gaps; ii) forming self-assembled monolayers (SAMs) and then applying a top-contact; and iii) forming monolayers parallel to the surface of nanogap electrodes.[14,15] We combined these approaches by forming SAMs on thin films (100 nm) of gold, evaporating a second layer of gold (100 nm) to form a gold/SAM/gold sandwich, and then slicing thin sections (50-100 nm) perpendicular to the plane of the SAM by nanoskiving. The resulting structures comprise two nanowires separated by the smallest dimension of a SAM. This method circumvents the high frequency of electrical shorts ($\sim$ 98.8% for alkanthiolates on gold[16]) that normally results from depositing metal contacts

directly onto SAMs because the total area of the skived SAM is only $\sim 50\ \mu m^2$. Nanoskiving has been used in combination with photolithographic techniques to produce electrically-addressable nanowires separated by a 30 nm-thick layer of SiO_2,[17] but applications in tunneling junctions require gaps below 10 nm. In addition, we greatly simplified the fabrication process and eliminated the use of photolithography by simply offsetting the evaporated gold features by hand. The entire procedure is summarized in Figure 3.1. A silicon wafer is cleaned with an air plasma and then passivated with a perfluorinated trichlorosilane. Rectangles of gold ($1 - 2$ mm) are deposited by evaporation through a Teflon mask. Epofix epoxy pre-polymer is poured over the entire wafer, covering the gold features, and the epoxy is cured before being template-striped[18] by separating the epoxy from the wafer; the gold features remain adhered to the epoxy. A SAM is formed by submerging these features in a 1 mM ethanolic solution of the appropriate thiol overnight. A second set of gold rectangles is deposited by placing the Teflon shadow mask over the SAM-covered gold features with an offset of $250 - 500\ \mu$m with respect to the first evaporation. This offset will eventually define the longest dimension of the gap, and it can be accurately measured using a micro-ruler before embedding the entire structure in epoxy for sectioning. Figure 3.2 is a schematic of the resulting SAM-templated addressable nanogaps (STANs) and how each dimension is defined; the longest dimension by the shadow mask, the smallest (the gap) by the thickness of the SAM, the width by the ultramicrotome, and the thickness by the evaporation of the gold.

The resulting structures are 2-4 mm in total length, but since the length of the gap (dimension E from Figure 3.2) is only $250 - 500\ \mu$m, $0.75 - 1.75$ mm of each wire is available for electrical contact, obviating the need for further lithography to connect the wires to an electrometer. The gold wires have square cross-sections of only 100 nm on a side and are therefore too fragile to contact directly using a probe station; however, contact pads can be applied by hand using small drops of a liquid conductor such as silver paste or conductive carbon paint. We used a combination of silver paste and micrometer-sized tips of eutectic Ga-In

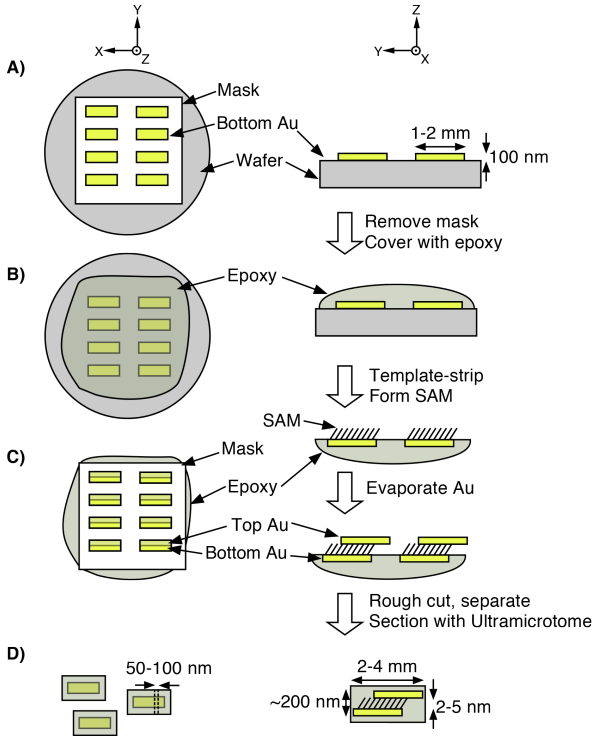

Figure 3.1: A schematic (not to scale) of the fabrication of STAN electrodes. The left column is the top-down view and the right column is the side-view. A) A 100 nm-thick layer of gold is deposited through a Teflon shadow mask onto a fluorinated silicon wafer via thermal evaporation to produce an array of millimeter-sized rectangles. B) The mask is removed and the gold features covered in epoxy. After the epoxy cures, it is separated from the wafer such that the gold features remain adhered to the epoxy. A SAM is then formed on the newly-exposed gold surfaces. C) The Teflon mask is placed over the SAM-covered gold features with an offset of $250-500\ \mu\mathrm{m}$ and another 100 nm-thick layer of gold is deposited. D) The mask is removed and the the gold/SAM/gold features are separated by rough-cutting the epoxy with a jewler's saw. The features are then embedded in epoxy and sectioned with an ultramicrotome. Reproduced with permission from Ref. [13].

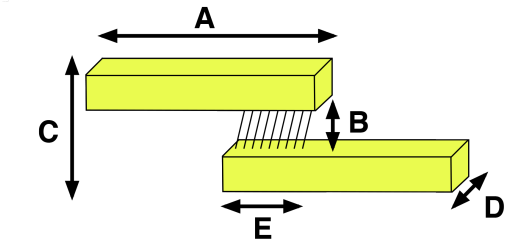

A)1-2 mm; defined by the shadow mask.

B) 2-5 nm; defined by the thickness of the SAM.

C) ~200 nm; defined by the two gold depositions.

D) 50-100 nm; defined by the Ultramicrotome.

E) 250-500 μm; defined by the offset in the second gold-deposition step.

Figure 3.2: A schematic (not to scale) of the dimensions of the STAN electrodes showing how each dimension is the defined. A) The length of each wire is defined by the shadow mask. B) The size of the gap between the wires is defined by the thickness of the SAM. C) The total width is defined by the two gold deposition steps. D) The depth is defined by the ultramicrotome. E) The amount of overlap–and the longest dimension of the nanogap–is defined by the offset between the first and second gold-deposition steps. Reproduced with permission from Ref. [13].

(EGaIn) formed at the tip of a syringe.[19] The ability to pick-and-place nanogaps and then contact them directly is unique to STAN electrodes. The typical trade-off between directly fabricating nanogaps via photo/e-beam lithography and forming them via chemical process in a template is that the former allows the gaps to be fabricated in-place, but is constrained by the resolution of lithography, while the latter may produce large numbers of gaps, but they must be addressed one-at-a-time using e-beam lithography to form contact pads. Nanoskiving falls somewhere between; STAN electrodes are fabricated serially at a rate of ~ 1 s^{-1} and each block can produce hundreds of thousands of STAN electrodes (and the blocks are fabricated dozens at a time). The individual sections can be placed onto arbitrary substrates (that are sufficiently wetted by water) with control over position and orientation, or they can be transferred from the boat as a ribbon of several sections by dipping a substrate into the water and slowly raising it from underneath the ribbon (Figure 3.3). Although we use silver paste for convenience, it is by no means necessary; the STAN structures could, for example, be placed onto pre-defined contact pads. Gaps of different sizes can also be combined onto one substrate simply placing different STAN structures next to each other. Thus, hundreds of nanogaps of various sizes can be fabricated, positioned, and wired up by hand, in matter of minutes, and directly on the bench top. The fabrication process presented in this paper also represents the low end of complexity for nanoskiving and utilizes a commercial ultramicrotome that is designed neither for high throughput nor automation.

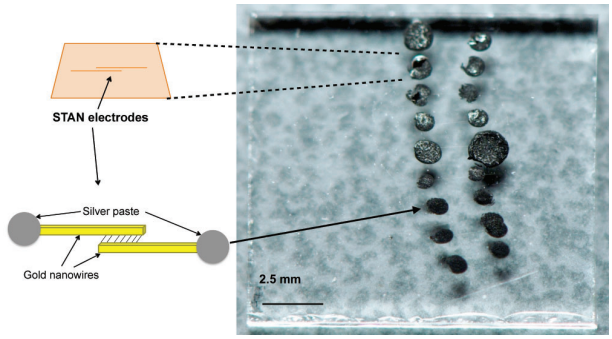

Figure 3.3: A photograph of a ribbon of 10 STAN electrodes on a glass substrate after applying silver paste to the two electrodes. This ribbon was transferred to the glass by dipping it into the boat of the knife of the ultramicrotome beside the ribbon and then removing it slowly from underneath the ribbon. Reproduced with permission from Ref. [13].

3.3 Electron Microscopy

I initially prepared STAN electrodes of four different gap-widths, one using hexadecane-1,16-dithiol (SC16S), one using tetradecane-1,14-dithiol (SC14), one using dodecane-1,12-dithiol (SC12S), and one using hexane-1-thiol (SC6). The end-to-end (S-S for the dithiols and S-C for SC6) length of each molecule in the extended (AM1 minimized) conformation is 21.7, 19.7, 17.0, and 7.8 Å respectively. In principle the SAMs of these molecules will produce STANs with gaps-widths of the hypotenuse formed from these lengths and the tilt-angle of the respective SAM on gold; however, SAMs of SC6 are disordered and liquid-like at room temperature, while SC12S, SC14S, and SC16S form well-ordered, (liquid) crystalline SAMs.[20] Moreover, the methyl-terminated SAMs of SC6 will likely have a lower-energy interaction with gold than the thiol-terminated SAMs of SC12S, SC14S, and SC16S. Thus, if the SAMs are able to template nanogaps, we have three expectations; i) SAMs of SC6 should not produce a gap; ii) both SC16S and SC12S should form gaps and these gaps should be stable due to the stronger interaction of thiols with gold; Thiols do not necessarily form

gold-thiolate bonds during the deposition of gold, rather thiols have a higher surface free-energy than methyl groups. And iii) the gaps produced by SC16S, SC14S, and SC12S should differ in size. This last expectation is experimentally challenging to observe, as the difference in widths of the gaps is expected to be less than one nanometer. While it is preferable to image the STAN structures as-fabricated, due to excessive charging of the Epofix resin, I had to ash the organics (including, presumably, the SAMs) using an oxygen plasma ($\sim$ 15 min) before imaging by SEM; representative electron micrographs are pictured in 3.4. There is no visible gap between the gold wires formed using SC6, implying that the liquid-like SAM was readily penetrated by the evaporated gold, however, the gaps formed from SC16S, SC14S and SC12S are clearly visible and the size of the gap appears to increase with the length of the molecule. The resolution limit of the SEM, however, precluded the accurate measurement of features below $\sim$ 4 nm. Thus, we conclude that the gap-width of these STANs is $<$ 4 nm. The gaps and total length of the wires cannot be resolved simultaneously (*i.e.*, at one magnification), but series of images across the STAN structures reveal uniform wires and gaps. An SEM image of the edge of the overlap between two wires is shown in Figure 3.5. Efforts to measure the gaps precisely using AFM, CP-AFM, and STM failed due to either the extreme aspect-ratios of the STANs and, for un-ashed STANs, the disparate properties of the materials (*i.e.*, gold, alkanedithiols, and epoxy).

To determine whether the gaps extended through the entire thickness of the STANs, I prepared STANs that were 50 nm thick (dimension D from Figure 3.2) to reduce the aspect ratio, and imaged them by TEM. For the gaps containing SC12S, SC14S, and SC16S, aligning the samples perfectly perpendicular to the electron-beam proved too challenging; these gaps are on the order of the wavelength of an electron and have an aspect-ratio of 50:1 (height:width). In addition to the SAMs of dithiols, I fabricated STANs using 16-mercaptohexadecanoic acid (SC15CO2H), which forms dense SAMs that are mechanically stable (due to internal hydrogen-bonding). I was able to resolve the gaps of these STANs more

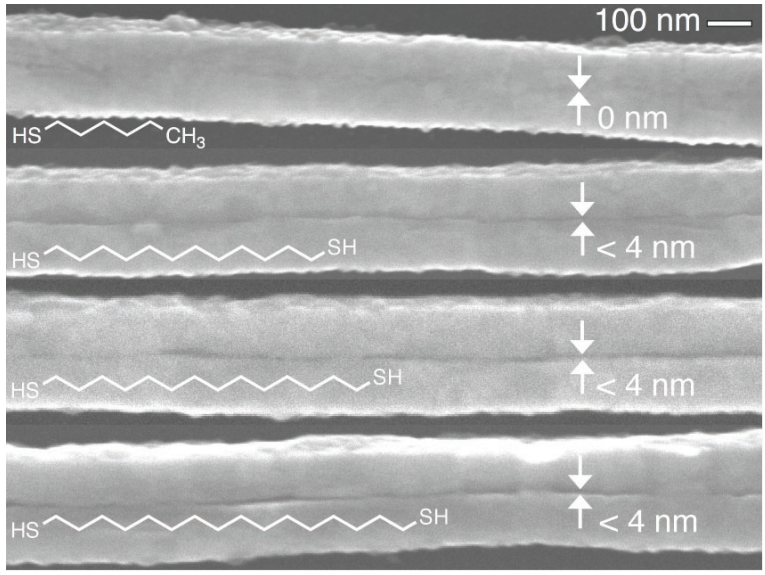

Figure 3.4: Scanning electron micrographs of the gaps of four different STAN electrodes prepared using different thiols as templates, after ashing the organics with oxygen plasma. From top to bottom; SC6 results in no visible separation between the two gold wires; SC12S shows a clearly-visible gap; SC14S shows a clearly-visible gap that is qualitatively larger than the gap formed by SC12S; SC16S shows a clearly-visible gap that is qualitatively larger than the gaps formed by SC12S and SC14S. All three of the gaps formed by SAMs of dithiols are below the resolution limit of the instrument (~ 4 nm), thus they are labeled as "< 4 nm". Reproduced with permission from Ref. [13].

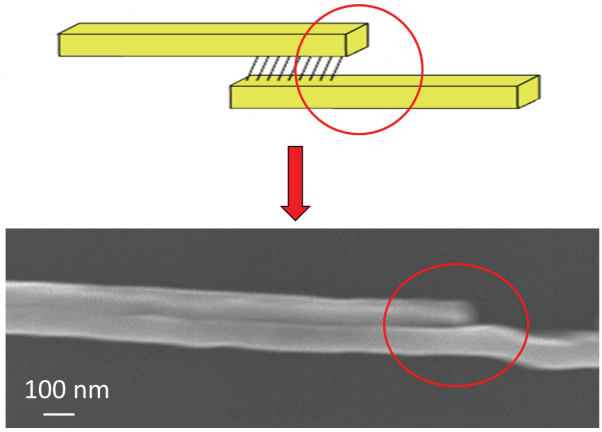

Figure 3.5: Scanning electron micrograph of the starting point of the overlap of STAN electrodes. The gap is clearly visible between two Au nanowires. Reproduced with permission from Ref. [13].

readily by SEM than the gaps from the dithiols due to the apparent poor adhesion of gold to the terminal carboxylic acid groups, which allowed one wire to shift slightly with respect to the other, making the sharp edges of the gaps clearer by electron microscopy and therefore easier to measure. The top image in 3.6 is an SEM of a STAN fabricated from SC15CO2H in which the edge of the lower electrode appears brighter than the face, drawing a sharp contrast with the gap, which appears dark. We were able to image the gap of one of these STANs by TEM (Figure 3.6; bottom) as well, from which we calculated a width of 2.6 ± 0.5 nm by comparing the pixel intensity versus displacement from five different regions distributed across the STAN structure. (The clarity of the gap is remarkable given the challenges of unambiguously resolving TEM images of gaps below 10 nm.[21]) More importantly, the TEM image shows that the gap extends through the entire thickness of the STAN, which implies that the deposited gold did not penetrate the SAM sufficiently to form filaments and that free-standing STANs (*i.e.*, after ashing the organics with oxygen plasma) with gaps of ~ 3 nm are mechanically stable.

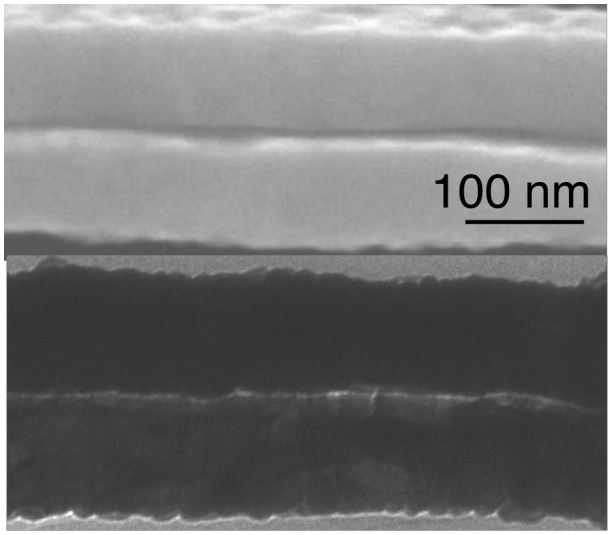

Figure 3.6: Scanning (top) and transmission (bottom) electron micrographs of gaps formed using 1-mercaptohexadecanoic acid, after ashing the organics with oxygen plasma. The light region in the bottom (TEM) image shows that the gap extends through the entire thickness of the gold wires ($100\ \mathrm{nm}$). The width of this light region is $2.6 \pm 0.5\ \mathrm{nm}$. The gap in the top (SEM) image appears to be significantly larger than $2.6\ \mathrm{nm}$ because the wires are tilted slightly downward, and are offset slightly, creating a high contrast between sharp edge of the lower wire (the cross section of the wires is rectangular) and the shadow from the upper wire. Reproduced with permission from Ref. [13].

3.4 Electrical Measurements

The disparate dimensions of STAN structures–nanometers in two dimensions and millimeters in the third–make it impossible to image them directly in their entirety. Electrical measurements, however, provide an indirect estimate of the size of a nanogap, provided the emission area can be estimated reasonably; we can measure the largest dimension (E from Figure 3.2) directly, and the other (D from Figure 3.2) is defined by the ultramicrotome. To measure the J/V characteristics, I made electrical contact by placing the epoxy sections containing STAN electrodes on a clean SiO_2 substrate and then applying drops of silver paste to each electrode under a light microscope. (While the electrodes themselves are too small to visualize, the index mismatch between the epoxy slab and gold nanostructures creates a line that is clearly visible to the naked eye.) I then placed the substrate in a home-build Faraday cage (in ambient temperatre and pressure) and grounded one of the electrodes using a small drop of EGaIn to connect the pad of silver paste to a tungsten probe. I contacted the other electrode by positioning a syringe with a sharp tip of EGaIn over the other pad of silver paste, bringing it in contact, and connecting the syringe to the electrometer. The Lo input was grounded at the electrometer. The schematic of the wiring of the source meter used to acquire I/V traces is shown in Figure 3.7. I observed four distinct behaviors; i) no-contact, characterized by noisy, hysteretic currents in the pA regime; ii) shorts, characterized by linear ohmic I/V curves with currents in the μA regime (Figure 3.8) (the S-shape curve refers to the I/V traces resulting form tunneling); iii) poor-contact, for which we initially observed no-contact I/V curves, but could observe shorts after placing the EGaIn tip between the two silver pads (*i.e.*, over the gap, bridging the two electrodes); and iv) working STAN electrodes, characterized by S-shaped I/V curves of reproducible, low-noise currents in the nA regime(S-shape curve refers to the tunneling current).

The transport of charges in metal-molecule-metal junctions in which one single

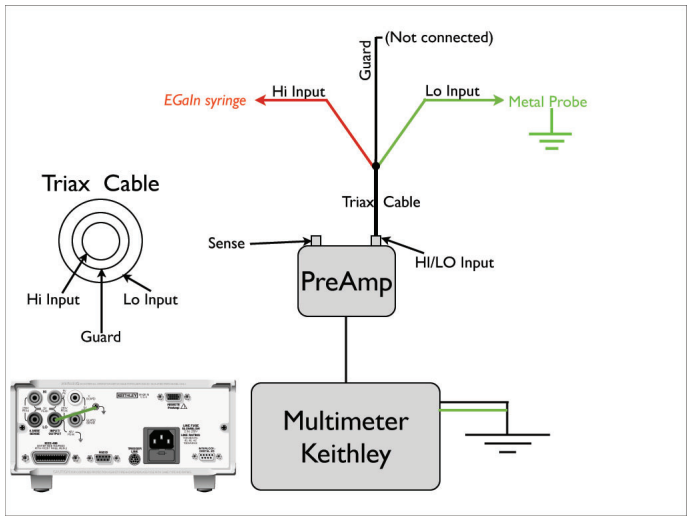

Figure 3.7: A schematic of the wiring of the source meter used to acquire I/V traces for the STAN electrodes. Metal Probe refers to the metal probe that contacts one of the silver pads and EGaIn syringes refers to the drop of EGaIn that contacts the other silver pad.

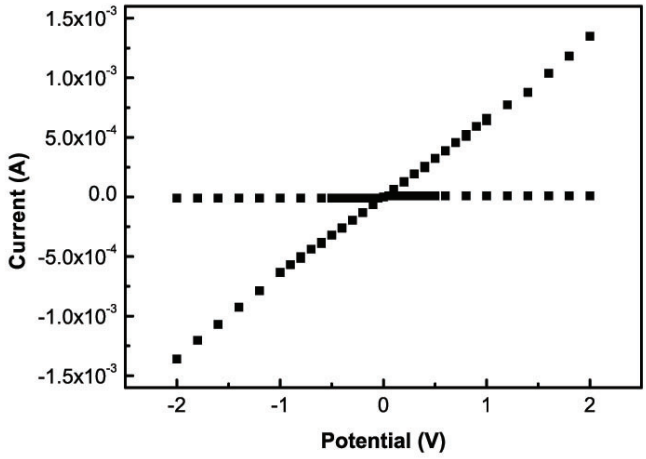

Figure 3.8: I/V plots from a section that was cycled between ± 500 mV and then increased to ± 2 V to deliberately induce a short; the S-shape of the curves for the pre-shorted junction is not visible because the data are plotted on a linear scale. Reproduced with permission from Ref. [13].

molecular orbital can bridge from one electrode to the other electrode, happens via tunneling. Charge transport is controlled by the energy difference between the Fermi level of metal and the Highest Occupied Molecular Orbital (HOMO) and Lowest Unoccupied Molecular Orbital (LUMO) levels of the molecules. Since this energy difference is larger than thermal energy kT, electrons can not pass and tunneling becomes the dominant mechanism. Tunneling is independent of temperature and dependent of width of the junction. SAMs of alkanethiols form with a tilt angle with respect to the surface of gold. Thus, electrons have two pathways, the shorter prependicular distance between two electrodes and a longer route through the backbone of the molecules. It has been shown that tunneling in molecular junctions is dominated by the transport through backbone of the molecules.[22,23]

The J/V data for SC12S, SC14S, and SC16S are plotted in Figure 3.9. We calculated J (A/cm^2) using the maximum theoretical emission area of the height, defined by the ultramicrotome and the width, defined by the shadow mask and measured using a micrometer during fabrication (*i.e.*, E and D from 3.2). Although the actual emission area may be smaller (due, for example, to deformation from mechanical stresses), this calculation assumes that any variations in size are systematic across all STANs and all three lengths of dithiols. The yields of working STAN electrodes are shown in Figure 3.1; the average yield for STAN electrodes fabricated using dithiols is 58%. The lowest yield of 13% (for SC15CO2H) and the highest yield of 71% (for SC14S) far exceed the $\sim$ 1.2% that is typical for evaporated gold top-contacts (without a buffer layer).[16] While this result is counterintuitive in that longer dithiols should form more mechanically robust SAMs, the quality of the diamond knife can adversely impact yields by introducing occasional breaks between where the silver paste is applied and the junction (*i.e.*, no-contacts) due to nicks in the cutting edge that can result from heavy usage. (Though likely not from fabricating the STANs, as gold films do not typically damage diamond knives.) We interpret poor-contacts and no-contacts as varying degrees of poor electrical contact between the silver paste and the

electrodes–and not defects in the STAN electrodes themselves–because we were able to deliberately short the former, and we did not observe any discontinuities in any of the (dozens of) STANs that we examined by SEM; however, the aspect ratios of the STANs makes inspecting the entire length of more than a few of them impractical. Thus the frequency of these phenomena is not intrinsic to the fabrication process and can therefore be reduced. Shorts are most likely caused by the gold penetrating through defects in the SAM during deposition and are therefore intrinsic to the choice of SAM, metal, and deposition method. For dithiols, these defects can arise from the molecules forming loops by attaching to the gold through both thiols, which can be mitigated by fine-tuning the concentration and exposure time during the formation of the SAM.[24] Other types of defects can be mitigated by improving the quality of the template-stripped gold surface, using silver (SAMs of alkanethiolates pack more densely on silver than gold), improving the mechanical stability of the molecules *via* functionalization, and sharpening the diamond knives regularly.

Table 3.1: The yields of working junctions from STAN electrodes fabricated using various thiols.

Thiol	**No-contact (%)**	**Shorted (%)**	**Working (%)**	**Devices**
SC12S	8	25	67	12
SC14S	15	14	71	14
SC16S	28	36	36	14
SC15CO2H	34	53	13	30

The simplest approach to determining the dimensions of a tunneling gap that is too small to measure directly is to fit I/V curves of the gap to Simmons' approximation for a rectangular tunneling barrier,[25] however that requires removing the molecules from the STAN electrodes, as this approximation is not valid for alkanedithiols. Unfortunately we were unable to remove the SAMs reliably

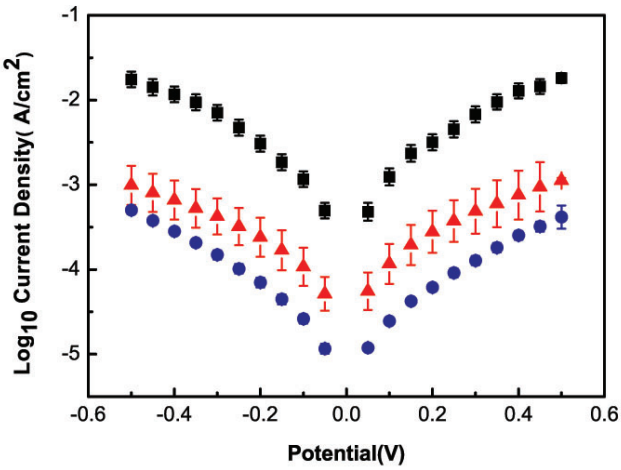

Figure 3.9: Log current-density versus potential plots for STAN electrodes fabricated from three different dithiols; SC12S (black squares), SC14S (red triangles), and SC16S (blue circles). Each plot is a log-average of at least ten scans from five different STAN electrodes; the error bars are the variance. Reproduced with permission from Ref. [13].

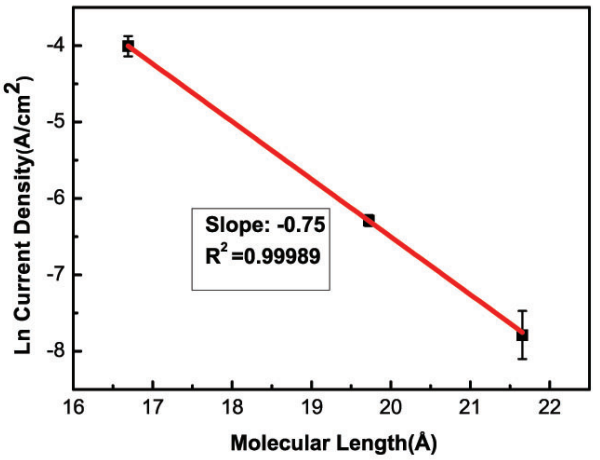

Figure 3.10: A plot of $ln(J)$ at 500 mV versus length (Å) from the data in 3.9 showing a linear fit ($R^2 = 0.99$) with a slope corresponding to $\beta = 0.75$ Å^{-1} ($0.94\ n_C^{-1}$). Reproduced with permission from Ref. [13].

while retaining reproducible I/V data. Treatment with oxygen plasma, while resulting in intact STAN structures by SEM and TEM, yielded large spreads in the I/V curves (Figure 3.11). Exposure to piranha solution (H_2SO_4 in H_2O_2) yielded similar results. These spreads may simply be due to the oxidation of the pads of silver paste; the average resistance of single gold nanowires connected through pads of silver paste decreases from 2.57 kΩ to 1.58 kΩ after 15 minutes of exposure to oxygen plasma. Regardless, using another form of Simmons' approximation, $J = J_0 e^{-d\beta}$ where d is the width of the junction and J_0 is the theoretical value of J at $d = 0$, the characteristic tunneling decay, β, can be extracted from a linear fit of J as a function of the width of a junction (or number of carbons, n_C). This method provides not only a measure of the width of a junction, but also how precisely it can be controlled. And, since β has been determined for SAMs of alkanthiols[26] and dithiols[27] in a variety of systems, it offers strong evidence that the dithiols are defining the width of the junction

and carrying the tunneling current; other possible carriers such as gold filaments or constriction points would yield a very different value for β. While there is a range of reported values of β for alkane backbones, the emerging consensus that it is $0.51 - 0.78$ Å^{-1} ($0.71 - 1.10$ n_C^{-1}) at 200-500 mV.[28–31] Figure 3.10 is a plot of $\ln J$ at 500 mV (from the data in Figure 3.9) versus length (Å) for STAN electrodes containing SC16S, SC14S, and SC12S. From the slope of this plot, $\beta = 0.75$ Å^{-1} (0.94 n_C^{-1}) which is in excellent agreement with literature values. Thus, we conclude that the gap-width of the STAN structures is defined by the SAMs used as templates, that those SAMs remain intact after fabrication, and that the size of the gap can be defined with a resolution as small as 2.5 Å. Further evidence that the SAM not only remains intact, but undamaged, is shown in Figure 3.12 which is a plot of data from two STAN electrodes of approximately equal width; one fabricated using SC16S and one using SC15CO2H, which is ~ 0.7 Å shorter than SC16S–in principle, too small of a difference to detect by conductance measurements. Changing the head group from a thiol (that is either physi- or chemisorbed) to a carboxylic acid is, however, expected to produce detectible, but minor (and, importantly, non-exponential) changes in conductance (and the shape of the J/V curves). We observed exactly that–a slight change in the magnitude and shape of the J/V curves and a slight change in rectification. While we cannot derive the emission area from length-dependence measurements alone, the magnitudes of the values of J in Figure 3.9 are comparable to other SAM-based tunneling junctions in which one of the thiols of an alkanedithiol is electronically de-coupled from the electrode.[27,32] This observation implies that the "top" electrode, formed by deposition onto the SAM, forms a physisorbed rather than chemisorbed interface with the thiol end-groups (*i.e.*, SH//Au, not S-Au). The nature coupling of contacts to molecules are important. Strong (chemisorption of molecules on contacts) coupling and weak (physorption of molecules on contacts) lead to the shift in energy levels of the molecular orbitals. In chemisorption more change in molecular energy leves happen. Thus, in strong coupling less resistance is

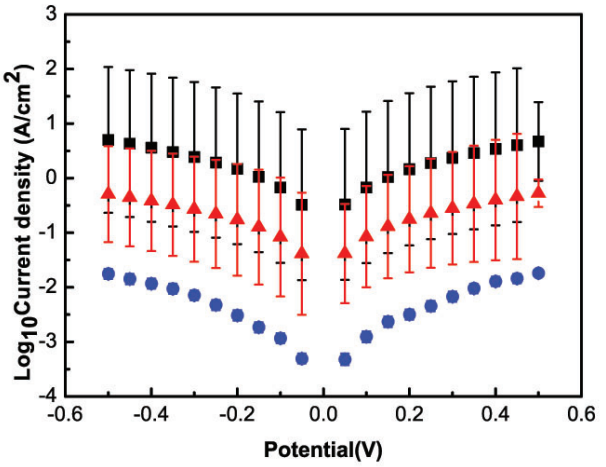

Figure 3.11: Log current-density versus potential plots for eight STAN electrodes fabricated using SC12S after different varying lengths of exposure to oxygen plasma; 0 min (blue circles), 15 min (black squares), and 30 min (red triangles). Each plot is a log-average of 32 scans.

observed in comparision to the weak coupling.

I performed control measurements on blank epoxy microtome sections without STAN structures (Figure 3.13), on blank SiO_2 substrates (Figure 3.14; *i.e.*, after ashing the blank epoxy sections) and the open circuit (*i.e.*, with the EGaIn electrode raised out of electrical contact with the substrate; Figure 3.15). These control measurements show that the observed currents were not the result of ionic conduction through the epoxy/SiO_2 or open-circuit artifacts.

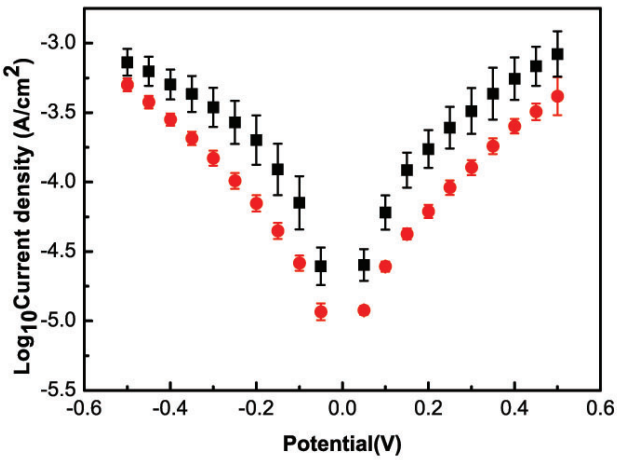

Figure 3.12: Log current-density versus potential plots for STAN electrodes fabricated from two different dithiols; SC15CO2H (black squares) and SC16S(red circles). Each plot is a log-average of at least 20 scans from four different STAN electrodes. The lengths of the two thiols are within 0.7 Å of each other, implying that the slight difference in conductance is due to the differences in electronic coupling to gold between CO_2H and SH. The small magnitude of this difference implies that the gold electrode formed by depositing gold directly onto the SAM of SC15CO2H forms a physisorbed and not a chemisorbed contact (*i.e.*, SH//Au, not S-Au). Reproduced with permission from Ref. [13].

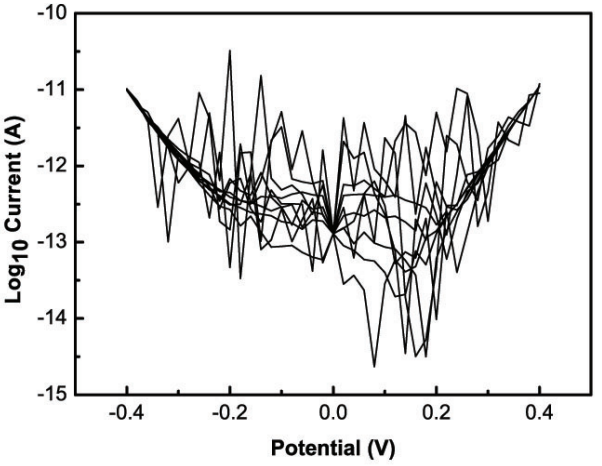

Figure 3.13: Log current versus potential plot for an epoxy section without a STAN electrode present.

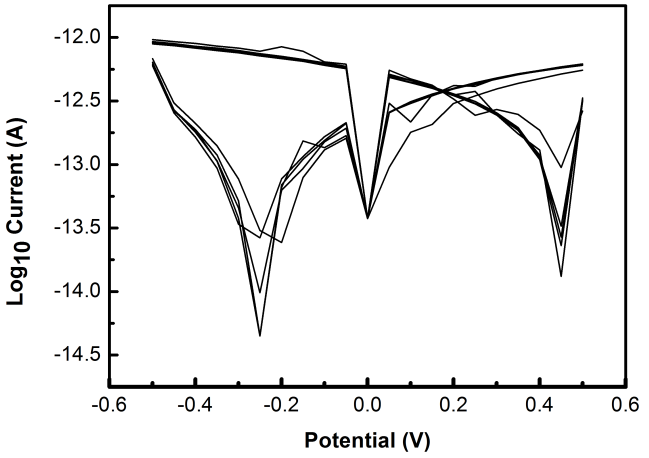

Figure 3.14: Log current versus potential plot for a blank SiO_2 substrate.

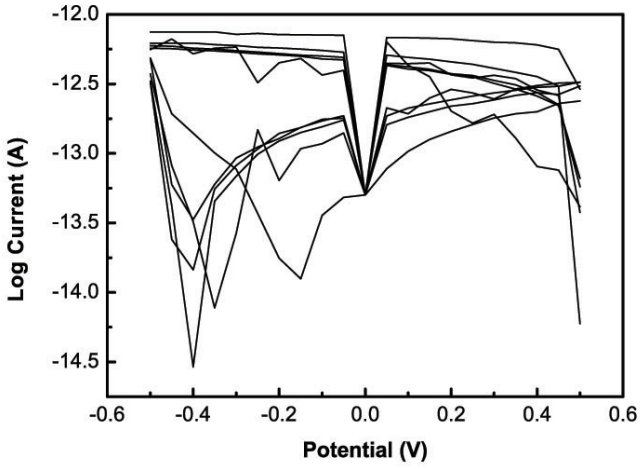

Figure 3.15: Log current versus potential plot of the open circuit resulting from raising the EGaIn tip.

3.5 Conclusions

Our overall goal with this work was to create a simple method for fabricating nanogaps on the order of the length scale of small molecules without any arduous lithography steps. Ideally, these nanogaps could be precisely defined by the thickness of a SAM–affording Angstrom-level control over the width of the gaps–that could later be removed and replaced with dithiols of similar lengths to form devices based on tunneling junctions. In this chapter I have demonstrated the basic concept by fabricating STAN structures with gaps of 1.7–2.2 nm using only nanoskiving and the hand-placement of mm-sized shadow masks to form gaps of $\sim$ 2 nm over areas of $\sim$ 500 μm^2. We can control all three dimensions of the STANs, pick-and-place them by hand, and they are directly electrically-addressable using a light microscope to apply contact pads of silver paste (or using EGaIn tips). Length-dependent electrical measurements on intact alkanedithiols (*i.e.*, before ashing the organics with oxygen plasma) clearly

show that charge transport is dominated by tunneling through the backbone of the SAM, demonstrating that the gaps are indeed defined by the lengths of the molecules in the SAMs. Thus, STAN electrodes offer an exceedingly simple platform for directly fabricating tunneling junctions comprising SAMs that pack densely enough to withstand the deposition of gold. These electrodes offer five advantages over existing methods for fabricating nanogaps; i) the resolution of the gap is at least 2.5 Å; ii) no special equipment or infrastructure is needed to fabricate them–only an ultramicrotome; iii) they are directly addressable as-fabricated, requiring no additional lithography steps; iv) they can be fabricated on-demand at the rate of about one per second (the epoxy blocks are stable for at least one year); and v) they can be placed onto almost any substrate with any orientation, and can be stacked and aligned. Although we were able to remove the SAM templates by plasma oxidation and exposure to piranha solution and image them by electron microscopy there was too much variance in the resulting electrical measurements to conclude that a uniform air-gap remained; however, the absence of shorts indicates that the gaps did not collapse.

3.6 Experimental Section

I treated a technical-grade 3" silicon wafer in an air plasma cleaner for 30 seconds and then exposed it to (tridecafluoro-1,1,2,2,-tetrahydrooctyl)trichlorosilane vapor for one hour. (This step is necessary to prevent the epoxy from adhering to the silicon wafer.) I deposited a layer of gold (usually 100 nm-thick, which defines the width of the wires) through a Teflon master (that defines the length of the resulting wires; 0.5 mm, 1 mm, or 1.5 mm) onto the pre-treated silicon wafer. Then, I covered the entire wafer with $\sim$ 8.5 mL of Epofix epoxy pre-polymer and cured it for three hours at 60 °C. In the next step, I template-stripped the gold layer by carefully peeling the epoxy from the wafer such that the gold remains attached to the cured epoxy. I inserted the edge of a razor blade at the interface between the silicon wafer and epoxy and then gently peeled the

epoxy layer from the silicon wafer. Because of the poor adhesion of gold to the fluorinated silicon wafer, the gold features remain adhered to the epoxy. I immersed the template-stripped gold on epoxy in a 1 mM solution of an alkanedithiol in ethanol (or any solvent that does not swell the epoxy) overnight in a closed chamber that is purged with nitrogen (to mitigate the spontaneous formation of disulfides). I used 1,12-dodecanedithiol, 1,14-tetradecanedithiol or 1,16-hexadecanedithiol, etc to produce gaps of various widths below 3 nm. After removing the template-stripped gold-on-epoxy substrate from the SAM-forming solution, I rinsed it with ethanol and dried it with nitrogen before drying at 60 °C for 2 minutes. I placed back the Teflon mask onto the epoxy substrate but laterally offset by $\sim$ 80% of the shortest dimension of the gold features. Then I deposited a second layer of gold or any other metal (100 nm in this case) through the mask. Afterwards I removed the Teflon mask, taking care not to scratch the features, which will result in broken nanowires. I re-embedded the entire substrate in Epofix pre-polymer ($\sim$ 8.5 mL) and cured it for at least three hours at 60 °C.

I cut the features out using a jeweler's saw (into $\sim$4 x 10 mm pieces) and placed each into a separate well in a polyethylene 'coffin' microtome mold, filled the mold with Epofix pre-polymer and cured it overnight at 60 °C.

I removed a block from the polyethylene mold and mounted it in the sample holder and attached it to the trimming attachment and mounted it in the ultramicrotome. Then, I cleaned a razor blade with ethanol to remove lubricant and metal fragments and inspected the edge of the razor blade under the stereoscope of the ultramicrotome. Any remaining fragments will damage the diamond knife during sectioning. I trimmed the block to the width of the diamond knife (I used 2 mm or 4 mm Diatome Ultra 35°) in a trapezoid shape (because it is the most stable shape for sectioning). In the next step, I aligned the edge of a glass knife parallel to the bottom edge of the face of the block. I started pre-cutting with the ultramicrotome (I used a Leica EMUC-6) equipped with a glass knife to define a smooth surface on the face of the block. To fabricate a metallic structure,

I replaced the glass knife with a diamond knife, re-aligned it, and sectioned the block to either 100 nm at 1 mm/s or 50 nm at 0.6 mm/s. Epofix sections are stable down to $\sim$ 30 nm. An easy verification of the thicknesses of the sections is their color, which varies predictable as a function of thickness and does not depend on the resin which has been used; reference cards are available.[33] I collected the epoxy sections containing the structures from the surface of the water in the reservoir of the knife either individually using a Perfect Loop (Electron Microscopy Sciences) or as ribbons of several sections to an Si/SiO_2 (for SEM) or SiO_2 (for electrical measurements) substrate by placing substrate under the surface of the water and raising it slowly. I dried the sections at 60 °C for 3 hours to improve their adhesion to the substrate.

To ash the epoxy, I exposed the samples to an oxygen plasma (15 minutes at 1 mbar is sufficient to remove all traces of the epoxy from 100 or 50 nm-thick sections).

Bibliography

[1] T. Li, W. Hu, and D. Zhu. Nanogap electrodes. *Adv. Mater.*, 22(2):286–300, 2010.

[2] R. L. Carroll and C. B. Gorman. The genesis of molecular electronics. *Angew. Chem. Int. Ed*, 41(23):4378–4400, 2002.

[3] M. A. Reed, C. Zhou, C. J. Muller, T. P. Burgin, and J. M. Tour. Conductance of a molecular junction. *Science*, 278(5336):252–254, 1997.

[4] W. Chen, H. Ahmed, and K. Nakazoto. Coulomb blockade at 77 k in nanoscale metallic islands in a lateral nanostructure. *Appl. Phys. Lett.*, 66(24):3383–3384, 1995.

[5] A.F. Morpurgo, C.M. Marcus, and D.B. Robinson. Controlled fabrication of metallic electrodes with atomic separation. *Applied Physics Letters*, 74(14):2084–2086, 1999.

[6] Y. Paska and H. Haick. Systematic cross-linking changes within a self-assembled monolayer in a nanogap junction: A tool for investigating the intermolecular electronic coupling. *J. Am. Chem. Soc.*, 132(6):1774–1775, 2010. PMID: 20088587.

[7] J. Park, A. N. Pasupathy, J. I. Goldsmith, C. Chang, Y. Yaish, J. R. Petta, M. Rinkoski, J. P. Sethna, H. D. Abruna, P.L. McEuen, and D. C. Ralph. Coulomb blockade and the kondo effect in single-atom transistors. *Nature*, 417:722–725, 2002.

[8] T. Nagase, T. Kubota, and S. Mashiko. Fabrication of nano-gap electrodes for measuring electrical properties of organic molecules using a focused ion beam. *Thin Solid Films*, 438-439(0):374 – 377, 2003. ¡ce:title¿The 5th International Conference on Nano-Molecular Electronics¡/ce:title¿.

[9] S. Kubatkin, A. Danilov, M. Hjort, J. Cornil, J. Brédas, N. Stuhr-Hansen, P. Hedegård, and T. Bjørnholm. Single-electron transistor of a single organic molecule with access to several redox states. *Nature*, 425:698–701, 2003.

[10] A. Notargiacomo, V. Foglietti, E. Cianci, G. Capellini, M. Adami, P. Faraci, F. Evangelisti, and C. Nicolini. Atomic force microscopy lithography as a nanodevice development technique. *Nanotechnology*, 10(4):458, 1999.

[11] L. Qin, S. Park, L. Huang, and C. A. Mirkin. On-wire lithography. *Science*, 309(5731):113–115, 2005.

[12] A. Hatzor and P. S. Weiss. Molecular rulers for scaling down nanostructures. *Science*, 291:1019–1020, 2001.

[13] P. Pourhossein and R. C. Chiechi. Directly addressable sub-3 nm gold nanogaps fabricated by nanoskiving using self-assembled monolayers as templates. *ACS Nano*, 6(6):5566–5573, 2012.

[14] H. B. Akkerman and B. de Boer. Electrical conduction through single molecules and self-assembled monolayers. *J. Phys.: Condens. Matter*, 20(1):013001, 2008.

[15] G. S. McCarty. Molecular lithography for wafer-scale fabrication of molecular junctions. *Nano Lett.*, 4(8):1391–1394, 2004.

[16] T.-W. Kim, G. Wang, H. Lee, and T. Lee. Statistical analysis of electronic properties of alkanethiols in metal–molecule–metal junctions. *Nanotechnology*, 18(31):315204, 2007.

[17] M. D. Dickey, D. J. Lipomi, P. J. Bracher, and G. M. Whitesides. Electrically addressable parallel nanowires with 30 nm spacing from micromolding and nanoskiving. *Nano Lett.*, 8(12):4568–4573, 2008.

[18] E. A. Weiss, G. K. Kaufman, J. K. Kriebel, Z. Li, R. Schalek, and G. M. Whitesides. Si/sio2-templated formation of ultraflat metal surfaces on glass, polymer, and solder supports: Their use as substrates for self-assembled monolayers. *Langmuir*, 23(19):9686–9694, 2007. PMID: 17696377.

[19] R. C Chiechi, E. A. Weiss, M. D. Dickey, and G. M. Whitesides. Eutectic Gallium–Indium (EGaIn): A Moldable Liquid Metal for Electrical Characterization of Self-Assembled Monolayers. *Angew. Chem. Int. Ed.*, 120(1):148–150, January 2008.

[20] R. Powell, M. H. Francombe, and A. Ulman. *Self-Assembled Monolayers of Thiols, Volume 24 (Thin Films)*. Academic Press, 1998.

[21] B. Y. Lee, K. Heo, A. L. Schmucker, H. J. Jin, J. K. Lim, T. Kim, H. Lee, K. Jeon, Y. D. Suh, C. A. Mirkin, and S. Hong. Nanotube-bridged wires with sub-10 nm gaps. *Nano Lett.*, 12(4):1879–1884, 2012.

[22] Krzysztof Slowinski, Richard V. Chamberlain, Renata Bilewicz, and Marcin Majda. Evidence for inefficient chain-to-chain coupling in electron tunneling through liquid alkanethiol monolayer films on mercury. *Journal of the American Chemical Society*, 118(19):4709–4710, 1996.

[23] Krzysztof Slowinski, Richard V. Chamberlain, Cary J. Miller, and Marcin Majda. Through-bond and chain-to-chain coupling. two pathways in electron tunneling through liquid alkanethiol monolayers on mercury electrodes. *Journal of the American Chemical Society*, 119(49):11910–11919, 1997.

[24] H. B. Akkerman, A. J. Kronemeijer, P. A. van Hal, D. M. de Leeuw, P. W. M. Blom, and B. de Boer. Self-assembled-monolayer formation of long alkanedithiols in molecular junctions. *Small*, 4(1):100–104, 2008.

[25] J. G. Simmons. Generalized formula for the electric tunnel effect between similar electrodes separated by a thin insulating film. *J. Appl. Phys.*, 34(6):1793–1803, 1963.

[26] K. Slowinski, H. K. Y. Fong, and M. Majda. Mercury-mercury tunneling junctions. 1. electron tunneling across symmetric and asymmetric alkanethiolate bilayers. *J. Am. Chem. Soc.*, 121(31):7257–7261, 1999.

[27] H. B. Akkerman, P. W. M. Blom, D. M. de Leeuw, and B. de Boer. Towards molecular electronics with large-area molecular junctions. *Nature*, 441(7089):69–72, May 2006.

[28] M. M. Thuo, W. F. Reus, C. A. Nijhuis, J. R. Barber, C. Kim, M. D. Schulz, and G. M. Whitesides. Odd–even effects in charge transport across self-assembled monolayers. *J. Am. Chem. Soc.*, 133(9):2962–2975, 2011.

[29] H. Song, Y. Kim, H. Jeong, M. A. Reed, and T. Lee. Coherent tunneling transport in molecular junctions. *The Journal of Physical Chemistry C*, 114(48):20431–20435, 2010.

[30] W. Wang, T. Lee, and M. A. Reed. Mechanism of electron conduction in self-assembled alkanethiol monolayer devices. *Phys. Rev. B*, 68:035416, Jul 2003.

[31] E. A. Weiss, R. C. Chiechi, G. K. Kaufman, J. K. Kriebel, Z. Li, M. Duati, M. A. Rampi, and G. M. Whitesides. Influence of defects on the electrical characteristics of mercury-drop junctions: Self-assembled monolayers of n-alkanethiolates on rough and smooth silver. *J. Am. Chem. Soc.*, 129(14):4336–4349, 2007. PMID: 17358061.

[32] S. Sek, R. Bilewicz, and K. Slowinski. Electrochemical Wiring of α,ω-Alkanedithiol Molecules into an Electrical Circuit. *Chem. Commun.*, pages 404–405, 2004.

[33] R. L. Mays, P. Pourhossein, D. Savithri, J. Genzer, R. C. Chiechi, and M. D. Dickey. Thiol-containing polymeric embedding materials for nanoskiving. *J. Mater. Chem. C*, 1:121–130, 2013.

Chapter 4

Fabrication of $> 5nm$ Nanogap Electrodes by Nanoskiving

4.1 Introduction

In this chapter I describe the fabrication of electrically addressable, high-aspect-ratio nanowires of gold separated by gaps of single nanometers using vacuum-deposited aluminum and silver as a sacrificial spacer layers for gaps of > 5 nm. I fabricated these nanostructures without a clean room or any photolithographic processes by sectioning sandwich structures of gold separated by a sacrificial spacer using nanoskiving.[1–3] Electrically addressable nanogap electrodes that are separated by < 100 nm gaps have application in sensors,[4,5] as electrodes for dielectrophoresis[6,7] and electrochemistry,[8,9] and in molecular junctions.[10,11] There are limited number of methods to fabricate nanogap electrodes that are easy to address electrically. Photolithographic techniques (*i.e.*, e-beam and FIB lithography) can be used to produce addressable nanogap electrodes but they

∗ Parts of this chapter have been published in: Parisa Pourhossein and Ryan C. Chiechi, J. Vis. Exp., 2013, 75, e50406.

are restricted to the class of materials and rigid planar substrates.[12,13] The application of nanolithographic methods such as shadow mask evaporation,[14] mechanical break junctions,[15] local etching of carbon nanotubes,[16] electromigration[17] and on-wire lithography[18] are experimentally challenging. A simple an inexpensive method capable of fabricating nanowires with nanoscale spacing is nanoskiving, which has advantages over conventional methods that make it an ideal technique to be used in academic laboratories. The fabrication of electrically addressable nanowires with 30 nm spacing using nanoskiving has been reported.[19]

As I have mentioned in previous chapters, nanoskiving is a combination of the deposition of thin films and sectioning using an ultramicrotome. Nanoskiving enables the rapid fabrication of electrically-addressable nanowires with spacings of single nanometers on the bench-top. I am interested in the rapid prototyping of nanostructures for Molecular Electronics, for which nano-fabricated electrodes should not require specialized or time-consuming techniques;[20] once a block is made, it can produce hundreds of thousands of nanostructures, (serially) on demand. However, the technique is not limited to SAMs–as I have shown in Chapter 3—or Molecular Electronics and is a general method for preparing a gap between two nanostructures. I used silver and aluminum as sacrificial layers to produce gaps of various sizes between gold nanowires, but the technique is not limited to these materials (or to metallic nanowires).[21] The wires are pick-and-place and are compatible with magnetic alignment, thus they can be placed on arbitrary substrates.[22]

4.2 Fabrication

Figure 4.1 summarizes the procedure that I used to produce nanowires with a well-defined spacing between them. Gold features ($1 - 2$ mm in length) are deposited by evaporation through a Teflon mask onto a silicon substrate. Epofix (Electron Microscopy Sciences) epoxy pre-polymer is poured over the

entire wafer, covering the gold features, when the epoxy is cured, the epoxy is separated from the wafer (*i.e.*, via template stripping); the gold features remain adhered to the epoxy. As metallic sacrificial layers, aluminum or silver is evaporated with the desired thickness through the teflon mask with an offset of $250 - 500$ μm over the gold features. The thickness of this layer will define the spacing of the nano-gap between the gold wires. The lower limit depends on the metal, but is $\sim$ 5 nm for aluminum and silver, below which the layers become discontinuous. The second layer of gold (or another metal) is deposited onto the aluminum or silver layer. The offset will eventually define the longest dimension of the gap, and it can be accurately measured using a micro-ruler before embedding the entire structure in epoxy for sectioning. Then the whole structure is embedded in a block of epoxy which is then ready for sectioning with an ultramicrotome.

4.2.1 Preparation of a block for sectioning

I treated a technical-grade 3" silicon wafer in an air plasma cleaner for 30 seconds and then exposed it to (tridecafluoro-1,1,2,2,-tetrahydrooctyl)trichlorosilane vapor for one hour. (This step is necessary to prevent the epoxy from adhering to the silicon wafer.) I deposited a layer of gold (usually 100 nm-thick, which defines the width of the wires) through a Teflon master (that defines the length of the resulting wires; 0.5 mm, 1 mm, or 1.5 mm) onto the pre-treated silicon wafer. then, I covered the entire wafer with $\sim$ 8.5 mL of Epofix epoxy pre-polymer and cured it for three hours at 60 °C. In the next step, I template-stripped the gold layer by carefully peeling the epoxy from the wafer such that the gold remains attached to the cured epoxy. I inserted the edge of a razor blade at the interface between the silicon wafer and epoxy and then gently peeled the epoxy layer from the silicon wafer. Because of the poor adhesion of gold to the fluorinated silicon wafer, the gold features remain adhered to the epoxy. I placed the same Teflon mask back over the gold features, but laterally offset by $\sim$ 80% of the shortest dimension of the gold features and deposited a layer of aluminum or silver through

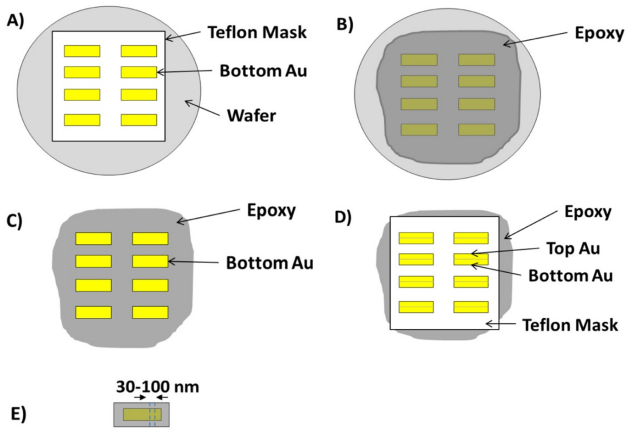

Figure 4.1: A schematic (not to scale) of the procedure used to fabricate nanogap structures. A) First layer (100 nm-thick) of gold is deposited through a Teflon shadow mask onto a fluorinated silicon wafer via thermal evaporation. B) After removal of the mask the whole surface of silicon is covered in epoxy. C) After the epoxy cures, it is separated from the wafer such that the gold features remain adhered to the epoxy (*i.e.*, Template stripping). D)The Teflon mask is placed over the gold features with an offset of $250 - 500\ \mu\mathrm{m}$ and aluminum or silver is evaporated with the desired thickness onto gold features. Afterwards, another 100 nm-thick layer of gold (or any other metal) is deposited. E) The mask is removed and the the resulting features are rough-cut with a jeweller's saw and are then embedded in epoxy in microtome mold to produce the blocks to be sectioned with an ultramicrotome. Reproduced with permission from Ref.[23].

the Teflon master. This offset will eventually define the length of the overlap between two gold electrodes and it can be measured with a micro-ruler. Then I deposited a second layer of gold or any other metal through the mask (This layer will typically be composed of the same metal at the thickness as the first which was 100 nm-thick in this case). Afterwards I removed the Teflon mask, taking care not to scratch the features, which will result in broken nanowires. I re-embedded the entire substrate in Epofix pre-polymer ($\sim$ 8.5 mL) and cured it for at least three hours at 60 °C. I cut the features out using a jeweler's saw (into $\sim$4 x 10 mm pieces) and placed each into a separate well in a polyethylene 'coffin' microtome mold, filled the mold with Epofix pre-polymer and cured it overnight at 60 °C.

Figure 4.2 shows images of each step of the procedure. In Figure 4.2A, deposited gold features on Si wafer is shown. The result of template-stripping–gold features with ultra smoth surface onto a epoxy substare–is shown in Figure 4.2B. After rough cutting using jeweler's saw, I ended up with individual strips (Figure 4.2C) Placing these strips in a microtome polyethylene mold and curing them in excess epoxy yeilds the final block (Figure 4.2D).

4.2.2 Sectioning

I removed a block from the polyethylene mold and mounted it in the sample holder, attached it to the trimming attachment and placed it in the ultramicrotome. Then, I cleaned a razor blade with ethanol to remove lubricant and metal fragments and inspected the edge of the razor blade under the stereoscope of the ultramicrotome. Any remaining fragments will damage the diamond knife during sectioning. I trimmed the block to the width of the diamond knife (I used 2 mm or 4 mm Diatome Ultra 35°) in a trapezoid shape (because it is the most stable shape for sectioning). In the next step, I aligned the edge of a glass knife parallel to the bottom edge of the block. I started pre-cutting with ultramicrotome (I used a Leica EMUC-6) equipped with a glass knife to define a smooth surface on the surface of the block. To fabricate a metallic structure,

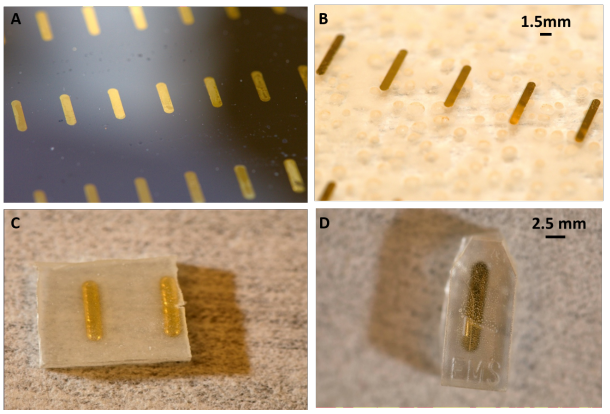

Figure 4.2: Images of the procedure that have been taken after each step. A) Gold features on Si wafer, B) Gold features transferred to epoxy after template-stripping, C) Strips after being cut out with jeweler's saw, D) Final block ready to be mounted in ultramicotome

I replaced the glass knife with a diamond knife, re-aligned it, and sectioned the block to either 100 nm at 1 mm/s or 50 nm at 0.6 mm/s. Epofix sections are stable down to $\sim$ 30 nm. An easy verification of the thicknesses of the sections is their color, which varies predictably as a function of thickness and does not depend on the resin; reference cards are available.[24] I collected the epoxy sections containing the structures from the surface of water in the reservoir of the knife either individually using a Perfect Loop (Electron Microscopy Sciences) or as ribbons of several sections to an Si/SiO_2 (for SEM) or SiO_2 (for electrical measurements) substrate by placing substrate under the surface of the water and raising it slowly. I dried the sections at 60 °C for 3 hours to improve their adhesion to the substrate.

4.2.3 Etching out the sacrificial layer

I placed 100 nm-thick sections containing 5 nm of aluminum in a 2 M aqueous solution of HCl for 2 hours and then rinsed them with ethanol and dried them with nitrogen before drying at 60 °C for 2 hours. I exposed 100 nm -thick

sections containing 5 nm silver to oxygen plasma for 10 minutes (The duration of plasma oxidation depends on the power of plasma oxdizer). The selection of materials allows either wet-etching (using HCl) or dry-etching (using oxygen plasma), however silver can be removed by wet etching as well.

4.3 Electron Microscopy

I prepared nanogap structures by incorporating two metallic sacrificial layers as the spacer: aluminum or silver. I etched these layers to obtain gaps of the desired thicknesses. As I described in Fabrication, after sectioning I exposed the structures containing silver to oxygen plasma, and those containing aluminum to aqueous HCl. Figure 4.3 shows scanning electron micrographs (SEMs) of the resulting nanowires with nanometer-scale separation. In both cases gaps are clearly visible and directly measurable. Figure 4.3A shows two nanowires of gold separated by a 5 nm gap produced after etching out aluminum. In Figure 4.3B, two nanowires of gold and aluminum are separated by a 5 nm gap after the removal of silver. The top electrode is gold and the bottom one is aluminum. Thus, we can use different metals to fabricate nanogap electrodes with different work functions. Using different metals as electrodes is not restricted to using metals as sacrificial layers. I fabricated STANs by incorporating gold and aluminum as electrodes. Figure 4.4 shows the SEM image of a STAN using 16-mercaptohexadecanoicacid as gap template. The top electrode is gold and the bottom one is aluminum.

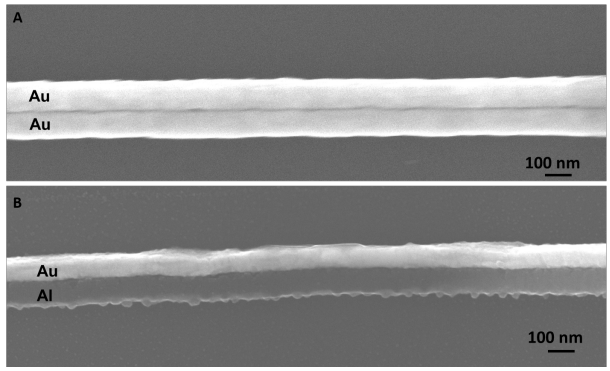

Figure 4.3: Scanning electron micrographs of the nanogaps produced using aluminum (top) and silver (bottom) as the spacer. The top image shows two nanowires of gold with the gap in between produced by etching out the aluminum layer with aqueous HCl. The bottom image shows two nanowires of gold and aluminum with the gap produced by etching out the silver layer with oxygen plasma. The gap is clearly visible in both cases. Reproduced with permission from Ref. [23].

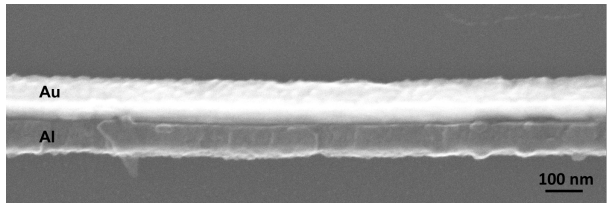

Figure 4.4: Scanning electron micrograph of a STAN produced using gold and aluminum as electrodes and SAM of 16-mercaptohexadecanoicacid as the template.

4.4 Conclusions

In this Chapter I demonstrated the fabrication of addressable nanogap electrodes using sacrificial layers of aluminum and silver to achieve gaps larger than 5 nm. I can control the gap size by depositing desired thickness of sacrificial layer. Wet-etching and dry-etching can be exploited to remove the sacrificial layers. I have shown that combination of different work function metals allows construction of asymetrical nanogap electrodes. Insertion of molecules that show photovoltaic effects in these gaps which their size is within the range of exciton diffusion length can be promising to construct organic solar cells with higher efficiencies. But one crucial step towards this application is to fabricate interdigitated nanogap electrodes.

Bibliography

[1] D. J. Lipomi, R. V. Martinez, and G. M. Whitesides. Use of thin sectioning (nanoskiving) to fabricate nanostructures for electronic and optical applications. *Angew. Chem. Int. Ed.*, 50(37):8566–8583, 2011.

[2] Q. Xu, R. M. Rioux, M. D. Dickey, and G. M. Whitesides. Nanoskiving: A new method to produce arrays of nanostructures. *Acc. Chem. Res.*, 41(12):1566–1577, 2008.

[3] Q. Xu, R. M. Rioux, and G. M. Whitesides. Fabrication of complex metallic nanostructures by nanoskiving. *ACS Nano*, 1(3):215–227, 2007.

[4] K. Ramanathan, M. A. Bangar, M. Yun, W. Chen, N. V. Myung, and A. Mulchandani. Bioaffinity sensing using biologically functionalized conducting-polymer nanowire. *J. Am. Chem. Soc.*, 127(2):496–497, 2005.

[5] M. Yun, N. V. Myung, R. P. Vasquez, C. Lee, E. Menke, and R. M. Penner. Electrochemically grown wires for individually addressable sensor arrays. *Nano Lett.*, 4(3):419–422, 2004.

[6] A. Bezryadin, C. Dekker, and G. Schmid. Electrostatic trapping of single conducting nanoparticles between nanoelectrodes. *Appl. Phys. Lett.*, 71(9):1273–1275, 1997.

[7] R. Hölzel, N. Calander, Z. Chiragwandi, M. Willander, and F. F. Bier. Trapping single molecules by dielectrophoresis. *Phys. Rev. Lett.*, 95:128102/1–128102/4, 2005.

[8] R. W. Murray. Nanoelectrochemistry: Metal nanoparticles, nanoelectrodes, and nanopores. *Chem. Rev.*, 108(7):2688–2720, 2008. PMID: 18558753.

[9] D. W. M. Arrigan. Nanoelectrodes, nanoelectrode arrays and their applications. *Analyst*, 129:1157–1165, 2004.

[10] N. J. Tao. Electron transport in molecular junctions. *Nat. Nanotechnol.*, 1:173–181, 2006.

[11] A. Nitzan and M. A. Ratner. Electron transport in molecular wire junctions. *Science*, 300(5624):1384–1389, 2003.

[12] F. Carcenac, L. Malaquin, and C. Vieu. Fabrication of multiple nano-electrodes for molecular addressing using high-resolution electron beam lithography and their replication using soft imprint lithography. *Microelectron. Eng.*, 61 - 62:657 – 663, 2002.

[13] B. D. Gates, Q. Xu, J. C. Love, D. B. Wolfe, and G. M. Whitesides. Unconventional nanofabrication. *Annu. Rev. Mater. Res.*, 34(1):339–372, 2004.

[14] J. Tang, Y. Wang, J. E. Klare, G. S. Tulevski, S. J. Wind, and C. Nuckolls. Encoding molecular-wire formation within nanoscale sockets. *Angew. Chem. Int. Ed*, 46(21):3892–3895, 2007.

[15] H. Ohnishi, Y. Kondo, and K. Takayanag. Quantized conductance through individual rows of suspended gold atoms. *Nature*, 395:780–783, 1998.

[16] X. Guo, J. P. Small, J. E. Klare, Y. Wang, M. S. Purewal, I. W. Tam, B. H. Hong, R. Caldwell, L. Huang, S. O'Brien, J. Yan, R. Breslow, S. J. Wind, J. Hone, P. Kim, and C. Nuckolls. Covalently bridging gaps in single-walled carbon nanotubes with conducting molecules. *Science*, 311:356–359, 2006.

[17] H. Park, A. K. L. Lim, A. P. Alivisatos, J. Park, and P. L. McEuen. Fabrication of metallic electrodes with nanometer separation by electromigration. *Appl. Phys. Lett.*, 75(2):301–303, 1999.

[18] L. Qin, S. Park, L. Huang, and C. A. Mirkin. On-wire lithography. *Science*, 309(5731):113–115, 2005.

[19] M. D. Dickey, D. J. Lipomi, P. J. Bracher, and G. M. Whitesides. Electrically addressable parallel nanowires with 30 nm spacing from micromolding and nanoskiving. *Nano Lett.*, 8(12):4568–4573, 2008.

[20] P. Pourhossein and R. C. Chiechi. Directly addressable sub-3 nm gold nanogaps fabricated by nanoskiving using self-assembled monolayers as templates. *ACS Nano*, 6(6):5566–5573, 2012.

[21] D. J. Lipomi, R. C. Chiechi, M. D. Dickey, and G. M. Whitesides. Fabrication of conjugated polymer nanowires by edge lithography. *Nano Lett.*, 8(7):2100–2105, 2008. PMID: 18517256.

[22] D. J. Lipomi, F. Ilievski, B. J. Wiley, P. B. Deotare, M. Lončar, and G. M. Whitesides. Integrated fabrication and magnetic positioning of metallic and polymeric nanowires embedded in thin epoxy slabs. *ACS Nano*, 3(10):3315–3325, 2009.

[23] P. Pourhossein and R. C. Chiechi. Fabricating nanogaps by nanoskiving. *J. Vis. Exp.*, 75:e50406, 2013.

[24] R. L. Mays, P. Pourhossein, D. Savithri, J. Genzer, R. C. Chiechi, and M. D. Dickey. Thiol-containing polymeric embedding materials for nanoskiving. *J. Mater. Chem. C*, 1:121–130, 2013.

Chapter 5

Construction of Tunneling Junctions from Arbitrary Dithiols

5.1 Introduction

Self-assembled monolayers (SAMs) are ordered molecular assemblies formed by the spontaneous adsorption of an active surfactant on a solid surface via static self-assembly (Figure 5.1).[1–3] Very complex systems in Nature result from the self-assembly of interlocking components.[4] Nuzzo and Allara showed that SAMs of alkanethiols can be prepared by the chemisorption of di-n-alkyl disulfides on gold substrates from dilute solutions.[5] Many self-assembly systems have since been studied, but SAMs of alkanethiols on gold are the most studied ones to date.[6–11]

It has been reported that once SAMs are formed on a surface, molecules desorb in a few days upon exposure to air in the absence of light.[12–14] Other studies show that well-packed SAMs of alkanethiols are stable in air for more than one month; by contrast, however, loosely packed SAMs undergo an undefined structural change over one month.[15] SAMs of alkanethiols readily desorb upon

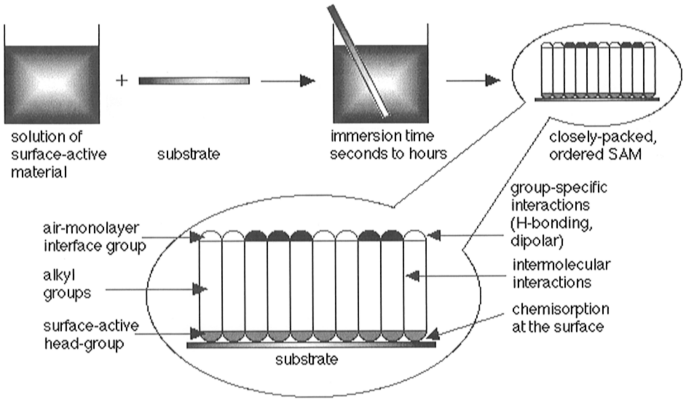

Figure 5.1: Self-assembled monolayers are formed by simply immersing a substrate in a solution of the surface-active material. The driving force for the spontaneous formation of the 2D assembly includes chemical bond formation of molecules with the surface and intermolecular interactions. Reproduced with permission from Ref. [1]

heating to elevated temperatures (*e.g.*, 70 °C) in a hydrocarbon solvent[16] and can be exchanged from the surface by immersion in a solution containing a different thiol.[16–18] Although the exact mechanism is not clear yet, it is accepted generally that the adsorption of thiols on gold proceeds with the cleavage of the SH bond.[19] Thus, the adsorption of an alkanethiol (RSH) on Au(s) produces RSAu(s) instead of RSHAu(s). The exchange of adsorbed thiol (R_1SAu) with a different thiol (R_2SH) in solution would also give R_2SAu. When R_1 and R_2 are different groups, many different methods can be used to measure the quantity of each molecule on the surface. For example, to monitor the exchange, Whitesides and co-workers measured contact angles for thiols of different terminal groups, normal alkanethiol and ω-hydroxyalkanethiols.[20]

We are interested in fabrication of SAM-templated addressable nanogap (STAN) electrodes from arbitrary dithiols (*e.g.*, OPEs) and not only alkanedithiols; we would like to have a general platform to construct tunneling junctions from molecules of interest. Unfortunately, not all SAMs can serve as gap templates directly (they are fragile or delicate); thus, we have to look for an alternative

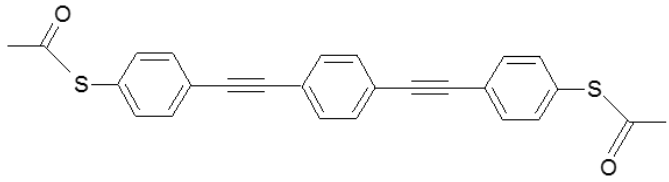

Figure 5.2: OPE3 molecule. Suffix 3 refers to the number of phenyl rings.

way of fabricating such devices. Conjugated molecules, namely oligo(phenylene ethynylenes) (OPEs) (Figure 5.2), serve as "molecular wires" in molecular electronic (ME) devices.[21,22] The first report on mixed SAMs containing conjugated thiols was given by Tour et.al.[23] In 2011, Valkenier et al. reported a systematic study on the formation of SAMs of OPEs for ME devices.[24] We are interested in incorporating OPE molecules in STAN electrodes. However, it is not possible to fabricate STANs from SAMs of OPE molecules directly. These moleules are delicate and will not survive the second metal deposition. Thus, we took advantage of the dynamic exchange phenomena in SAMs to replace alkanethiols with OPEs and construct tunneling junctions.

5.2 Experimental Section

I used STAN electrodes fabricated using SAMs of alkanedithols to insert OPE3 molecules in the gaps via exchange. I chose STANs of 1,14-tetradecanedithiol and 1,16-hexadecanedithiol so that the gap size was within the same length as OPE3 molecules—I put STANs on glass substrates that were cleaned with Piranha solution to increase the adhesion of sections to the substrate. I incubated these STANs in a 0.45 mM soultion of OPEs in THF and triethylamine. OPE3 molecules are not compatible with protic solvents, therefore aprotic solvents such as THF are used. I took out STANs from OPE3 solution with certain time intervals, rinsed them with THF and dried them with nitrogen flow. Using the same procedure to electrically address nanogap electrodes that I have described

in Chapter 3, I performed electrical characterization.

5.3 Results and Discussion

OPEs are more conductive than alkanedithiols; Thus, electrical measurements provide us an indirect estimate to verify the insertion of OPEs in the gap. Figure 5.3 shows the plot of current density versus immersion time for STANs of 1,14-tetradecanedithiol incubated in OPE3 solution with different time intervals. The value of current density that is shown is the value collected at 500 mV. As is shown in this plot, the highest current density obtained is for one hour incubation. Increasing the immersion time results in a decrease in current density which, after 8 days (as it is depicted in the inset of Figure 5.3), almost reaches the initial value of current density which corresponds to alkanedithiol. The yield of working STANs decreases dramatically as we increase the incubation time. We know that THF swells the epoxy, which likely causes the STANS to deform upon prolonged exposure.

Finding out that the incubation of STANS in OPE3 solution for one hour gives the highest current density, I continued all the measurements after one hour of immersion. The general platform that I have used to exchange alkanedithiols with OPE3 is shown in Figure 5.4. The red box shows the procedure to exchange 1,14-tetradecanedithiol with OPE3. Blue and pink boxes refer to two control experiments that I have performed. The pink box refers to the exchange of 1,14-tetradecanedithiol with octanethiol. Exchange with OPE3 and again re-incubation in 1,14-tetradecanedithiol solution is shown in the blue box. The results are shown in Figure 5.5. As is shown in the J/V plot, after incuabtion of STANs in OPE3 solution for one hour, the current density increases by almost 1.5 orders of magnitute; Black squares are the data for STANs of 1,14-tetradecanedithiol and red circles are the data corresponding to exchange with OPE3. This incease in conductance was expected due to the higher conductivity of OPE3s; however, we have no estimate of how many OPE3s re-

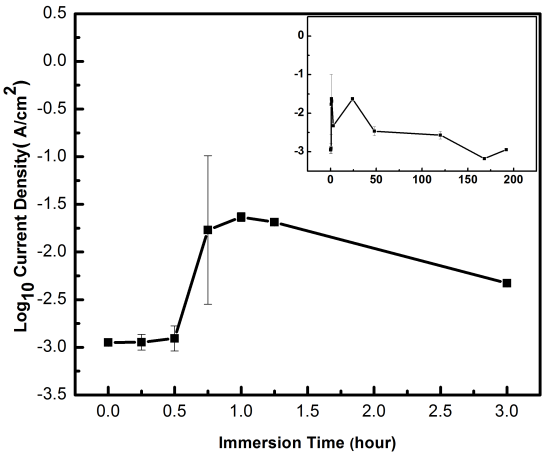

Figure 5.3: A plot of current density versus immersion time for STANs of 1,14-tetradecanedithiol incubated in OPE3 solution with different time intervals. The inset is the same plot for incubation up to 8 days (192 hours).

place alkanedithiols. It is known from the literature that even 15 percent of any defects with higher conductance will dominate the conductance characteristics of a junction. To prove that this increase in current density is indeed the result of insertion of OPE3s in the gap, I incubated the STANS of 1,14-tetradecanedithiol in a solution containing octanethiol. Octanethiol molecules are much shorter than the gap size and can not span the distance between two electrodes. Thus, we would expect lower current densities in this case. As it is shown in Figure 5.5, the current density decreases once we incubate STANs of 1,14-tetradecanedithiol in octanethiol solution (pink downward triangles). I performed another control experiment to check whether the exchange phenomenon is reversible in the nanogaps or not. For this experiment, I incubated the STANS of 1,14-tetradecanedithiol in OPE3 solution for one hour and after rinsing them with THF, I re-incubated them in a solution containing 1,14-tetradecanedithiol. The J/V data shows that the current density drops down and it is within the

error bars of current density for 1,14-tetradecanedithiol.

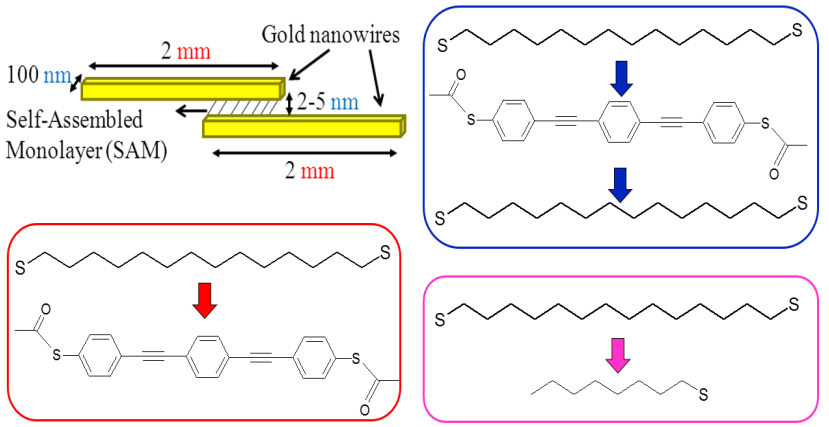

Figure 5.4: The general platform to do exchange. Red box shows the exchange of alkanedithiol with OPE3s. Pink box is the exchenge of alkanedithiol with a short alkanethiol. In blue box, exchange with OPE3 and again with alkanedithiol is shown.

To verify that the increase in current upon incubation in OPE3 is not the effect of solvent (THF), I did measurements on STANs that were incubated in THF for one hour. J/V data in Figure 5.6 indicates that this incubation results in an increase in current (red circles) but this increase is not as high as the increase when OPE3s are in solution. This results confirm that the OPE3s are indeed playing a role in increasing the current. I repeated the same experiments with ethanol and DCM. In both cases, the current density remained within the same value. Incubation in chloroform for one hour destroyed the STANS, as chloroform swells epoxy considerably and detaches the sections from substrate.

I incubated STANs of 1,16-hexadecanedithiol in OPE3 solution for one hour. The corresponding J/V plot is shown in Figure 5.7. The incresae in current density as a result of exchange is obtained in this case as we expected (red cir-

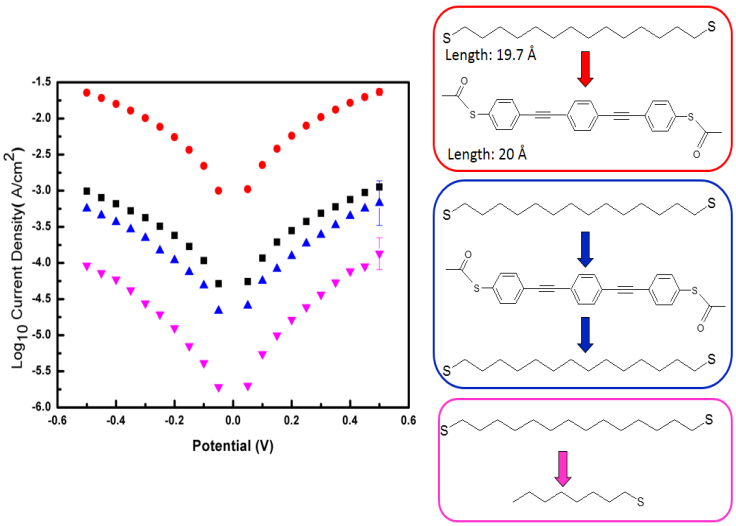

Figure 5.5: Plots of current density versus potential for STANs of 1,14-tetradecanedithiol (black squares), exchange with OPE3 (red circles), exchange with octanethiol (pink downward triangles) and exchange with OPE3 and again re-incubation in 1,14-tetradecanedithiol solution (blue upward triangles). Each plot is an average of at least ten scans from ten different STAN electrodes. The error bars are the variance.

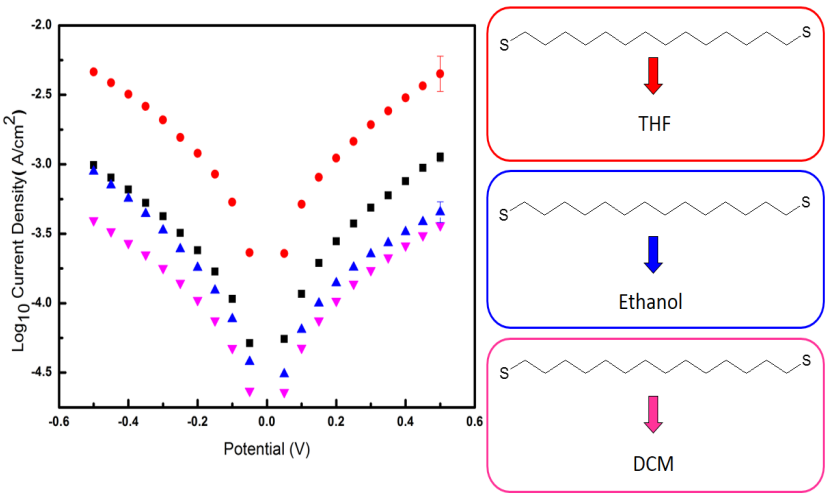

Figure 5.6: Plots of current density versus potential for STANs of 1,14-tetradecanedithiol (black squares), incubation in THF (red circles), incubation in DCM (pink downward triangles) and incubation in ethanol (blue upward triangles). Each plot is an average of at least ten scans from ten different STAN electrodes. The error bars are the variance.

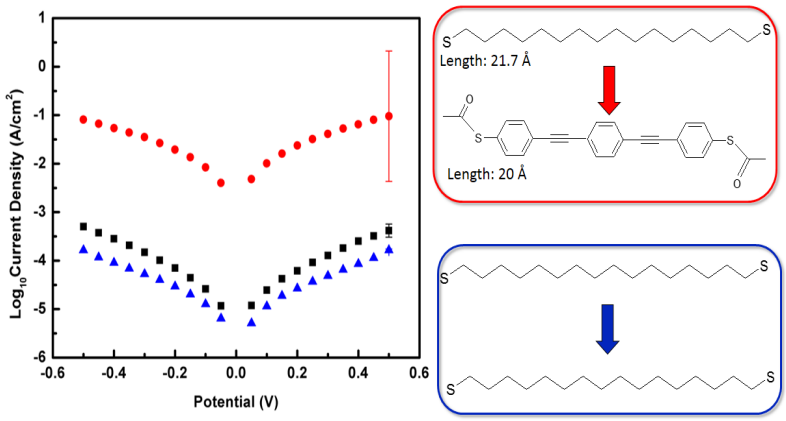

Figure 5.7: Plots of current density versus potential for STANs of 1,16-hexadecanedithiol (black squares), incubation in OPE3 solution for one hour (red circles) and incubation in 1,16-hexadecanedithiol (blue triangles). Each plot is an average of at least ten scans from ten different STAN electrodes. The error bars are the variance.

cles); This incease is almost two orders of magnitute. If I incubate the STANs of 1,16-hexadecanedithiol in soultion containing the same alkanedithiols, I predict to obtain the same current density as the same molecules are going to exchange in the gap. This is indeed the outcome of measurements (blue triangles in Figure 5.7).

5.4 Conclusions

The goal of this work was to provide a simple and general platform to construct tunneling junctions from conjugated molecules such as OPEs. I have demonstrated that taking advantage of exchange phenomena, we can fabricate junctions from arbitrary symmetrical dithiols that can not directly serve as the template for STANs. Once the blocks using different length alkanedithiols are

fabricated, we can choose the right gap size, nanoskive them and incubate them in a solution of the desired molecule. The facile nature of this procedre allows us to construct nanodevices for molecular electronics. The combination of nanoskiving method and the dynamic exchange of SAMs enables rapid prototyping of molecular electronic devices which are truly solid state devics and not just spectroscopic platforms for fundemental investigations which is far from practical applications.

Bibliography

[1] A. Ulman. Formation and structure of self-assembled monolayers. *Chem. Rev.*, 96(4):1533–1554, 1996.

[2] A. Ulman. *Thin Films- Self-Assembled Monolayers of Thiols*. Academic Press: Boston, MA, 1998.

[3] G. M. Whitesides and P. E. Laibinis. Wet chemical approaches to the characterization of organic surfaces: self-assembled monolayers, wetting, and the physical-organic chemistry of the solid-liquid interface. *Langmuir*, 6(1):87–96, 1990.

[4] H. Kuhn and A. Ulman. *Supramolecular assemblies: vision and strategy*. Academic Press: New York, 1995.

[5] R. G. Nuzzo and D. L. Allara. Adsorption of bifunctional organic disulfides on gold surfaces. *J. Am. Chem. Soc.*, 105(13):4481–4483, 1983.

[6] C. D. Bain and G. M. Whitesides. Formation of monolayers by the coadsorption of thiols on gold: variation in the length of the alkyl chain. *J. Am. Chem. Soc.*, 111(18):7164–7175, 1989.

[7] M. M. Walczak, C. Chung, S. M. Stole, C. A. Widrig, and M. D. Porter. Structure and interfacial properties of spontaneously adsorbed n-alkanethiolate monolayers on evaporated silver surfaces. *J. Am. Chem. Soc.*, 113(7):2370–2378, 1991.

[8] K. Shimazu, I. Yagi, Y. Sato, and K. Uosaki. In situ and dynamic monitoring of the self-assembling and redox processes of a ferrocenylundecanethiol monolayer by electrochemical quartz crystal microbalance. *Langmuir*, 8(5):1385–1387, 1992.

[9] G. K. Rowe and S. E. Creager. Redox and ion-pairing thermodynamics in self-assembled monolayers. *Langmuir*, 7(10):2307–2312, 1991.

[10] T. W. Schneider and D. A. Buttry. Electrochemical quartz crystal microbalance studies of adsorption and desorption of self-assembled monolayers of alkyl thiols on gold. *J. Am. Chem. Soc.*, 115(26):12391–12397, 1993.

[11] F. Nüesch, F. Rotzinger, L. Si-Ahmed, and L. Zuppiroli. Chemical potential shifts at organic device electrodes induced by grafted monolayers. *Chem. Phys. Lett*, 288(5 - 6):861 – 867, 1998.

[12] M. H. Schoenfisch and J. E. Pemberton. Air stability of alkanethiol self-assembled monolayers on silver and gold surfaces. *J. Am. Chem. Soc.*, 120(18):4502–4513, 1998.

[13] M. Lee, C. Hsueh, M. S. Freund, and G. S. Ferguson. Air oxidation of self-assembled monolayers on polycrystalline gold:the role of the gold substrate. *Langmuir*, 14(22):6419–6423, 1998.

[14] J. R. Scott, L. S. Baker, W. R. Everett, C. L. Wilkins, and I. Fritsch. Laser desorption fourier transform mass spectrometry exchange studies of air-oxidized alkanethiol self-assembled monolayers on gold. *Anal. Chem.*, 69(14):2636–2639, 1997.

[15] Y.-S. Shon and T. R. Lee. Desorption and exchange of self-assembled monolayers (sams) on gold generated from chelating alkanedithiols. *J. Phys. Chem. B*, 104(34):8192–8200, 2000.

[16] C. D. Bain, E. B. Troughton, Y. T. Tao, J. Evall, G. M. Whitesides, and R. G. Nuzzo. Formation of monolayer films by the spontaneous assembly of organic thiols from solution onto gold. *J. Am. Chem. Soc.*, 111(1):321–335, 1989.

[17] J. B. Schlenoff, M. Li, and H. Ly. Stability and self-exchange in alkanethiol monolayers. *J. Am. Chem. Soc.*, 117(50):12528–12536, 1995.

[18] C. Chung and M. Lee. Exchange of self-assembled thiol monolayers on gold: characterization by ft-ir external reflection spectroscopy. *Journal of Electroanalytical Chemistry*, 468(1):91 – 97, 1999.

[19] C.-J. Zhong and M. D. Porter. Evidence for carbon-sulfur bond cleavage in spontaneously adsorbed organosulfide-based monolayers at gold. *J. Am. Chem. Soc.*, 116(25):11616–11617, 1994.

[20] C. D. Bain, J. Evall, and G. M. Whitesides. Formation of monolayers by the coadsorption of thiols on gold: variation in the head group, tail group, and solvent. *J. Am. Chem. Soc.*, 111(18):7155–7164, 1989.

[21] N. Weibel, S. Grunder, and M. Mayor. Functional molecules in electronic circuits. *Org. Biomol. Chem.*, 5:2343–2353, 2007.

[22] R. L. McCreery and A. J. Bergren. Progress with molecular electronic junctions: Meeting experimental challenges in design and fabrication. *Adv. Mater.*, 21(43):4303–4322, 2009.

[23] J. M. Tour, L. Jones, D. L. Pearson, J. J. S. Lamba, T. P. Burgin, G. M. Whitesides, D. L. Allara, A. N. Parikh, and S. Atre. Self-assembled monolayers and multilayers of conjugated thiols, .alpha.,.omega.-dithiols, and thioacetyl-containing adsorbates. understanding attachments between potential molecular wires and gold surfaces. *J. Am. Chem. Soc.*, 117(37):9529–9534, 1995.

[24] H. Valkenier, E. H. Huisman, P. A. van Hal, D. M. de Leeuw, R. C. Chiechi, and J. C. Hummelen. Formation of high-quality self-assembled monolayers of conjugated dithiols on gold: Base matters. *J. Am. Chem. Soc.*, 133(13):4930–4939, 2011.

Chapter 6

Optical Gating in Molecular Junctions

6.1 Introduction

Molecular electronics can benefit from utilizing molecules whose conductivity changes by an external stimuli such as light,[1] temperature,[2] magnetic field,[3] etc.[4–9] However, one of the challenges that still remains in the field is being able to control the conductance of the molecules upon applying such stimuli.[10] Optoelectronic devices like these, in which their key components are photochromic species, have great potential for various applications. Once a molecule absorbs a photon, an electron is promoted to an excited state and this excitation can result in photoisomerization. To the best of our knowledge the difference in conductance for molecules as a result of irradiation reported in literature is attributed only to different isomers of the molecule, *i.e.*, photoisomerization. In all of these cases, to have reversible switching two different external stimuli (light with another wavelength or heat) are required and usually it is not a fast reaction (it can take 45 minutes).[20] Charge transport through

photochromic molecules has been investigated both in single molecule and self-assembled monolayer (SAM) systems. Current-probe atomic force microscopy (CP-AFM),[11,12] scanning tunneling microscopy (STM),[13] mecanically controllable break junctions (MCBJ)[14,15] and other methods[16–18] have been used to address this issue. Most of the experimental studies have been focused on dithienylethene,[19] stilbene[16] and azobenzene[18] as the photo-switchabe components. Recently, Wandlowski and co-workers reported charge transport in reversible photo-thermal switching of a bispyridine-appended dimethyldihydropyrene/cyclophanediene system using single-molecule conductance in MCBJs.[20] However, what was reported was the difference in conductivity of molecules sampled from a population in solution that was photoisomerized; they did not switch molecules in a tunneling junction. Graphene-molecule junctions have been investigated using azobenzene as the photoswitchabe component; In these devices, reversible switching occurs by using an external stimuli such as light with different wavelengths or different pH values.[5] Li et al. have used transparent graphene oxide films as top contacts to investigate photo switching in dihydroazulene/vinylheptafulvalene systems.[21] Photoswitchable monolayers of aryl azobenzenes sandwiched between two transparant graphene electrodes have been reported by Seo et.al.[22] These, too, required different external stimuli to affect reversible switching. The photovoltaic effect of SAMs of hemicyanines with donor and acceptor moieties on a gold substrate in a Au/SAM/liquid junction has been studied.[23] The electron donating strength of the donor part of the molecule influences photocurrent generation. In this chaper, we investigate the difference in transient conductance of SAMs of these hemicyanine molecules (Figure 6.1) upon exposure to light with certain wavelengths. I fabricated SAM-templated addressable nanogap (STAN) electrodes using hemicyanine molecules and studied the charge transport in STANs under illumination and in the dark.

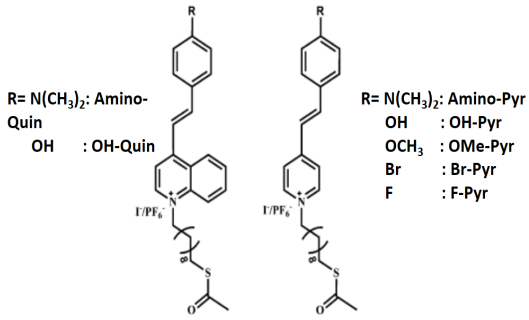

Figure 6.1: Chemical structure of hemicyanine molecules

6.2 Fabrication

I used the same procedure that I described in Chapter 3 to fabricate STAN electrodes. The only difference is that instead of alkanedithiols, I used SAMs of hemicyanine molecules; all dimensions are the same except for the gap size which in these devices is defined by the thickness of SAMs of hemycyanine molecules. Vijayaraghavan et al. reported the procedure to form dense monolayers of these hemicyanines.[23] I followed the same protocol, using 1 mM solutions of hemicyanines, 1 equivalent of 1,8-diazabicyclo[5.4.0]undec-7-ene (DBU) as base and 1 equivalent of tri-n-butyl-phosphine in methanol. Hemicyanines with I^- as counterions are less stable than hemicyanines with PF_6^- counterions under basic conditions. I fabricated STANs of Amino-Quin and OMe-Pyr successfully. Unfortunately the other molecules are too fragile to serve as gap templates.

6.3 Results and Discussion

Normalized absorption spectra of the molecules (shown in Figure 6.1) in dilute chloroform solution is depicted in Figure 6.2. The Amino-Quin molecule has the most red-shifted absorption, whereas the most blue-shifted absorption in the

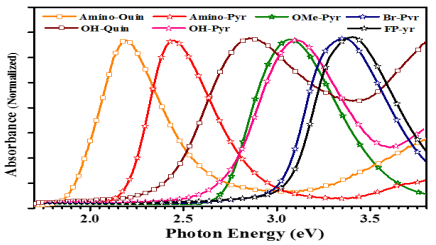

Figure 6.2: Normalized absorption spectra of hemicyanine molecules in chloroform. Reproduced with permission from Ref. [23].

spectra corresponds to F-Pyr. In SAMs of hemicyanines on gold substrates, the maximum of the absorption spectra is blue-shifted and broadening of the band is observed which is due to the formation of H-aggregates of the molecules.[23]

To see if photo–gating of the fabricated STANs has any effect on their conductance characteristics, I performed electrical measurements in the dark and under illumination. I used the same procedure to address the STANs as I have described in Chapter 3. I collected I/V data in four different situations: 1) Irradiation with green laser pointer ($\lambda = 532$ nm), 2) Irradiation with purple laser pointer ($\lambda = 405$ nm), 3) Irradiation with red laser pointer ($\lambda = 650$ nm), 4) No irradiation. The power of laser pointers are listed in Table 6.1.

Table 6.1: The power of laser pointers

Wavelength (nm)	**Power (mW)**
Green - 532	12.5
Purple - 405	1.5
Red - 650	2.8

In Figure 6.3, I/V plot for STANs of OMe-Pyr is shown. The data have

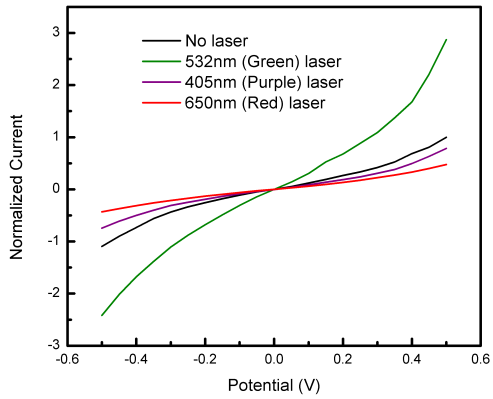

Figure 6.3: Normalized current versus potential for STANs of OMe-Pyr in four different situations; When there is no irradiation with lasers (black line), irradiation with green laser (green line), irradiation with prurple laser (purple line) and irradiation with red laser (red line). Each plot is an average of at least ten scans from ten different STAN electrodes.

been normalized to the value of current with no irradiation. As it is abvious from this plot, upon exposure of STANs to different wavelength lasers, a change in tunneling current is observed. The highest change occures when green laser pointer is used. To check if isomerization happens upon irradiation (*i.e.*, any ring open/closure), I irradiated OMe-Pyr molecules with UV light for 8 minutes. I used two UV wavelengths of 365 nm and 245 nm. The absorption spectra are depicted in Figure 6.4. We do not see any change in the position of the maximum of the spectra or any broadening. With this we can rule out the possibility of ring open/closure in the molecules. Our hypothesis to explain this phenomenon is that there is no photoisomerization involved here as this process is fast and we do not need any stimuli to drive the reaction back; right after turning off the laser we see that the current goes back to the initial value. Thus, this change in conductivity may be due to a different rate of tunneling in the ground and excited state of the molecule.

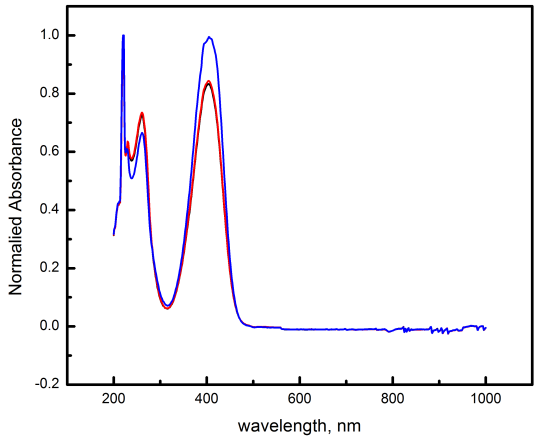

Figure 6.4: Normalized absorption spectra for OMe-Pyr molecules; Black spectra refers to the absorption in the absence of irradiation with UV light, red line refers to the absorption upon exposure to UV light with wavelength of 365 nm and blue line corresponds to the absorption after irradiation with UV light with wavelength of 245 nm.

I did electrical measurements on STANs of Amino-Quin in the dark and under illumination. The results are shown in Figure 6.5. In this case, we see that unlike the results for STANs of OMe-Pyr, conductance changes upon irradiation with all lasers. We do not have an explanation for this trend as in STANs of both OMe-Pyr and Amino-Quin, changes in the conductance do not match with the maximum in absorption spectra of molecules in solution. As a control, if we investigated this effect in the molecules that they do not comprise donor-acceptor moieties, I fabricated STANs of 1-octadecanethiol. As it is shown in Figure 6.6, no change in conductance as a result of irradiation occurs. Thus, we can conclude that optical-gating of the STANs of hemicyanine molecules can change the conductance but so far we were unable to explain the wavelength dependence.

One of the features of these junctions is that we have observed the irradiation/no irradiation cycles for more than 150 scans and the junctions are still stable and responsive; although after 150 scans the STANs are still functional, in order to collect data from more STAN electrodes, I start measuring new junctons. To summarize the results obtained for all STANs, I plotted the current at 500 mV for each STAN (Figure 6.7). I mentioned earlier that we do not see any trend in the conductance after irradiation, but we do see the response only for the molecules with donor-acceptor moieties.

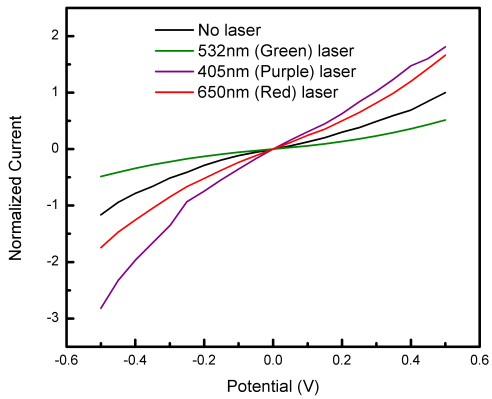

Figure 6.5: Normalized current versus potential for STANs of Amino-Quin in four different situations; When there is no irradiation with lasers (black line), irradiation with green laser (green line), irradiation with prurple laser (purple line) and irradiation with red laser (red line). Each plot is an average of at least ten scans from ten different STAN electrodes.

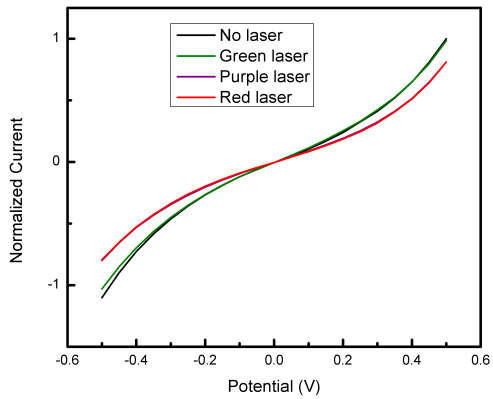

Figure 6.6: Normalized current versus potential for STANs of 1-octadecanethiol in four different situations; When there is no irradiation with lasers (black line), irradiation with green laser (green line), irradiation with prurple laser (purple line) and irradiation with red laser (red line). Each plot is an average of at least ten scans from ten different STAN electrodes.

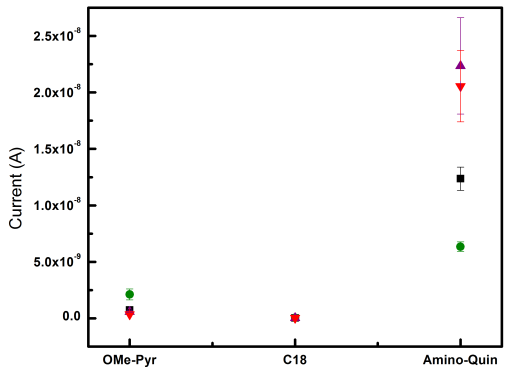

Figure 6.7: Current for STANs of OMe-Pyr, Amino-Quin and 1-octadecanethiol at 500 mV in four different situations; when there is no irradiation with lasers (black squares), irradiation with green laser (green dots), irradiation with prurple laser (purple upward triangles) and irradiation with red laser (red downward triangles). The error bars are variance.

6.4 Conclusion

The data presented here show unambiguously that the rate of tunneling, which we observe as current, in STANs comprising SAMs of hemicyanines changes upon irradiation with different wavelengths. This investigation is still in its first stages and further studies are required to understand the behavior of these photo-gated devices. Also, using substrates other than gold may help clarifying this issue. Utilizing molecules like hemicyanines that show reversible and fast change in conductance upon using external stimuli (*e.g.*, light) can be promising candidates for functional devices in molecular electronics.

With an eye towards the application of nanogap electrodes in solar cells, the incorporation of such molecules that show photovoltaic effects in STANs may pave the road towards new generation of organic solar cells based on interdigitaed nanogap electrodes.

Bibliography

[1] M. Irie. Diarylethenes for memories and switches. *Chem. Rev.*, 100(5):1685–1716, 2000.

[2] Q. Lu, K. Liu, H. Zhang, Z. Du, X. Wang, and F. Wang. From tunneling to hopping: A comprehensive investigation of charge transport mechanism in molecular junctions based on oligo(p-phenylene ethynylene)s. *ACS Nano*, 3(12):3861–3868, 2009. PMID: 19916506.

[3] M.-H. Jo, J. E. Grose, K. Baheti, M. M. Deshmukh, J. J. Sokol, E. M. Rumberger, D. N. Hendrickson, J. R. Long, H. Park, and D. C. Ralph. Signatures of molecular magnetism in single-molecule transport spectroscopy. *Nano Lett*, 6(9):2014–2020, 2006.

[4] S. Y. Quek, M. Kamenetska, M. L. Steigerwald, H. J. Choi, S. G. Louie, M. S. Hybertsen, J. B. Neaton, and L. Venkataraman. Mechanically controlled binary conductance switching of a single-molecule junction. *Nat. Nanotechnol.*, 4:230, 2009.

[5] Y. Cao, S. Dong, S. Liu, Z. Liu, and X. Guo. Toward functional molecular devices based on graphene-molecule junctions. *Angew. Chem. Int. Ed*, 52(14):3906–3910, 2013.

[6] J. Repp, G. Meyer, F. E. Olsson, and M. Persson. Controlling the charge state of individual gold adatoms. *Science*, 305:493, 2004.

[7] S. Grunder, R. Huber, V. Horhoiu, M. T. González, C. Schönenberger, M. Calame, and M. Mayor. New cruciform structures: Toward coordination induced single molecule switches. *J. Org. Chem*, 72(22):8337–8344, 2007. PMID: 17915927.

[8] S. J. van der Molen and P. Liljeroth. Charge transport through molecular switches. *Journal of Physics: Condensed Matter*, 22(13):133001, 2010.

[9] B. L. Feringa. *Molecular Switches*. Weinheim: Wiley-VCH, 2001.

[10] J. C. Cuevas and E. Scheer. *Molecular Electronics: An Introduction to Theory and Experiment*. World Scientific: Singapore, 2010.

[11] J. M. Mativetsky, G. Pace, M. Elbing, M. A. Rampi, M. Mayor, and P. Samoì. Azobenzenes as light-controlled molecular electronic switches in nanoscale metal-molecule-metal junctions. *Journal of the American Chemical Society*, 130(29):9192–9193, 2008. PMID: 18576645.

[12] K. Uchida, Y. Yamanoi, T. Yonezawa, and H. Nishihara. Reversible on/off conductance switching of single diarylethene immobilized on a silicon surface. *J. Am. Chem. Soc.*, 133(24):9239–9241, 2011.

[13] G. Pace, V. Ferri, C. Grave, M. Elbing, C. von Hänisch, M. Zharnikov, M. Mayor, M. A. Rampi, and P. Samorì. Cooperative light-induced molecular movements of highly ordered azobenzene self-assembled monolayers. *Proceedings of the National Academy of Sciences*, 104(24):9937–9942, 2007.

[14] Y. Kim, A. Garcia-Lekue, D. Sysoiev, T. Frederiksen, U. Groth, and E. Scheer. Charge transport in azobenzene-based single-molecule junctions. *Phys. Rev. Lett.*, 109:226801, Nov 2012.

[15] D. Dulić, S. J. van der Molen, T. Kudernac, H. T. Jonkman, J. J. D. de Jong, T. N. Bowden, J. van Esch, B. L. Feringa, and B. J. van Wees. One-way optoelectronic switching of photochromic molecules on gold. *Phys. Rev. Lett.*, 91:207402, 2003.

[16] S. Martin, W. Haiss, S. J. Higgins, and R. J. Nichols. The impact of e–z photoisomerization on single molecular conductance. *Nano Lett.*, 10(6):2019–2023, 2010. PMID: 20499909.

[17] M. del Valle, R. Gutierrez, C. Tejedor, and G. Cuniberti. Tuning the conductance of a molecular switch. *Nat. Nanotechnol.*, 2:176, 2007.

[18] V. Ferri, M. Elbing, G. Pace, M. D. Dickey, M. Zharnikov, P. Samorì, M. Mayor, and M. A. Rampi. Light-powered electrical switch based on cargo-lifting azobenzene monolayers. *Angew. Chem. Int. Ed*, 47(18):3407–3409, 2008.

[19] Y. Kim, T. J. Hellmuth, D. Sysoiev, F. Pauly, T. Pietsch, J. Wolf, A. Erbe, T. Huhn, U. Groth, U. E. Steiner, and E. Scheer. Charge transport characteristics of diarylethene photoswitching single-molecule junctions. *Nano Lett.*, 12(7):3736–3742, 2012.

[20] D. Roldan, V. Kaliginedi, S. Cobo, V. Kolivoska, C. Bucher, W. Hong, G. Royal, and T. Wandlowski. Charge transport in photoswitchable dimethyldihydropyrene-type single-molecule junctions. *J. Am. Chem. Soc.*, 135(16):5974–5977, 2013.

[21] T. Li, M. Jevric, J. R. Hauptmann, R. Hviid, Z. Wei, R. Wang, N. E. A. Reeler, Er. Thyrhaug, S. Petersen, J. A. S. Meyer, N. Bovet, T. Vosch, J. Nygård, X. Qiu, W. Hu, Y. Liu, G. C. Solomon, H. G. Kjaergaard, T. Bjørnholm, M. B. Nielsen, B. W. Laursen, and K. Nørgaard. Ultrathin reduced graphene oxide films as transparent top-contacts for light switchable solid-state molecular junctions. *Adv. Mater.*, 25(30):4164–4170, 2013.

[22] S. Seo, M. Min, S. M. Lee, and y. Lee. Photo-switchable molecular monolayer anchored between highly transparent and flexible graphene electrodes. *Nature Communications*, 4:1920, 2013.

[23] R. K. Vijayaraghavan, F. Gholamrezaie, and S. C.J. Meskers. Photovoltaic effect in self-assembled molecular monolayers on gold: Influence of orbital energy level alignment on short-circuit current generation. *The Journal of Physical Chemistry C*, 117(33):16820–16829, 2013.

Summary

The focus of this thesis is the simple fabrication of nanogap electrodes (metal/ molecule/ metal junctions). Due to the potential applications of nanogap electrodes in Molecular Electronics (ME), solar cells etc., several methods of fabricating nanogap electrodes have been developed. Mechanically controllable break junctions, electrochemical and chemical deposition, electromigration, molecular rulers and on-wire lithography are some of these methods, which I discuss in Chapter 1. Each of these methods have their own advantages and disadvantages but none of them combines simplicity, high throughput, direct addressability and ease of fabrication. The fabrication of nanogap electrodes using nanoskiving is a new method that we have developed to overcome these drawbacks.

In Chapter 2 I provide an overview of nanoskiving and how this method works. Different nanostructures can be fabricated by nanoskiving that are difficult or impossible to fabricate using other methods. Also, in this chapter I introduce a new embedding resin that we developed in collaboration with Prof. M. D. Dickey's group at North Carolina University. Gold is commonly used in nanoskiving and in the fabrication of nanogap electrodes due to its properties (*e.g.*, it is easy to deposit, it is not brittle and does not oxidize readily). Thus, good adhesion of gold to the embedding resin is crucial. To improve this adhesion, our newly developed resin contains free thiols. Several properties of this thiol-containing resin are discussed and specifically those which are important for nanoskiving.

In Chapter 3 I present the fabrication of sub-3 nm nanogap electrodes using self-assembled monolayers (SAMs) as gap template. I have fabricated SAM-templated addressable nanogap electrodes (STANs) using different alkanethiols. I characterized them using electron microscopy and electrical measurements, proving that that alkanedithiols can be used as gap templates. The I/V curves of three alkanedithiols with different lengths show that the current decreases exponentially with increasing length of the molecules, which is expected in tunneling junctions. The tunneling decay constant (β) obtained from length dependent electrical measurements shows an excellent agreement with values reported for alkanethiols in literature and indicates that molecules indeed defining the gap size and tunneling happens through the backbone of molecules. As a result, we have control over the gap size with angstrom-level resolution; a carbon-carbon

bond.

In Chapter 4 I show that nanogap electrodes with gaps larger than 5 nm can be fabricated using sacrificial layers of Al and Ag as spacer. Dry or wet etching of these layers result in gaps of the desired size. The fabrication of nanogaps using different metals is another issue that I present in this chapter. Fabrication using different metals allows us to make nanogaps with different work function metals. These results show that we are not limited to use gold as electrode material and SAMs as the gap template.

To be able to make tunneling junctions from arbitrary dithiols (which are delicate to be used as gap template directly) such as oligo(pheniylene ethynylene) (OPE) molecules, I take advantage of exchange phenomena in SAMs. The results are depicted in Chapter 5. I used electrical measurements to characterize the junctions. Dynamic exchange of alkanedithiols in STANs with OPE molecules via incubation of them in OPE3 solution results in higher current densities. These promising results suggest that we may have a generalizable platform to construct tunneling junctions from any arbitrary dithiols.

In Chapter 6 I show the results of the fabrication of STANs using hemicyanine molecules as gap template. Photovoltaic effects of these molecules have been studied before. Using electrical measurements, we investigated the change in currents upon photo-gating the junctions. Irradiation of junctions with different wavelengths and comparing these results with the measurements in dark (no irradiation) indicates that current changes upon irradiation with different wavelengths. This change is reversible and fast; however, to fully understand this behavior further studies need to be performed.

Samenvatting

De focus van dit proefschrift ligt op de eenvoudige fabricage van electroden waartussen zich een spleet bevindt in de range van nanometers (metaal-molecuul-metaalkoppelingen). Door de mogelijke toepassingen van deze electroden met daartussen een nanospleet in bijvoorbeeld moleculaire electronica en zonnecellen zijn verschillende fabricagemethoden ontwikkeld. Een aantal van deze methoden zoals mechanisch-controleerbare breekkoppelingen, (electro)chemische depositie, electromigratie, zogenaamde moleculaire heersers en draadlithografie zullen worden beschreven in hoofdstuk 1. Elk van deze methoden heeft eigen voor- en nadelen, maar geen is in staat om eenvoud, hoge doorvoersnelheid, directe adresseerbaarheid en gemak van fabricage te combineren. Daarom hebben wij een nieuwe methode ontwikkeld om electroden te maken met daartussen een nanospleet, geheten nanoskiving, die dit wel kan.

In hoofdstuk 2 wordt uitgelegd wat nanoskiving is. Met behulp van nanoskiving kun je verschillende nanostructuren fabriceren die met behulp van andere methoden moeilijk of haast onmogelijk te produceren zijn. In dit hoofdstuk zal ik ook een inbeddende hars beschrijven die we ontwikkeld hebben in samenwerking met de groep van prof. M.D. Dickey van de universiteit van North Carolina. Nanoskiving maakt vaak gebruik van goud door zijn eigenschappen (makkelijke depositie van het materiaal, het is niet broos en het oxideert niet makkelijk). Een goede adhesie van goud aan de inbeddende hars is cruciaal. Om deze adhesie te verbeteren zitten er vrije thiolen in de hars. Verschillende eigenschappen van deze thiolhoudende hars en dan vooral diegene die van belang zijn voor nanoskiving worden besproken.

In hoofdstuk 3 behandel ik de fabricage van electroden met daartussen een spleet in de orde van sub-3 nanometer, gebruik makend van zelf-assemblerende monolagen (afkorting SAMs) als matrijs voor de nanospleet. Met verschillende alkaanthiolen zijn zogenaamde SAM-templated addressable nanogap electrodes (STANs) gefabriceerd. Deze zijn gekarakteriseerd met behulp van een electronenmicroscoop en electrische metingen om te bewijzen dat alkaanthiolen geschikt zijn als matrijs voor nanospleten. De I/V curves van 3 alkaandithiolen met verschillende ketenlengte laten zien dat de stroom exponentieel afneemt als de ketenlengte van het molecuul toeneemt, zoals verwacht wordt bij tunnelingkoppelingen. De tunnelingvervalconstante (β) die bepaald werd tijdens elektrische metingen van ketenlengte-afhankelijkheid, komt goed overeen met waardes uit de literatuur die gemeld zijn voor alkaanthiolen. Dit betekent dat moleculen in-

derdaad de spleetgrootte bepalen en dat tunneling plaatsvindt via de ruggegraat van moleculen. Daardoor hebben we controle over de grootte van de spleet met een resolutie op het Angstrmniveau: het niveau van een C-C binding.

In hoofdstuk 4 laat ik zien dat met behulp van kunstmatige aluminium- en zilverlagen als tussenlaag electrodes met een spleet ertussen van meer dan 5 nanometer gefabriceerd kunnen worden. Het droog of nat etsen van deze kunstmatige tussenlagen leidt tot spleten met de gewenste grootte. De fabricage van nanospleten met behulp van verschillende metalen is een ander issue dat behandeld wordt in dit hoofdstuk. Elk metaal heeft zijn eigen werkfunctie, waardoor verschillende soorten nanospleten gefabriceerd kunnen worden. De resultaten tonen aan dat we niet beperkt zijn tot het gebruiken van goud als electrode en/of SAMs als matrijs voor de nanospleet.

Om tunnelingkoppelingen te verkrijgen van willekeurige dithiolen (welke te delicaat zijn om direct te gebruiken als matrijs voor nanospleten) zoals oligo (pheniyleen ethynyleen) (OPE) moleculen, maak ik gebruik van uitswisselingsfenomenen in SAMs. De resultaten hiervan staan in hoofdstuk 5. Electrische metingen worden gebruikt om de koppelingen te karakteriseren. Dynamische uitwisseling van alkaandithiolen in STANs met OPE moleculen via incubatie van STANs in een oplossing van OPE3 resulteert in hogere stroomdichtheden. Deze veelbelovende resultaten suggereren dat we een algemeen, breed platform ontwikkeld hebben om tunnelingkoppelingen te bouwen van elk willekeurig dithiol.

In hoofdtuk 6 laat ik de resultaten zien van de fabricage van STANs met hemicyanine moleculen als matrijs voor nanospleten. Photovoltaische effecten van deze moleculen zijn al bestudeerd in de literatuur. Met behulp van electrische metingen hebben we de verandering in stroomdichtheid onderzocht door middel van de invloed van licht op de werking van onze metaal-molecuul-metaal koppelingen. Het bestralen van koppelingen met verschillende golflengtes en het vergelijk van de resultaten met metingen uitgevoerd in het donker (zonder bestraling) geeft aan dat de stroom verandert door bestraling met verschillende golflengtes. Deze verandering is reversibel en snel; echter, om dit gedrag volledig te begrijpen zijn verdere studies nodig.

Acknowledgments

Words cannot express my sincere gratitude to those whose support and profound impacts made this dissertation possible. I would like to apologize in advance if I have forgotten to mention those who have helped and supported me along this way.

My first and foremost thanks go to my supervisor Dr. Ryan Chiechi. Ryan, I owe you a great deal. You gave me the opportunity to be part of your group despite the fact that I did not have any experimental background! I feel privileged to have done my PhD under your supervision. Your unreserved support, help and patience allowed me to develop my skills as a scientist. You were not just my mentor but a true friend; not just a good scientist but a good person. Your sense of humor, understanding and kindness enabled me to discuss openly almost every single issue with you. I will never forget our conversations about everything and your general knowledge in different areas has always astonished me. I cannot express enough how much I have learned from you. Thanks for everything!

I would like to thank Prof. Dr. Kees Hummelen for his support and assistance during the four years of my PhD. Kees, I truly appreciate the chance of being part of your group. The door of your office was always open to me. Ik heb veel van je geleerd tijdens mijn promotieonderzoek.

I would like to express my gratitude to the members of reading committee Prof. Dr. Sabeth Verpoorte, Prof. Dr. Stefan Meskers and Prof. Darren Lipomi for their time and effort in improving my dissertation.

I would like to thank Renate Hekkema for her endless help in arranging the enormous amount of paper work that accompanies a PhD. Renate, you were always so kind to me and I will never forget your cheerful character.

I cannot imagine woking in the lab without the help of our great technician, Reinder Gooijaarts. Reinder, I was always amazed by your creativity in making tools and devices to ease the difficulties involved in our experiments. Bedankt!

I would like to thank my collaborators in North Carolina State University,

specially Prof. Michael Dickey for the fruitful collaboration. Also, I would like to thank Ratheesh Vijayaraghavan and Prof. Dr. Stefan Meskers for providing the hemicyanine molecules.

I would like to thank Dr. Marc Stuart for assistance with TEM measurements.

I am grateful to all my colleagues and friends in CBMD group. Cindy, Hennie, Davide, Zhiyuan, Wenqiang, Jelmer, Ricardo, Jermio, Mehrnoosh, Thomas, Jenny, Olga, Thijs, Bouke, Difei, Dang and Piet, thank you all for making such a nice and friendly atmosphere in the group. Special thanks to Cindy for the translation of the summary of the present dissertation to Dutch. Cindy, that meant a lot to me. Jenny and Mehrnoosh, thanks for accepting to be my paranymphs.

Also, I would like to thank my bachelor and master students who did their projects under my supervision. Laaya, Tadesse, Henrieke and Jim, I have learned a lot and enjoyed working with you while I was your daily supervisor.

Being far from family is difficult, but having nice friends from your home country makes it easier to cope with the situation. My sincere appreciation goes to all my Persian friends in Groningen. I have to admit that my life here would have been boring without you! Saeedeh, our friendship goes back almost 10 years (how old we are ;-)). I believe that the world is not as big as we think. Thanks for everything that you have done for me. Mehrsima, I am so lucky to have you as a friend and will never forget our trip to Prague with a fruitful ending :-) Amir Hossein and Sara, thanks for all the time that we have spend together especially the times that we played hours of Settlers of Catan! Sara, special thanks goes to you for being my dance partner. Also, your daily messages (you know what I mean!!) have inspired me a lot. Sahar and Ismaiel, I wish I knew you earlier. I will carry the memory of being together for the rest of my life. Mehrnoosh, Ali (Ghavami), Fariba, Saleh, Shaghayegh, Qader, Ali (Najafi) and Zahra, thank you guys for all your sweet company.

Parinaz, my sweetheart! You are the best sister that one could ever have. You know how difficult it is for me being far from you. Kochoolooye man, thanks for your endless support, care and kindness. I miss you every moment...

Mom and dad! I am writing these lines with tears in my eyes. How can I ever thank you both enough. You have done everything for me, including sacrificing the joys of your own lives so that I could be happy and can pursue my dreams. I can not express my feelings in words. "Mamani", you are a symbol of patience and assiduity for me. You have always encouraged me to go on."Babaie" I am deeply indebted to you. You are the reason I never understood what difficulty, complexity and struggle really mean. Thank you both for all your endless and sincere support and care.

Finally, I would like to thank my one and only one, Mehdi. How can I possibly thank you for what you have done for me. You are the best thing that has happened to me in my life. You are the one who made my dreams come true. Thank you for every single moment that we have spent together. Thanks for your infinite and unconditional love, care and support. This thesis could not have been accomplished without your patience.

May 8, 2014
Parisa